Consequences of a lack of adult intravenous data on the prediction accuracy of pediatric physiologically based pharmacokinetic (PBPK) modeling

by

Rabiya Chandani

A thesis

presented to the University of Waterloo

in fulfillment of the

thesis requirement for the degree of

Master of Science

in

Pharmacy

Waterloo, Ontario, Canada, 2015

Author's declaration

I hereby declare that I am the sole author of this thesis. This is a true copy of the thesis, including any required final revisions, as accepted by my examiners.

I understand that my thesis may be made electronically available to the public.

Abstract

Lack of pediatric clinical data has led to a large gap in knowledge concerning drug efficacy, safety and dosing guidelines within the pediatric population. Many pediatric off-label doses are based largely on adult studies with little or no pediatric experience; this has the potential to lead to treatment failures, toxicities, and various other drug-related adverse events. Given that recruitment to pediatric trials is difficult, researchers have recently used physiologically-based pharmacokinetic (PBPK) models as a means to efficiently plan pediatric clinical studies. PBPK models are mechanistic in nature and mathematically describe the disposition of drugs in an organism. This *in silico* technique predicts pharmacokinetic (PK) profiles based on compound physicochemical properties and multiple physiological input parameters of the individual, such as organ volumes, tissue composition, blood flow, and clearance (CL). Pediatric PK parameters are typically predicted using a pediatric PBPK model that has been developed using an adult PBPK model and clinical PK data. Within this workflow for pediatric PBPK model development, adult intravenous (IV) data is typically used; however, there are many instances where there may not be an IV formulation available for certain compounds. As a result, the question remains if the workflow for pediatric PBPK modeling produces accurate pediatric PK predictions in the absence of adult IV data. In this case, IV data from pre-clinical species (i.e. rat) may be an alternative to human IV data. The objective of this study was to assess the ability of pediatric PBPK models to predict observed pediatric PK parameters using a model development workflow that uses rat IV PK data, as opposed to adult human IV PK data. The implications of both workflows were assessed by comparing the precision and bias of the predicted vs. observed PK exposure metrics in children. This study demonstrated that rat IV data is a viable alternative to using adult IV PK data within the pediatric PBPK model development workflow and the majority of exposure metrics were within 2 fold from the observed pediatric data, regardless of workflow or Biopharmaceutics Classification System (BCS) class of the compound. Ultimately, the model was not hindered in its prediction accuracy, despite a lack of distribution and clearance data that would otherwise have been derived from human IV data. Overall, the application of rat IV data as a substitute for human IV data in PBPK modeling is a novel approach that has significant potential for future application.

Acknowledgements

I would like to extend my sincerest gratitude to my advisor, Dr. Andrea Edginton for giving me the opportunity to work under her guidance as one of her MSc students. I would not have been able to complete this project without Dr. Edginton's ongoing support, patience, and encouragement. Filling the entire 153 pages of this document praising Dr. Edginton for her time, and mentorship could not possibly do justice in summarizing my eternal gratitude for this opportunity and all that she has done for me.

I would like to acknowledge Dagmar M. Hajducek for her advice pertaining to the statistical analysis of my research. Special thanks go to my advisory committee members for guiding me through the milestones of this degree.

I extend my deepest gratitude to Anil Maharaj for his ongoing expertise during the project as a mentor, and dear friend. Many thanks to Jessica Nicastro, fellow lab mates, and all the wonderful close friends I've had the pleasure to get to know within the last few years.

Lastly, I would like to thank my family for their unconditional love, and support during this experience. I could always turn to them for my daily dose of sanity, through the good times and the bad.

Dedication

I would like to dedicate this thesis to my father, Ali, my sister, Zahra, my late mother, Zainab, and to my close friends and colleagues who supported me throughout my graduate career.

Table of Contents

Author's declaration ii
Abstract iii
Acknowledgements iv
Dedication v
Table of Contents vi
List of Tables ix
List of Figures xiv
List of Abbreviations xx
1. Introduction 1
2. Objectives & Hypotheses 10
3. Methods 11
3.1 Data collection 11
3.2 Software for PBPK model development 12
3.3 Project workflow overview 12
3.4 Pediatric PK predictions for BCS class 1 compounds 13
3.4.1 Acetaminophen 13
Workflow 1 of acetaminophen 13
Workflow 2 of acetaminophen 21
3.4.2 Levofloxacin 28
Workflow 1 of levofloxacin 28
Workflow 2 of levofloxacin 32
3.4.3 Lorazepam 35
Workflow 1 of lorazepam 35
Workflow 2 of lorazepam 39
3.5 Pediatric PK predictions for BCS class 2 compounds 42
3.5.1 Ofloxacin 42
Workflow 1 of ofloxacin 42
Workflow 2 of ofloxacin 46
3.5.2 Ciprofloxacin 50
Workflow 1 of ciprofloxacin 50
Workflow 2 of ciprofloxacin 54

3.5.3 Valsartan 57
Workflow 1 of valsartan 57
Workflow 2 of valsartan 61
3.6 Pediatric PK predictions for BCS class 3 compounds 65
3.6.1 Acyclovir 65
Workflow 1 of acyclovir 65
Workflow 2 of acyclovir 69
3.6.2 Cimetidine 73
Workflow 1 of cimetidine 73
Workflow 2 of cimetidine 77
3.6.3 Azithromycin 80
Workflow 1 of azithromycin 80
Workflow 2 of azithromycin 84
3.7 Comparison of model predictive performance 87
3.7.1 Post-hoc ANOVA based tests (Aim 1 & 2) 87
3.7.2 Assessing precision and bias of model derived predictions (Aim 3) 88
3.7.3 Assessing how BCS level influences pediatric model accuracy (Aim 4) 89
4 Results 90
4.1 Results for BCS class I compounds 90
Acetaminophen 90
Levofloxacin 93
Lorazepam 96
4.2 Results for BCS class II compounds 98
Ciprofloxacin 98
Ofloxacin 100
Valsartan 102
4.3 Results for BCS class III compounds 105
Acyclovir 105
Cimetidine 107
Azithromycin 109
4.4 Summary of aim 1 and aim 2 111
4.5 Summary of Chi squared statistic of BCS class comparison (Aim 3 & 4) 112
5. Discussion 114

6. Conclusion.......... 119
References.......... 120

List of Tables

Table 1. Acetaminophen physicochemical input parameters for the rat and adult models within Workflow 1 13

Table 2. Optimized total hepatic CL_{spec}, and intestinal permeability (P_{int}) for three simulated adult oral profiles. The arithmetic mean of the three studies is presented. 15

Table 3. CL proportions for the adult oral model following oral acetaminophen administration 16

Table 4. Optimized CL_{spec} and GFR fraction for each of three simulated profiles following oral dose administration in adults 16

Table 5. Relative proportions of individual pathways of CL within the adult oral model 16

Table 6. Population variability of acetaminophen incorporated into population model simulations of acetaminophen 19

Table 7. Relative proportions of individuals pathways of Cl within the adult IV model in Workflow 2 22

Table 8. Numerically optimized P_{int} for each of three simulated profiles following oral dose administration in adults within Workflow 2 22

Table 9. Pediatric inter-individual variability factors applied to the pediatric population of acetaminophen 27

Table 10. Levofloxacin initial input, and optimized final model parameterization for Workflow 1 and Workflow 2 28

Table 11. Numerically optimized P_{int}, TS and UGT1A1 parameters for the oral model of levofloxacin 30

Table 12. Population variability incorporated into the adult population model simulations in PK-Sim and MoBi for levofloxacin 31

Table 13. Numerically optimized P_{int}, TS, UGT1A1 CL_{spec}, LogP for the adult PBPK model of levofloxacin within the standard workflow 33

Table 14. Lorazepam initial input, and optimized final model parameterization for Workflow 1 and Workflow 2 35

Table 15. Mean optimized P_{int} and hepatic UGT2B7 CL_{spec} 36

Table 16. Population variability incorporated into the adult population model simulations in PK-Sim for lorazepam..... 37

Table 17. Numerically optimized P_{int}, LogP, UGT2B7 CL_{spec} for the standard workflow of lorazepam 40

Table 18. Physicochemical initial parameter inputs for ofloxacin within Workflow 1..... 42

Table 19. Workflow 1- optimized CL parameters for adult oral model of ofloxacin..... 44

Table 20. Population variability incorporated into the adult population model of ofloxacin..... 45

Table 21. Optimized P_{int}, TS, and Hepatic CL for the standard workflow of ofloxacin 47

Table 22. Population variability incorporated into the adult population model simulations in MoBi for ofloxacin..... 48

Table 23. Population variability incorporated into the pediatric population model for ofloxacin 49

Table 24. Ciprofloxacin physicochemical input parameters for the rat and adult models within Workflow 1..... 50

Table 25. Optimized total hepatic CL_{spec}, P_{int} for three simulated adult oral profiles..... 52

Table 26. Population variability incorporated into the adult population model simulations of ciprofloxacin..... 52

Table 27. Numerically optimized parameters of P_{int}, TS, CYP1A2 CL and LogP for the standard workflow of ciprofloxacin..... 55

Table 28. Population variability incorporated into the pediatric population model simulations for Ciprofloxacin..... 56

Table 29. Physicochemical initial parameter inputs for valsartan in the Rat and adult model..... 57

Table 30. Optimized distribution and CL parameters of valsartan..... 59

Table 31. Population variability incorporated into the adult population model simulations for valsartan 60

Table 32. Optimized absorption and CL parameters of valsartan 62

Table 33. Population variability incorporated into the adult population model simulations of valsartan 63

Table 34. Population variability incorporated into the pediatric population model simulations in PK-Sim and MoBi for Workflow 1 and 2 64

Table 35. Physicochemical initial parameter inputs for acyclovir 65

Table 36. Numerically optimized P_{int}, TS CL_{spec} for each of three simulated profiles following oral dose administration in adults 67

Table 37. Population variability incorporated into the adult population model simulations of acyclovir 68

Table 38. Numerically optimized P_{int}, TS, and hepatic CL parameters for acyclovir within the standard workflow 70

Table 39. Population variability incorporated into population model simulations for acyclovir 71

Table 40. Population variability parameters incorporated into the pediatric population model for Workflow 1 and 2 72

Table 41. Physicochemical parameters of cimetidine for initial input into Workflow 1 and 2 73

Table 42. Numerically optimized P_{int}, TS CL_{spec}, and hepatic CL parameters based on observed data . 75

Table 43. Population variability incorporated into the adult population model simulation in PK-Sim and MoBi 76

Table 44. Numerically optimized parameters of LogP, P_{int}, TS, and hepatic CL spec 78

Table 45. Population variability parameters incorporated into the pediatric model for Workflow 1 and 2 of cimetidine 79

Table 46. Physicochemical initial parameter inputs for azithromycin in the Rat and adult model 80

Table 47. Optimized parameters of P_{int}, biliary CL, CYP 3A4 CL and TS within Workflow 1 of azithromycin 82

Table 48. Population variability incorporated into the adult population model simulations of azithromycin 83

Table 49. Optimized P_{int}, CYP3A4 CL, Biliary CL, TS and Log P for cimetidine within the standard workflow 85

Table 50. Population variability parameters incorporated into the pediatric model for Workflow 2 of azithromycin 86

Table 51. ANOVA F-test summary comparing model derived vs. observed means of acetaminophen 91

Table 52. P-values from post-hoc multiple comparison tests, of model derived PK predictions of observed data for acetaminophen. 91

Table 53. Precision and bias measurements for Workflow 1 and Workflow 2 derived PK estimates based on observed studies of acetaminophen 92

Table 54. ANOVA F-test summary between model derived vs. observed means of levofloxacin 93

Table 55. P-values from post-hoc multiple comparison tests, of model derived PK predictions of observed data of levofloxacin 94

Table 56. Precision and bias measurements for Workflow 1 and Workflow 2 derived PK estimates based on observed studies for levofloxacin 95

Table 57. ANOVA F-test summary between model derived vs. observed means of lorazepam 96

Table 58. P-values from post-hoc multiple comparison tests, of model derived PK predictions of observed data for lorazepam 97

Table 59. Precision and bias measurements for Workflow 1 and Workflow 2 derived PK estimates based on observed studies of Lorazepam 97

Table 60. ANOVA F-test summary between model derived vs. observed means for ciprofloxacin 98

Table 61. P-values from post-hoc multiple comparison tests, of model derived PK predictions of observed data for ciprofloxacin 99

Table 62. Precision and bias measurements for Workflow 1 and Workflow 2 derived PK estimates based on observed studies of ciprofloxacin 99

Table 63. ANOVA F-test summary between model derived vs. observed means of ofloxacin 100

Table 64. P-values from post-hoc multiple comparison tests, of model derived PK predictions of observed data for ofloxacin 101

Table 65. Precision and accuracy measurements for workflow 1 and workflow 2 derived PK estimates based on observed studies of ofloxacin 101

Table 66. ANOVA F-test summary between model derived vs. observed means for valsartan 102

Table 67. P-values from post-hoc multiple comparison tests, of model derived PK predictions of observed data for valsartan 103

Table 68. Precision and bias measurements for workflow 1 and workflow 2 derived PK estimates based on observed studies of valsartan 103

Table 69. ANOVA F-test summary between model derived vs. observed means of acyclovir 105

Table 70. P-values from post-hoc multiple comparison tests, of model derived PK predictions of observed data for acyclovir 106

Table 71. Precision and bias measurements for Workflow 1 and Workflow 2 derived PK estimates based on observed studies of acyclovir 106

Table 72. ANOVA F-test summary between model derived vs. observed means 107

Table 73. P-values from post-hoc multiple comparison tests, of model derived PK predictions of observed data for cimetidine 107

Table 74. Precision and bias measurements for Workflow 1 and Workflow 2 derived PK estimates based on observed studies 108

Table 75. ANOVA F-test summary between model derived vs. observed means of azithromycin 109

Table 76. P-values from post-hoc multiple comparison tests, of model derived PK predictions of observed data 109

Table 77. Precision and bias measurements for Workflow 1 and Workflow 2 derived PK estimates based on observed studies of azithromycin 110

Table 78. Summary of aim 1 and aim 3 ANOVA and pairwise comparison 112

Table 79. Chi squared statistic comparing overall predictive performance of each workflow to predict pediatric parameters within 2 fold AAFE 112

Table 80. Chi squared statistic comparing overall influence of BCS class on model prediction. 113

List of Figures

Figure 1. Schematic representation of a mechanistic whole-body PBPK model 2

Figure 2. Standard workflow employed in the development of a PBPK model for pediatrics based on an adult IV model 4

Figure 3. Alternate workflow for creating a whole-body PBPK model in pediatrics based on rat IV data as a substitute for human IV data 9

Figure 4. Biopharmaceutics Classification System (BCS) based on degree of compound permeability and solubility 9

Figure 5. Simulated (line) and observed (symbols) plasma concentration data following a 1 mg/kg IV bolus administration of acetaminophen to rats. Dose normalized observed data is taken from Watari et al[41]. 14

Figure 6. Simulated (line) and observed (symbols) plasma concentration data following a A) 325 mg [43] B) 500 mg [44] and C) 1000 mg [45] oral dose of acetaminophen in adults. Simulated profiles are optimized for P_{int} and CL 17

Figure 7. Simulated mean (central line) and standard deviation (dotted line) plasma concentration data in 100 individuals as compared to observed (symbols) mean and standard deviation plasma concentration data following a 500 mg oral dose of acetaminophen in adults Rawlins et al [43]. Observed SD has been calculated from standard error mean (SEM) reported by Rawlins et al. 20

Figure 8. Simulated (line) and observed (symbols) plasma concentration data following an IV dose of acetaminophen in adults, including simulated fe (dotted line). IV profile was optimized for CL and distribution (i.e. LogP) based on data from Rawlins et al [43]. 21

Figure 9. Simulated (line) and observed (symbols) plasma concentration data following a A) 325 mg B) 500 mg and C) 1000 mg oral dose of acetaminophen in adults, as well as simulated fe (dotted line). Simulated profiles are optimized for Pint and hepatic CL. 22

Figure 10. Simulated mean (central line) and standard deviation (dotted line) plasma concentration data in 100 individuals as compared to observed (symbols) mean and standard deviation plasma concentration data following a 500 mg oral dose of acetaminophen in adults Rawlins et al [43]. Observed SD have been calculated from standard error mean (SEM) reported by Rawlins et al. *Building the acetaminophen pediatric population model for Workflow 1 and 2* 23

Figure 11. Simulated (line) and observed (symbols) plasma concentration data following 20 mg/kg levofloxacin to rats. Observed data was taken from Fujieda et al [59]. 28

Figure 12. Simulated (line) and observed (symbols) plasma concentration profiles, and fe (dotted line) for a 500 mg oral levofloxacin administration. B) and C) have been dose normalized from 750 mg and 1000 mg respectively. All graphs were optimized for CL and P_{int}. 30

Figure 13. Simulated mean (central line) and standard deviation (dotted line) plasma concentration data in 100 individuals as compared to observed (symbols) mean and standard deviation plasma concentration data following a 500 mg oral dose of levofloxacin [61] 31

Figure 14. Simulated (line) and observed (symbols) plasma concentration data following a 500 mg IV infusion of levofloxacin in adults, including simulated fe (dotted line). IV profile was optimized for CL and distribution (i.e. LogP) Based on data from Chien et al [64]. Adult IV model optimized for LogP and CL. 32

Figure 15. Simulated (line) and observed (symbols) plasma concentration profiles of 500 mg [63] oral levofloxacin. B) and C) have been dose normalized from 750 mg [64] and 1000 mg [64] respectively. All graphs were optimized for CL and P_{int}. 33

Figure 16. Simulated mean (central line) and standard deviation (dotted line) plasma concentration data in 100 individuals as compared to observed (symbols) mean and standard deviation plasma concentration data following data following a 500 mg oral dose of levofloxacin in adults ... 34

Figure 17. Simulated (line) and observed (symbols) plasma concentration data following 0.05 mg/kg mg lorazepam to rats. Observed data was taken from Atack et al[69] 35

Figure 18. Simulated (line) and observed (symbols) plasma concentration profiles of 1.5 mg oral lorazepam. A-C have been dose normalized to reflect a 1.5 mg dose. All graphs were optimized for P_{int} and total CL 37

Figure 19. Simulated mean (central line) and standard deviation (dotted line) plasma concentration data in 100 individuals as compared to observed (symbols) mean and standard deviation plasma concentration data following a 1.5 mg oral dose of lorazepam 38

Figure 20. Simulated (line) and observed (symbols) plasma concentration data following a 2 mg IV bolus dose of levofloxacin in adults. IV profile was optimized for CL and distribution (i.e. LogP) Based on data from Greenblatt et al [74] 39

Figure 21. Simulated (line) and observed (symbols) plasma concentration profiles of 1.5 mg oral lorazepam. All graphs were optimized for CL and P_{int} 40

Figure 22. Simulated mean (central line) and standard deviation (dotted line) plasma concentration data in 100 individuals as compared to observed (symbols) mean and standard deviation plasma

concentration data following a 1.5 mg oral dose of lorazepam 41

Figure 23. Simulated (line and observed (symbols) plasma concentration data following a 40 mg/kg IV bolus administration of ofloxacin to rats. IV profile optimized for LogP, based on data from Wang et al [90] 43

Figure 24. Simulated (line) and observed (symbols) plasma concentration data following a 400 mg oral dose administration of ofloxacin in humans, including fe (dotted). Data is taken from A) Lehto [87] B) Lode [84] C) Yuk [88] 44

Figure 25. Simulated mean (central line) and standard deviation (dotted line) plasma concentration data in 100 individuals as compared to observed (symbols) mean and standard deviation plasma concentration data following data following a 400 mg oral dose of ofloxacin in adults 45

Figure 26. Simulated (line) and observed (symbols) plasma concentration profile of ofloxacin following a 100 mg IV bolus. Observed data was taken from Lode et al [80]. 46

Figure 27. Simulated (line) and observed (symbols) plasma concentration data following a 400 mg oral dose administration of ofloxacin in humans, including fe (dotted). Data is taken from A) Lehto [87] B) Lode [84] C) Yuk [88] 47

Figure 28. Simulated mean (central line) and standard deviation (dotted line) plasma concentration data in 100 individuals as compared to observed (symbols) mean and standard deviation plasma concentration data following data following a 400 mg oral ofloxacin in adults 48

Figure 29. Rat IV PBPK model following 5 mg/kg of ciprofloxacin, optimized for LogP, based on observed data. 50

Figure 30. Simulated (line) and observed (symbols) plasma concentration profiles, including fe (dotted), of ciprofloxacin following A) 100 mg [86] B) 250 mg [85] and C)750 mg [86] or oral ciprofloxacin. 52

Figure 31. Simulated mean (central line) and standard deviation (dotted line) plasma concentration data in 100 individuals as compared to observed (symbols) mean and standard deviation plasma concentration data following data following a 100 mg oral dose of ciprofloxacin in adults [85, 86] 53

Figure 32. Simulated (line) and observed (symbols) plasma concentration data following a 100 mg IV bolus of ciprofloxacin in adults, including simulated fe (dotted line). IV profile was optimized for CL and distribution (i.e. LogP) Based on data from Wise et al[98]. Adult IV model optimized for LogP and CL 54

Figure 33. Simulated (line) and observed (symbols) plasma concentration profiles of ciprofloxacin following A) 100 mg B)250 mg and C)750 mg oral dose administration within Workflow 2

.....55

Figure 34. Simulated mean (central line) and standard deviation (dotted line) plasma concentration data in 100 individuals as compared to observed (symbols) mean and standard deviation plasma concentration data following data following a 100 mg oral dose of ciprofloxacin in adults. 56

Figure 35. Simulated (line) and observed (symbols) valsartan Rat IV profile optimized for LogP, following 1 mg/kg IV bolus dose administration based on data from Yamashiro et al [87]..58

Figure 36. Simulated (line) and observed (symbols) plasma concentration profiles of valsartan following 80 mg oral dose administration, based on data from A) Flesch et al [103] B)Criscione et al [100] C) Macek et al [104] including fe (dotted) 59

Figure 37. Simulated mean (central line) and standard deviation (dotted line) plasma concentration data in 100 individuals as compared to observed (symbols) mean and standard deviation plasma concentration data following data following a 80 mg oral dose of valsartan in adults 60

Figure 38. Simulated (line) and observed (symbols) plasma concentration data of a 20 mg IV bolus of valsartan in humans, including fe (dotted) optimized for distribution and CL. Observed data taken from Flesch et al [103].....61

Figure 39. Simulated (line) and observed (symbols) plasma concentration profiles of valsartan following 80 mg oral dose administration, based on data from A) Flesch et al [93] B)Criscione et al [90] C) Macek et al [94].....62

Figure 40. Simulated mean (central line) and standard deviation (dotted line) plasma concentration data in 100 individuals as compared to observed (symbols) mean and standard deviation plasma concentration data following data following a 80 mg oral valsartan in adults.....63

Figure 41. Simulated (line) and observed (symbols) plasma concentration data following a 1 mg/kg IV bolus of acyclovir in rats. Observed data taken from Ogiso et al [108], and YE et al [109].66

Figure 42. Simulated (line) and observed (symbols) plasma concentration data following a 400 mg oral dose of acyclovir, including fe (dotted). Observed data taken from A) Bangaru et al [116] B) Vergin et al [118] C) Yuen et al [117] 67

Figure 43. Simulated mean (central line) and standard deviation (dotted line) plasma concentration data in 100 individuals as compared to observed (symbols) mean and standard deviation plasma concentration data following data following a 400 mg oral dose of acyclovir in adults.....68

Figure 44. Simulated (line) and observed (symbols) plasma concentration data in adults following a 350 mg IV infusion of acyclovir. Observed data taken from [119].....69

Figure 45. Simulated (line) and observed (symbols) plasma concentration data following a 400 mg oral dose of acyclovir. Observed data taken from A) Bangaru et al [116] B) Vergin et al [118] C) Yuen et al [117] 70

Figure 46. Simulated mean (central line) and standard deviation (dotted line) plasma concentration data in 100 individuals as compared to observed (symbols) mean and standard deviation plasma concentration data following data following a 400 mg oral dose of acyclovir in adults. Observed data taken from Bangaru et al [116], Vergin et al [118], Yuen et al [117]. 71

Figure 47. Simulated (line) and observed (symbols) plasma concentration data following a 40 mg/kg IV dose of acyclovir in rats; based on observed data from Adedoyin et al [121]. 73

Figure 48. Simulated (line) and observed (symbols) plasma concentration data following a 200 mg oral dose of cimetidine in adults. Observed data taken from A) Yamasaki et al [124] B) Jantratid et al [122] fe (dotted) included Table 42. Numerically optimized P_{int}, TS CL_{spec}, and hepatic CL parameters based on observed data 75

Figure 49. Simulated mean (central line) and standard deviation (dotted line) plasma concentration data in 100 individuals as compared to observed (symbols) mean and standard deviation plasma concentration data following data following a 200 mg oral dose of cimetidine in adults. 76

Figure 50. Simulated (line) and observed (symbols) plasma concentration data following an IV dose of cimetidine in adults. Observed data was taken from Jantratid et [122]. 77

Figure 51. Simulated (line) and observed (symbols) plasma concentration data following a 200 mg oral dose of cimetidine in adults. Observed data taken from A) Yamasaki et al [124]B) Jantratid et al [122] 78

Figure 52. Simulated mean (central line) and standard deviation (dotted line) plasma concentration data in 100 individuals as compared to observed (symbols) mean and standard deviation plasma concentration data following data following a 200 mg oral dose of cimetidine in adults. 79

Figure 53. Simulated (line) and observed (symbols) azithromycin Rat IV plasma concentration profile optimized for LogP, following 20 mg/kg IV bolus dose administration of cimetidine 81

Figure 54. Simulated (line) and observed (symbols) plasma concentration data following 500 mg of oral azithromycin. Observed data obtained from A) Najib et al [126] B) Matzneller et al [124] C) Iqbal et al[125]. Fe (dotted) included 82

Figure 55. Simulated mean (central line) and standard deviation (dotted line) plasma concentration data in 100 individuals as compared to observed (symbols) mean and standard deviation plasma concentration data following data following a 500 mg oral dose of azithromycin in adults. . 83

Figure 56. Simulated (line) and observed (symbols) plasma concentration data, and fe (dotted), following a 500 mg IV infusion study. Workflow 2 adult iv model optimized for distribution and CL. Observed data taken from Foulds et al[130]..... 84

Figure 57. Simulated (line) and observed (symbols) plasma concentration data following 500 mg of oral azithromycin. Observed data obtained from A) Najib et al [126] B) Matzneller et al [124] C) Iqbal et al [125] 85

Figure 58. Simulated mean (central line) and standard deviation (dotted line) plasma concentration data in 100 individuals as compared to observed (symbols) mean and standard deviation plasma concentration data following data following a 500 mg oral dose of azithromycin in adults.. 86

List of Abbreviations

FDAMA – Food and Drug Administration Modernization Act

PBCA – Best Pharmaceuticals for Children Act

PBPK – Physiologically-Based Pharmacokinetic

AUC – Area under the curve

Cmax – Maximum concentration

Tmax – Time at which maximum concentration has occurred

CL – Clearance

LogP – Lipophilicity

pKa – Ionization constant

fu – Fraction Unbound

K_p – Tissue to plasma partition co-efficient

Css_{tissue} – Steady state concentration of a drug in tissue

Css_{plasma} – Steady state concentration of a drug in plasma

V_T – Volume of tissue

Q_{art} – Rate of arterial blood flow

Q_{ven} – Rate of venous blood flow

C_{art} – Concentration of a compound entering systemic circulation via the arterial route

E(t) – Rate of organ specific drug elimination

V_{cell} – Volume of the cellular space

P – Compound specific membrane permeability

SA – Organ specific membrane surface area

$C_{ex-cell}$ – Concentration of drug outside the cell

C_{cell} – Concentration of drug inside the cell

IV – Intravenous

P_{int} – Intestinal permeability

V_{ss} – Volume of distribution at steady state

V_{plasma} - Physiologic volume of plasma

V_{tissue} - physiologic volume of tissue

E – Extraction ratio

CL_h – Hepatic plasma CL

CL_r – Renal plasma CL

F_a – Fraction of drug absorbed into the portal vein

F_h – Fraction of drug that bypasses the liver and reaches the portal vein

CL_{int} – Intrinsic CL

F – Oral bioavailability

TS – Tubular secretion

TR – Tubular reabsorption

GFR – Glomerular filtration rate

fe – Fraction excreted unchanged in urine

HLM – Human liver microsomes

UGT – Glucuronosyltransferase

CYP – Cytochrome P450

BCS – Biopharmaceutics Classification System

H1 – Null hypothesis 1

H2 – Null hypothesis 2

H3 – Null hypothesis 3

ACAT – Advanced Compartmental Absorption and Transit model

MW – Molecular Weight

CL_{spec} – Specific clearance

P_{int} – Transcellular intestinal permeability

ANOVA – Analysis Of Variance

FE – Fold error

AAFE - Absolute average fold error

AFE – Average fold error

RMSE – Root mean square error

SD – Standard deviation

NHANES - National Health and Nutrition Examination Survey

CV – Coefficient of variation

GET – Gastric emptying time

SITT – Small intestinal transit time

1. Introduction

An alarmingly large number of drugs prescribed to children lack dosing information specific to pediatric populations, leading to off-label dosing of many drugs in children [1]. This has the potential to lead to treatment failures, toxicities, and various other drug-related adverse events[2]. Unfortunately, conducting clinical trials in pediatric participants has many challenges both ethical and logistical [3, 4]. A recent study indicates only 46% of drug products listed in the 2009 *Physician's Desk Reference* for pediatric use, are appropriately labeled and tested for this demographic [4], and as high as 60-90% of prescribed drug products are used off-label [5, 6]. Many of these doses are based largely on adult studies with little or no pediatric experience. Lack of pediatric clinical data has led to a large gap in knowledge concerning drug efficacy, safety and dosing guidelines within the pediatric population [6].

In recognition of the lack of substantial pediatric clinical data, the Food and Drug Administration (FDA) has implemented multiple initiatives and regulations to try and close this knowledge gap. In the late 90s, the FDA Modernization Act (FDAMA) was created with the purpose of offering a monetary incentive to drug companies for performing pediatric research [7]. Companies would be offered an additional six months of patent exclusivity of their drug product as encouragement to conduct pediatric research [7]. Other significant regulations implemented include the Pediatric Rule Regulation in 1998, the Pediatric Research Equity Act in December 2003, and the Best Pharmaceuticals for Children Act (BPCA) in January 2002 which was renewed in the FDA Safety and Innovation Act (2012) [7]. The purpose of each mandate was to encourage and guide pediatric research in the USA using a combination of industry incentives and requirements.

Given that recruitment to pediatric trials is difficult, researchers have recently used physiologically-based pharmacokinetic (PBPK) models as a means to replicate pediatric clinical studies to show the potential applications of PBPK models in clinical investigation [8]. PBPK modeling and simulation is a novel *in silico* technique that may potentially aid in the prediction and estimation of pharmacokinetic (PK) parameters [2]. Fundamental PK parameters examined within clinical studies are area under the curve (AUC), maximum concentration (Cmax) and time at which Cmax has occurred (Tmax). AUC is the measure of systemic exposure of a drug over a given time interval and is a function of dose administered. Cmax and Tmax help to quantify absorption of a compound administered by non-intravenous routes. PBPK models are mechanistic in nature and mathematically describe the disposition of drugs in an organism. This *in silico* technique predicts PK profiles based on compound physicochemical properties and multiple physiological input parameters of the individual, such as organ volumes, tissue composition, blood flow, and clearance (CL) [9]. PBPK models have been previously used for prediction of human bioavailability, and extrapolation across species and within human age groups to predict human PK parameters [10]. This method has been widely adopted for toxicological risk assessment as well as in

pharmaceutical research and development [9]. Provided sufficient data, a PBPK model has the ability to generate predictions of pharmacokinetic behaviour in virtual individuals and populations, and is beneficial in aiding clinical trial planning [9]. Figure 1 illustrates an example of a whole body PBPK model, whereby each organ is represented by a compartment that is interconnected through systemic circulation. Oxygenated arterial blood is circulated throughout the organs, and subsequently ends up as venous blood which returns to the lungs for subsequent oxygenation and re-circulation [10]. Each compartment representing individual organs is defined by a tissue blood flow rate and tissue volume specific to the species of interest [11].

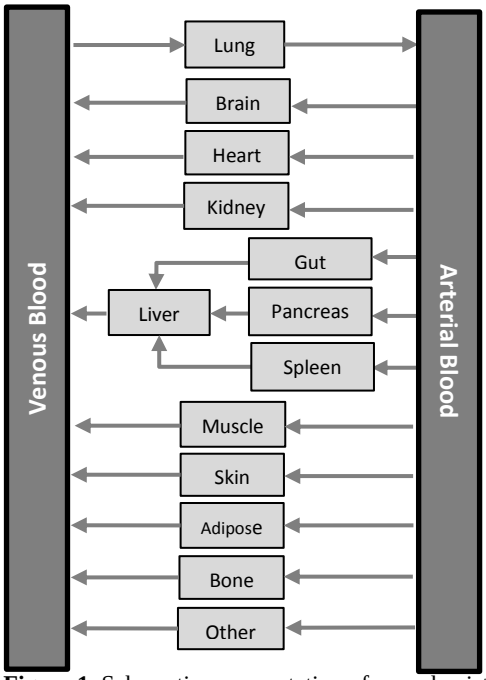

Figure 1. Schematic representation of a mechanistic whole-body PBPK model

Each compartment within the model has a respective tissue to plasma partition coefficient which depends on a compound's physicochemical properties such as lipophilicity (LogP), ionization constant (pKa), and fraction unbound (fu) of drug in plasma [10, 12]. The partition coefficient (K_p) more specifically represents the concentration of drug in tissue (Css_{tissue}) relative to plasma (Css_{plasma}) at steady state, and is defined as in equation 1:

$$K_p(tissue) = \frac{Css\,(tissue)}{Css(plasma)} \qquad (1)$$

K_ps are important input parameters for a PBPK model and they are usually derived using prediction algorithms that link drug physico-chemistry with tissue specific parameters [13]. Not only do K_p estimates aid in determining the extent of tissue specific drug exposure relative to plasma concentrations, but they can also estimate the extent of total distribution. Two of the most commonly used methods for predicting K_p in humans are the correlation-based and the tissue composition based techniques. The

correlation-based method provides a means of estimating human K_ps based on empirically derived regression equations using drug physicochemical properties relative to K_ps for muscle and adipose tissues derived experimentally in preclinical animal species [14]. The tissue composition based method for predicting K_ps is mechanistic in nature, as it relies on drug specific parameters such as protein binding, lipophilicity, and pKa as well as tissue specific parameters such as relative fractions of water, neutral lipids, phospholipids, and proteins in organs [15].

The uptake of compound into a tissue can be identified as either permeability rate limited or perfusion rate limited. Permeability rate limited conditions occur under conditions in which the permeability-surface area product (P·SA) for large polar molecules across membranes is less than blood flow, thereby creating resistance towards drug transport across membranes, irrespective of drug delivery to the tissue via perfusion. Alternatively, perfusion rate limited conditions occur typically under conditions in which the permeability-surface area product (P·SA) for small lipophilic molecules across membranes exceeds blood flow, thus organ uptake is limited primarily by blood flow. The rate of change of a total drug concentration (C_T) within an organ that is rate-limited by perfusion is defined as in equation 2:

$$\frac{dC_T}{dt} = \frac{1}{V_T}\left(Q_{art}C_{art} - Q_{ven} \cdot \frac{C_T}{f_u \cdot K_p}\right) - E(t) \qquad (2)$$

Where V_T is the volume of the tissue, Q_{art} and Q_{ven} are the rate of arterial and venous blood flow, respectively, through the tissue, C_{art} refers to the drug concentrations found in systemic plasma concentration entering via the arterial route, the overall term $\frac{C_T}{f_u \cdot K_p}$ represents venous plasma concentration where K_p is the tissue-blood partition coefficient in that tissue, fu is fraction unbound in blood, and lastly E(t) is the rate of organ specific drug elimination; in non-eliminating organs E(t) = 0 [13, 16]. Permeability rate limited kinetics are often represented by equations (3) and (4) [17]:

$$\frac{d(fu \cdot C_{cell})}{dt} \cdot V_{cell} = P \cdot SA \cdot (fu \cdot C_{ex-cell}) - P \cdot SA \cdot (fu \cdot C_{cell}) \qquad (3)$$

$$\frac{d(fu \cdot C_{ex-cell})}{dt} \cdot V_{ex-cell} = Q \cdot (fu \cdot C_{art}) - P \cdot SA \cdot (fu \cdot C_{ex-cell}) + P \cdot SA \cdot (fu \cdot C_{cell}) - Q \cdot (fu \cdot C_{ven}) \qquad (4)$$

In equation (3), $\frac{dC_{cell}}{dt}$ is the rate of change of concentration of a drug found in the cellular space, where V_{cell} is volume of the cellular space, P represents compound specific membrane permeability, SA is the organ specific membrane surface area, $(fu \cdot C_{ex-cell})$ and $(fu \cdot C_{cell})$ refer to unbound drug concentration entering and leaving the cells respectively, thus incorporating both drug and organ specific components [10, 17]. Generic PBPK models often operate under the assumption of perfusion rate limited kinetics although organ structure can be altered to account for permeability rate limitations.

Pediatric PBPK models are developed to help predict age-related changes of exposure to drugs from adults to children, when there is a lack of observed pediatric PK data [18]. These predictions can be extended to help design clinical trials that will generate relevant pediatric data for the purpose of drug labeling, and also reduce the number of children required for clinical trials [19]. The development of a pediatric PBPK model requires the model structure and inputs as described in the above paragraphs however, to be relevant in the pediatric population, the scaling of factors such as age-dependant CL, and age related body composition must be appropriately defined to effectively predict pharmacokinetic parameters [20]. Typically the creation of a pediatric PBPK model begins with the development of an adult PBPK model, as shown in Figure 2:

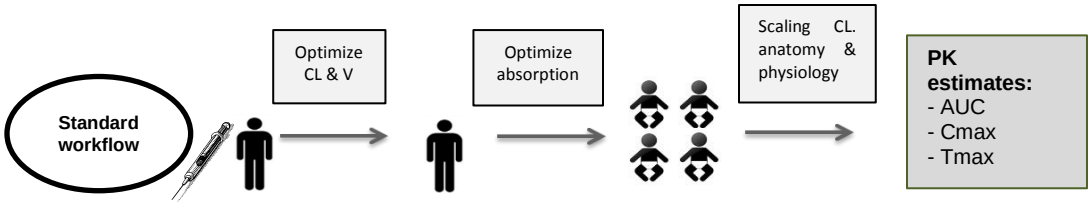

Figure 2. Standard workflow employed in the development of a PBPK model for pediatrics based on an adult IV model

Since PBPK model outcomes are only as good as the accuracy of their inputs and the underlying understanding of mechanism, inputs can be optimized and mechanisms more greatly understood with *in vivo* data, of which there exists much in the case of adults. The understanding that emerges from the development process of an adult PBPK model is carried over to the pediatric models of which there exists, usually, no *in vivo* PK information, especially in the early phases of the drug development process. The simulation process begins by gathering compound specific physicochemical data, physiological information, as well as drug CL information to develop a naïve adult PBPK model for the prediction of concentration time profiles in adults. The input of CL as well as the input of distribution, generally dominated by K_p, can be optimized by comparing the naïve prediction to the *in vivo* plasma concentration time data following intravenous (IV) administration. Once CL inputs and inputs related to the rate and extent of distribution are optimized and the simulation of IV data represents observed data, an oral profile is simulated using the optimized CL and distribution inputs. The method holds the assumption that the optimized CL and distribution parameters do not vary between routes of administration [10]. The generated adult oral PBPK model is then evaluated using observed PK data from studies conducted in adults. Optimization of absorption inputs, mainly dissolution profile and intestinal permeability (P_{int}), may be required at this stage. Once parameters have been optimized to minimize error between the experimental and simulated concentration time points, an adult population model must be created to incorporate inter-individual variability with regards to anthropometric parameters [21]. Creating a virtual adult population, will assist in the understanding of PK estimate variability within individuals of a population while incorporating demographic constraints and intrinsic enzymatic variability [21]. Once

confidence is gained that the adult PBPK and population models accurately represent various *in vivo* adult PK data, the model can be scaled to children. Any systematic deviations of simulated and observed data in adults is very likely to also manifest in the same misspecification in the pediatric model as was demonstrated by Maharaj et al using lorazepam [22]. The scaling of the model to children involves the scaling of physiological and anatomical input parameters such as organ volumes, blood flows, and ontogeny factors relating to transporters (i.e. efflux and influx), glomerular filtration rate (GFR) as well as hepatic enzymatic activity related to CL. Drug specific inputs are assumed the same between adults and children. Once all relevant inputs are scaled, pediatric IV or oral plasma concentration time profiles are generated [20].

Typically it is very important to have clinically derived adult IV data for a drug, as it is the only way to accurately derive CL and volume of distribution, given the assumption of complete absorption into systemic circulation. Volume of distribution at steady state (V_{ss}) can often be estimated from K_p values, which help identify the extent of drug distribution in each organ. The relationship between K_p and Vss is denoted in equation (5) as:

$$V_{ss} = V_{plasma} + \sum_{i=1}^{n} Kp_i \times V_{tissue,i} \times (1 - E_i) \qquad (5)$$

Where V_{plasma} and V_{tissue} are physiologic volumes of plasma and tissue, and E is the extraction ratio of the eliminating tissue [23]. V_{ss} is more specifically a metric that describes the extent of drug distribution in an individual. As a primary pharmacokinetic parameter, V_{ss} acts as foundational building block to aid in the prediction of estimating loading dose, and deriving half-life when applied in conjunction with observed CL values [24]. In the absence of adult human IV data, the optimization of distribution parameters must be completed using *in vivo* PK data from a pre-clinical species, e.g. rat. Since curve shape following IV administration is greatly affected by distribution parameters (as well as CL), and humans and rats are both mammals with assumed similar organ compositions, an assumption is made that the K_p for unbound drug distribution, the ratio of unbound drug concentration in the tissue vs. plasma, is the same between all mammalian species. In the study conducted by Jones et al., Vss in humans was predicted by assuming that the unbound K_p in human was equivalent to that in preclinical species [25]. Although the assumption holds for many tissue types of several mammals, recent literature would suggest an exception for lipid-rich tissue, wherein there exists a manifold difference of inter-species K_p measure [26]. In the absence of adult IV data, which would allow for a more confident prediction of K_p measures, an alternate workflow must rely on human K_p measures derived directly from the optimization of K_ps from IV data in preclinical (i.e. rat) species to derive an operational estimate of V using equation (5).

CL estimates are extremely important PBPK model inputs as they are the backbone for establishing dosing rates. CL is the volume of reference fluid (i.e. plasma) within a system that is completely cleared of drug over a given time interval. Multiple organs and enzymes are responsible for drug elimination such

as the gastrointestinal wall, liver, lungs, and kidneys, however total plasma CL can be derived via the addition of each unique plasma CL [27]. The two main organs responsible for CL of a drug are the kidneys and liver, a factor that must be considered when designing a PBPK model simulation. *In vivo* drug CL is typically derived from plasma concentration time profiles using equations (6) and (7) following IV and oral dose administrations, respectively:

$$CL_{IV} = \frac{Dose}{AUC_{(0\rightarrow\infty)}} \qquad (6)$$

$$CL_{oral} = \frac{Dose \cdot Fa \cdot Fh}{AUC_{(0\rightarrow\infty)}} \qquad (7)$$

Where Dose, in equation (6) is the IV dose administered and AUC is the area under the plasma concentration curve from 0 to infinity. Within equation (7), F_a and F_h are the fraction of drug absorbed into the portal vein, and the fraction of drug making it to the portal vein that is not subject to elimination by the liver, respectively [27].

Within a PBPK model framework, intrinsic CL (CL_{int}) is the CL input. For active processes where perfusion rate limits organ uptake, plasma CL and CL_{int} are correlated as described by the well-stirred model using equation (8):

$$CL_H = \frac{Q_h \cdot fu_b \cdot CL_{int}}{Q_h + fu_b \cdot CL_{int}} \qquad (8)$$

Using the liver as an example, the well stirred model is an approach that integrates total hepatic plasma CL (CL_H) with hepatic blood flow (Q_h), intrinsic CL (CL_{int}), as well as fraction of unbound drug in blood (fu_b).

Derivation of the input parameter estimates that define both plasma CL, (CL_{int}), and Vss, (K_p), is impeded by noise when oral absorption profiles are used to understand these parameters. Prediction of CL and V when IV data is unavailable is limited to CL/F and V/F where F is oral bioavailability [10]. F is the fraction of orally administered dose that is available to the systemic circulation, therefore considering the effects of both absorption and elimination via first pass metabolism [10]. As a result, the amount of drug available to systemic circulation is limited to the product of drugs escaping the intestines, liver, and lung [10]; CL and Vss are not directly knowable following an oral administration. This adds emphasis to the value clinical adult IV data contributes to the prediction accuracy of these inputs. IV data also provides a means of assessing curve shape which is a function of the rate of distribution. For instance, assumption of a perfusion limited uptake into organs may not be reasonable for larger drug molecules and this would be evident if an observed IV profile were overlaid onto a predicted profile that assumed instantaneous

mixing of organs. These modifications are integral components of the development of an adult PBPK model and, if poorly executed, will result in poor pediatric PBPK models.

The mechanistic nature of PBPK modeling allows for extrapolation of an adult PBPK model to children, based on age related differences in physiology, anatomy, as well as drug- and organism-specific properties such as CL and protein binding [18]. Once the adult IV and oral profiles have been simulated, and the PBPK model optimized and subsequently evaluated for accuracy, data must be collected from literature with respect to pediatric anatomical values for organ volumes and blood-flows [18, 28]. Parameters such as pediatric organ blood flows are generally derived from adult values while operating under the assumption that the proportion of cardiac output to the organs is similar to that in adults [18, 28]. Other input parameters such as maturation functions for hepatic and renal CL processes and age dependant protein binding would also be required [12, 18].

Scaling CL in children is largely based upon organ size and flow, fu and ontogeny of relevant processes. Fraction unbound has successfully been scaled in children by McNamara et al. and has been explained in further details within the method section of this study [29]. CL process maturation specific to hepatic and renal processes were adapted from successful methods presented by McNamara et al [30] and Rodin et al.[31] respectively, as well as Edginton et al [32]. The next step in the workflow requires the simulation of a virtual pediatric population, as described in Edginton 2010 and Maharaj et al., 2013, to allow for evaluation of variability [20-22]. The appeal of PBPK modeling is strongly based on the ability to integrate models that define the age dependence of ADME in a single platform [20]. This approach provides the means to generate an age dependant dosing regimen that may support a translational approach to pediatric trial design, as well as the potential to simulate pediatric dosing scenarios for a defined target exposure [20].

Assessing pathways of CL for a drug in the absence of IV data poses a large source of uncertainty. Having IV data and conducting a mass balance elimination study allows one to assess how much of a substance is eliminated through each route relative to an absolute administered dose. Renal CL is dependent on various physiological parameters such as renal blood flow, renal vascular resistance, as well as drug specific physicochemical factors [33]. The net balance of renal CL is a function of the physiological processes of tubular secretion (TS), tubular reabsorption (TR), and glomerular filtration rate (GFR). Total renal CL is usually derived following an IV study whereby the amount of drug excreted unchanged in urine can be quantified and divided by dose to generate the fraction excreted unchanged in urine (fe). Total plasma CL times fe is total renal CL in the case of the use of IV data and renal CL/F in the case of using data following oral administration. As a result, the oral absorption model that is used to generate F within the PBPK model is relied upon with CL being optimized based on matching AUC or terminal slope to observed data following oral administration. As such, if F is wrongly predicted, renal

CL inputs are inaccurate. The maximum renal CL due to GFR is GFR_{max} and can be calculated as defined in equation (9) below:

$$GFR_{max} = GFR \cdot f_u \qquad (9)$$

The mean GFR value used in this study was assumed to be 120 mL/min per 70kg [31]. TS cannot be measured directly, however if renal plasma CL of a substance is greater than the GFR_{max}, it is assumed that TS has occurred. Similarly, if renal plasma CL is less than GFR_{max}, it is assumed that TR has occurred and, within a PBPK model, is represented as an appropriately reduced GFR fraction input. Defining renal CL using human IV data is relatively straightforward whereas defining renal CL following oral administration is less certain. Like renal CL, hepatic CL may be quantifiable when only oral data is available, as a function of F (i.e. CL/F), but its quantification will be less certain in the absence of IV data. Hepatic plasma CL is dependent upon many factors such as liver blood flow, fu, enzymatic and various transport processes [32]. Data from a combination of published human liver microsomal (HLM), recombinant enzyme, and hepatocyte assays can be obtained to determine the extent of phase I and/or phase II metabolism on the metabolic fate of compounds [34]. Human liver microsomal assays determine the major pathway of metabolism responsible for the fate of a compound between phase I oxidative, primarily cytochrome P450 enzymes, or phase II conjugation, primarily glucuronosyltransferase (UGT) enzymes [34]. Subsequently, the application of recombinant cytochrome P450 (CYP) and UGT enzyme assays determine which specific enzyme(s), within the individual phases, are responsible for the metabolism of the parent compound. Hepatocyte assays aim to closely mimic *in vivo* conditions, as they contain all drug metabolising enzymes as well as influx/efflux transporters [34]. As a result, *in vitro* hepatocyte assays are valuable in their utility to closely approximate CL_{int} of various enzymes *in vivo*.

Although the workflow for development of the pediatric PBPK model typically follows Figure 2 [22], there are instances where an integral component is missing and may affect the predictive accuracy of the pediatric PBPK model outcome. This may be the case when an IV formulation for humans has not been developed and therefore no IV PK information is available in adults. Absence of IV adult data would result in an alternate workflow (Figure 3) where obtained CL and V inputs may be less certain. In this case, another means of assessing these inputs would be required and we suggest IV data from preclinical species, for example the rat. In a recent study, published in 2011 by Parrot et al., a group aimed to assess whether human adult and pediatric data for the prodrug oseltamivir, and its metabolite, can be scaled from marmoset monkey data [35]. This study focused on pre-clinical rat IV data due to the abundance of published rat IV data for various compounds. Pre-clinical rat IV data has been shown to effectively derive predictions in adult humans, using a PBPK modeling approach, for hepatic metabolism, renal excretion, as well as prediction of absorption and volume of distribution using tissue composition equations within 1-3 fold error for observed and predicted data [25]. If V was predicted with accuracy and only adult oral PK data were available, CL_{int} could be optimized with confidence by optimizing CL_{int} to match the

terminal phase of the *in vivo* data; a phase that is reliant only on the ratio of CL to V once absorption has been completed.

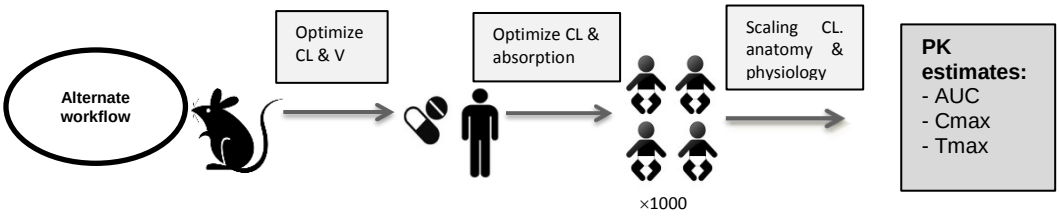

Figure 3. Alternate workflow for creating a whole-body PBPK model in pediatrics based on rat IV data as a substitute for human IV data

The biopharmaceutics classification system (BCS) is a framework for cataloguing orally administered drugs into four classes based on their magnitudes of permeability and solubility (Figure 4). The rate and extent of absorption for orally administered drug products is governed primarily by a combination of their gastrointestinal permeability, aqueous solubility, and *in vitro* dissolution profile [26]. According to the FDA, a drug product is considered "highly permeable" when the extent of absorption in an adult is ≥ 90% of the administered dose in comparison to an IV reference dose or as quantified by a mass balance study [36]. FDA guidelines also state that a drug is considered highly soluble when it is soluble in 250 mL of aqueous media between a pH range of 1-7.5 at 37 ± 1.8°C [26, 36]. BCS Class I drugs are characterized by high permeability and high solubility, thus resulting in a high rate and extent of absorption, or bioavailability. BCS Class II drugs are characterized by high permeability and low solubility. As a result, it is assumed that the oral absorption of a Class II drug product is limited by its ability to dissolve. Inverse to Class II drugs, BCS Class III drugs are highly soluble and are permeability limited throughout the gastrointestinal tract [24]. In the prediction of pediatric PK, the BCS of the target drug may influence the predictive accuracy of the pediatric PBPK model. Solubility and permeability can alter *in vivo* bioavailability or F and, since CL and V estimates in the absence of human IV data are dependent on F, the alternate workflow (Figure 3) may or may not be accurate for any BCS class other than BCS I where is F is close to 1.

	High solubility	Low solubility
High permeability	Class 1 High solubility High permeability	Class 2 Low solubility High permeability
Low permeability	Class 3 High solubility Low permeability	Class 4 Low solubility Low permeability

Figure 4. Biopharmaceutics Classification System (BCS) based on degree of compound permeability and solubility

2. Objectives & Hypotheses

Objectives

The objective of this study was to assess the ability of pediatric PBPK models, developed under Workflow 1 (Figure 3) and Workflow 2 (Figure 2), to predict observed PK parameters and to assess the implications to model accuracy when there is a lack of adult IV data.

Aim 1: To assess the ability of Workflow 1 and Workflow 2 to predict observed pediatric PK parameters.
Null hypothesis 1 (H1): Workflow 1 and Workflow 2 derived predictions of pediatric PK data will not be significantly different from observed data.

Aim 2: To determine if predictions from Workflow 1, where human IV data is not available, are equivalent to predictions from Workflow 2, where human IV data is available.
Null hypothesis 2 (H2): PK predictions from Workflow 1 will not be significantly different from Workflow 2.

Based on H1 and H2, the question of the need for human IV data will be answered using the following logic:
In the event that H1, for both workflows, and H2 are accepted, the conclusion is that human IV data is not a necessary component of the workflow for model development and models were accurate.
In the event that H1 for both workflows is accepted and H2 is rejected, the conclusion is that human IV data is not a necessary component of the workflow for model development and models were accurate.
In the even that H1 for Workflow 1 is accepted, H1 for Workflow 2 is rejected and H2 is also rejected, then we must conclude that human IV data is not a necessary component of model development.
In the event that H1 for Workflow 1 is rejected, H1 for Workflow 2 is accepted and H2 is rejected, the conclusion is that human IV data is a necessary component of the workflow for model development.
In the event that H1 for either workflow is rejected and H2 is accepted, the conclusion is that human IV data is not a necessary component of the workflow for model development and models were not accurate.
If H1 is rejected for both workflows and H2 is also rejected, then it is unknown if human IV data is a necessary component for model development.

Aim 3 To compare pediatric PK prediction accuracy using Workflow 1 vs. Workflow 2.
Null hypothesis 3 (H3): Pediatric predictions of observed data using Workflow 1 will be more accurate and less bias as compared to Workflow 2.

Aim 4: To assess how BCS level influences pediatric PBPK model accuracy.

3. Methods

3.1 Data collection

Each of nine drugs examined within this study were selected from literature and FDA summary databases for drugs that have passed the approval process in adult and pediatric populations [37, 38]. Experimentally derived *in vivo* pre-clinical and clinical study data requirements for each of the nine drugs consisted of:

1. Plasma concentration time profiles obtained from rat and adult IV studies
2. Plasma concentration time profiles obtained from adult oral studies
3. Plasma concentration time profiles obtained from pediatric IV or oral studies or PK parameters obtained from pediatric IV or oral studies including AUC, Cmax, and Tmax.

The following additional parameters were also required:

1. Molecular weight and chemical structure to evaluate presence of halogens
2. Acid dissociation constants (i.e. pKa)
3. Solubility and dissolution profile, ideally in a buffer medium representative of physiological conditions
4. Fraction unbound in plasma and binding partner (e.g. Albumin or Alpha 1-acid glycoprotein)
5. A measure of experimentally derived lipophilicity (e.g. LogP)
6. An understanding of the CL pathways and proportions of each pathway to total CL in adults.

Of the nine compounds, three are from each of BCS I, II, and III; BCS IV compounds were not considered due to their poor predictability of drug disposition in humans. Drugs pertaining to BCS I include:

1. lorazepam
2. acetaminophen
3. levofloxacin

BCS II drugs examined in this study include:

1. ciprofloxacin
2. ofloxacin
3. valsartan

Lastly, BCS class III drugs examined in this study include:

1. acyclovir
2. cimetidine
3. azithromycin

3.2 Software for PBPK model development

Key model development software programs utilized in this study were PK-Sim® (ver. 5.2, Bayer Technology Services GmbH, Leverkusen, Germany) and MoBi® (ver. 3.2, Bayer Technology Services GmbH, Leverkusen, Germany). PK-Sim® is a tool that allows the user to create whole-body physiologically based pharmacokinetic models based on anatomical and physiological parameters for humans and many common pre-clinical animal species. It consists primarily of 17 organs and tissues that further consist of sub-compartments such as red blood cells, plasma, interstitial space, and cellular space. The gastrointestinal compartment within the whole-body PBPK model is further divided using the advanced compartmental absorption and transit model (ACAT), which incorporates first pass metabolism and colonic absorption [39]. The ACAT model is employed as a method to predict the bioavailability of compounds and can include liver and gut metabolism, efflux and influx transport within the gut [39]. The versatility of the ACAT model stems from the intricate dissection of linear and non-linear metabolism kinetics, various states of compound release/uptake, and the transit flow of a drug compound throughout the several sub-divisions of the stomach, small intestine and colon [39]. Input parameters in the whole body PBPK model, ACAT inclusive, encompass physicochemical properties that are used to predict K_p, cellular permeability and intestinal permeability. CL_{int} information is a user defined input. All K_p algorithms incorporated into the PBPK models within this study follow mechanistic equations proposed by Rodgers and Rowland, 2006 [40]. MoBi® was used for parameter optimization using a 1/y weighted least squares regression function. MoBi was also implemented for population modeling which incorporates PK-Sim® models and MATLAB (version 7.0, Mathworks, MI, USA) functions for this purpose [9].

3.3 Project workflow overview

Two workflows were implemented throughout the study to assess the prediction accuracy of pediatric PK estimates derived via the standard workflow and the alternate workflow. As presented previously, Workflow 2 (Figure 2) follows the standard format [22] while Workflow 1 follows the alternate workflow, where adult IV data are missing and substituted with preclinical rat *in vivo* IV data (Figure 3). Workflow 1 was consistently simulated before Workflow 2, so as to eliminate any knowledge bias of a compound's pharmacokinetic profile in adults and children. Pediatric PK predictions for BCS class 1 compounds.

3.4 Pediatric PK predictions for BCS class 1 compounds

3.4.1 Acetaminophen

Workflow 1 of acetaminophen

Development of the Rat PBPK model following IV administration

A rat PBPK model was created for the drug acetaminophen, based on a rat IV study conducted by Watari et al. 1983 [41]. Organism specific anatomy and physiology parameters incorporated into PK-Sim, pertaining to a generic rat, were applied. Physicochemical properties such as fu in rat, pKa, molecular weight, and observed total plasma CL [41] were obtained from literature (Table 1). Three experimental plasma concentration data sets were obtained from Watari et al. 1983, each of which was dose normalized to plasma concentrations following a 1 mg/kg dose [41]. Following simulation of the rat PBPK model, experimentally derived *in vivo* data was superimposed upon the simulated plasma concentration profile [41]. Given that the simulated data points did not reflect the curve shape of the observed data, model parameters influencing distribution (e.g. LogP) and CL were numerically optimized using a Monte Carlo algorithm. The Monte Carlo algorithm randomly samples multiple iterations of designated model parameters until a global minimum is located within defined boundaries; Figure 5 presents the results of this optimization. Overall curve shape was not sensitive to LogP within a ten percent range, therefore the observed value of 0.49 was used [41] (Table 1). Total hepatic plasma CL was optimized to 52 mL/min/kg from an observed CL of 51 mL/min/kg [41]. Although CL within the rat model was not scaled to humans in subsequent models, rat plasma CL was optimized for overall goodness of fit assessment and comparison based on observed data obtained from literature.

Table 1. Acetaminophen physicochemical input parameters for the rat and adult models within Workflow 1

Initial input	Initial Value	Reference	Value in final model
Fu (rat)	0.82	[41]	0.82
Fu (human)	0.95	[42]	0.95
LogP (log units)	0.49	[42]	0.49
pKa	9.5 (acid)	[42]	9.5 (acid)
Solubility at ref pH	14.5 mg/mL (pH=7.0)	[42]	14.5 mg/mL
Dissolution profile	50% at 10 min	[43-45]	50% at 10 min

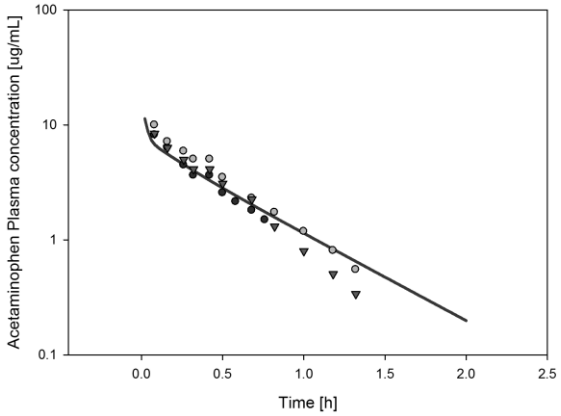

Figure 5. Simulated (line) and observed (symbols) plasma concentration data following a 1 mg/kg IV bolus administration of acetaminophen to rats. Dose normalized observed data is taken from Watari et al[41].

Development of the acetaminophen adult PBPK model following oral administration

Using the rat model as a base, all species specific inputs were changed to reflect an average 30 year old European human male. This included anatomical and physiological inputs. All drug-specific inputs were maintained as in the rat PBPK model (Table 1) with the addition of compound specific solubility and dissolution data. Three adult PBPK models were simulated, and were based upon three oral studies following a 325 mg [43], 500 mg [44] and 1000 mg [45] oral administration. A 10 minute dissolution time for each oral formulation [43-45] was also included. Observed data was superimposed upon the simulated plasma concentration time profiles for an initial visual goodness of fit assessment.

Given that the simulated data points did not fall within the range of observed data, model parameters influencing absorption (i.e. P_{int}) and total plasma CL (Table 2) were numerically optimized respective to each simulation (Figure 6a-c). An oral PK profile is regarded as 2 phases, an initial phase of drug absorption and a terminal phase dominated by elimination. The absorption phase is highly sensitive to intestinal permeability. This value is calculated by PK-Sim as a function of the input physicochemical parameters (i.e. Molecular weight, LogP) and therefore is the most uncertain parameter in the absorption component of the model. Other absorption parameters are physiological in nature (e.g. small intestinal transit time, gastric emptying time) and are less likely to be incorrect. As a result, intestinal permeability is the first parameter that is optimized. Only if this parameter is incapable of explaining observed absorption will physiological inputs be considered for optimization. In the case of the terminal phase, if Vss is accurately predicted (confidence gained from rat IV data) and absorption is over, the terminal phase of the observed data can be used to estimate CL. Due to the absence of CL information from a human IV application, matching the terminal phase of the simulated profile to observed data provides us with the greatest certainty towards estimating CL. Intestinal permeability and CL parameters were

optimized for each study (Table 2, Figure 6a-c) where, ideally, the $AUC_{0\text{-}inf}$ of the simulation is optimized to within ±10% of the corresponding observed AUC. Within the PBPK model, CL optimizations are expressed through specific CL (CL_{spec}) which is the intrinsic CL divided by the volume in which the process occurs, expressed in units of $L/min/L_{intracellular\ volume}$, or 1/min. For the final adult oral model, the arithmetic mean of each optimized parameter was used (Table 2) in all subsequent models.

Table 2. Optimized total hepatic CL_{spec}, and intestinal permeability (P_{int}) for three simulated adult oral profiles. The arithmetic mean of the three studies is presented.

Oral dose administration simulation	**P_{int} (cm/min)**	**Specific hepatic CL (CL_{spec}) optimized (1/min)**
325 mg dose [43]	1.01 E-05	0.273
500 mg dose[44]	3.49 E-04	0.389
1000 mg dose [45]	7.67 E-05	0.225
Arithmetic mean	**1.45 E-04**	**0.296**

CL pathway partitioning

Within the adult PBPK model, CL was input as a hepatic process only, as hepatic CL is the greatest proportion of overall CL. The next step was to proportion this CL into individual pathways that are responsible for acetaminophen metabolism, as determined from literature sources. The CL pathways were determined through literature searches which incorporated *in vitro* and *in vivo* data, as was done in Edginton 2006 [18]. Types of data that were sourced included mass balance data following oral administration to adults and *in vitro* studies that incorporated microsomes, recombinant microsomes and human hepatocytes. Since this section of the project workflow must operate under the assumption of an alternate workflow, any data derived from an adult human IV study could not be used to assess CL proportions.

In a mass balance study following an oral acetaminophen administration conducted by Prescott et al, 55% of total administered dose was recovered in urine as glucuronide metabolites [46]. Court et al [47] assessed *in vitro* UGT metabolism and determined that UGT 1A9 (61% of total intrinsic CL), UGT1A1 (29%) and UGT1A6 (10%) were responsible for acetaminophen glucuronidation. For the PBPK model, UGT1A9 and UGT1A1 were weighted to account for 100% of total intrinsic CL related to glucuronidation; 68% and 32% respectively [47]. In the study conducted by Prescott et al, 32% of total administered dose was recovered as a sulfonation product [46]. Adjei et al [48] determined *in vitro* that the responsible enzyme was primarily SULT1A1. Prescott et al. determined 5% of total administered dose was renally cleared [46], and 8% of total administered dose was a metabolite [46] produced primarily by CYP2E1 [49]. Prescott et al had a total recovery of acetaminophen of 93% with only 7% unchanged in feces [46]. As a result of this high bioavailability, of approximately 93%, the proportions of CL can be directly used without correction for the fraction not absorbed to systemic circulation.

Table 3 presents the CL proportions used in the adult PBPK model. Since the optimized CL was 100% hepatic, 5% of the total plasma CL was removed in order to account for fe. To achieve a 5% fe, GFR fraction was numerically optimized, due to the occurrence of TR, for each study as was total hepatic CL_{spec} (Table 4). The arithmetic mean of the three total hepatic CL_{spec} was further subdivided into one of four hepatic enzymes and their importance to overall hepatic CL is presented in Table 3. In the final model, the simulated AUC matched the observed AUC within a ±10% boundary (Figure 6). A final mean adult oral PBPK model was created and ready for population modeling and pediatric scaling.

Table 3. CL proportions for the adult oral model following oral acetaminophen administration

Pathway	**Proportion of acetaminophen CL**	**Notes and reference**
Glucuronide (UGT)	55% (0.55)	CL proportions determined by Prescott et al [46] following an oral acetaminophen administration, mass-balance study. 55% of total administered dose was glucuronide metabolites [46].
UGT 1A9	68%	Court et al [47] assessed *in vitro* UGT metabolism. UGT 1A9 (61% of total intrinsic CL), UGT1A1 (29%) and UGT1A6 (10%) were isoforms responsible for acetaminophen glucuronidation. UGT1A9 and UGT1A1 were weighted to accounted for 100% of total intrinsic CL.
UGT 1A1	32%	
Sulfonation (SULT1A1)	32% (0.32)	32% of total administered dose was sulfonation products [46]. Adjei et al [48] determined *in vitro* that the responsible enzyme was primarily SULT1A1.
Renal	5% (0.05)	5% of total administered dose was renally cleared unchanged [46].
CYP 2E1 (toxic metabolite)	8% (0.08)	8% of total administered dose was a metabolite [46] produced primarily by CYP2E1 [49].

Table 4. Optimized CL_{spec} and GFR fraction for each of three simulated profiles following oral dose administration in adults

Study group by oral dose	**Hepatic CL_{spec} (1/min)**	**GFR fraction**
325 mg dose [43]	0.172	0.19
500 mg dose[44]	0.24360	0.27
1000 mg dose [45]	0.1418	0.16
Arithmetic mean	**0.186**	**0.21**

Table 5. Relative proportions of individual pathways of CL within the adult oral model

Enzyme	**Percent contribution to overall hepatic CL (%)**	**Proportion of CL_{spec} = 0.186 1/min**
UGT1A9	39.4	0.0733
UGT1A1	18.5	0.0345
SULT1A1	33.7	0.0627
CYP2E1	8.4	0.0156

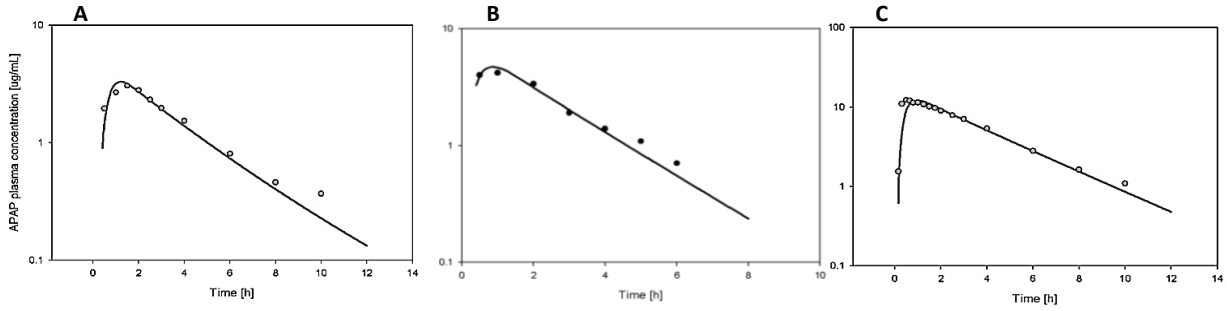

Figure 6. Simulated (line) and observed (symbols) plasma concentration data following a A) 325 mg [43] B) 500 mg [44] and C) 1000 mg [45] oral dose of acetaminophen in adults. Simulated profiles are optimized for P_{int} and CL.

Development of an adult oral population PBPK model

Inter-individual variability in drug disposition due to differences in physiology (e.g. organ volumes, organ blood flows, and CL) between study participants is important to consider. Predictive population modeling permits an *a priori* or "bottom up," speculation of the pharmacokinetic variability of a drug without conducting clinical studies beforehand. Application of a virtual population of individuals in this study serves as a surrogate to assess the correctness of inter-individual variability parameterization. This application lends itself to ensure a greater probability of deriving biologically sound PK variability estimates in children, assuming similar input variability between adults and children [21]. Virtual population generation followed the method of Willmann et al 2007 [21]. A range of body weights and heights are set by the user or constrained by realistic populations values using databases such as the National Health and Nutrition Examination Survey (NHANES) database [21]. For each virtual individual with a specific weight and height, organ weights and blood flows are assigned [21]. In order to ensure that individuals of the same weight and height are not identical, inter-individual variability of anatomical and physiological parameters is incorporated using a stochastic Monte Carlo method. The Monte Carlo algorithm randomly samples from designated model parameters with defined means, limits, and variability, based on user-defined distributions (i.e. normal, log normal, uniform). Inter-individual variability of all organ volumes and blood flows is already incorporated into PK-Sim using variability (e.g. coefficients of variation (CV) and distributions derived from literature [21]. Other inputs not varied in PK-Sim but requiring variability include those associated with the gastrointestinal tract (e.g. gastric emptying time, small intestinal transit time, small intestinal surface area) as well as CL-related variability in GFR and to account for the differences in, primarily, enzymatic protein concentration differences per gram of liver amongst different people.

For the population model of acetaminophen, 100 virtual individuals were generated within an age range of 18-55 years. In order to reflect the observed study, in which all participants were male, all virtual individuals were male. Additional variability, over and above organ volumes and blood flows, was also

included (Table 6) and followed variability estimates and distributions from literature. Once the population had been generated, the population was administered a 500 mg oral dose to reflect the study conducted by Rawlins et al [43]. The observed data obtained from Rawlins et al was superimposed onto the model predictions (Figure 7). Progression of the workflow depends on a visual check of whether or not the population model is able to encompass a significant portion of observed data (Figure 7). The standard deviation of the observed data was smaller than simulated in the terminal phase although this comparison is difficult to make as there were only 6 individuals within the observed study. Only if the number of individuals within the study is deemed high enough to accurately represent the population would the variability metrics be substantially changed. The risk of changing variability in the PBPK model based on a very small sample size is that it may or may not represent variability in another, much larger or much different, population. Methods for dealing with this are an emerging area of research. Observed data fell towards the lower limit of the population curve. This may be largely due to a potentially larger mean weight within the study population (n = 6); weights were not presented in the study. The mean weight of the simulated population was approximately 70 kg, which could be lower than the sample mean weight. Since this could not be confirmed and because the mean oral profiles for which the pediatric predictions are based were very well simulated, the model was deemed reasonable enough to move forward to pediatric prediction.

Table 6. Population variability of acetaminophen incorporated into population model simulations of acetaminophen			
Pathway	**Value**	**Distribution**	**Notes and reference**
Gastric emptying time (GET)	CV = 24%	Log normal	Gastric emptying time was obtained from Willmann 2007 [50]. GET was derived statistically in the population module of PK-Sim following normal distribution.
Small intestinal transit time (SITT)	CV = 22.5%	Log normal	Small intestinal transit time was obtained from Willmann et al. [50]. SITT was derived statistically in the population module of PK-Sim following log normal distribution.
Small intestinal surface area	9 fold variation in a uniform distribution (mean*3 – mean/3). Each individual had the same surface enhancement factor applied.	Uniform	As taken from Willmann et al [50]
GFR (specific)	CV = 25%	Normal	Determined from Van Biesen et al [51]
CYP2E1 (specific)	CV = 16 %	Log normal	CV of CYP2E1 protein activity Vmax was obtained from Bourrie et al., using human liver microsomal assays to assess protein activity and metabolite production for Aniline [52].
SULT1A1 (specific)	CV = 29%	Log normal	CV of sulfonation Vmax was obtained from Alhusainy et al. using human liver microsomal assays to assess protein activity and sulfonated metabolite production [53].
UGT1A1 (specific)	CV = 20%	Log normal	CV of glucuronidation by UGT1A1 Vmax was obtained from Borlak et al. using human liver microsomal assays to assess protein activity and glucuronide metabolite production [54]
UGT1A9 (specific)	CV = 50%	Log normal	CV of glucuronidation by UGT1A9 Vmax was obtained from Borlak et al. using human liver microsomal assays to assess protein activity and glucuronide metabolite production [54].

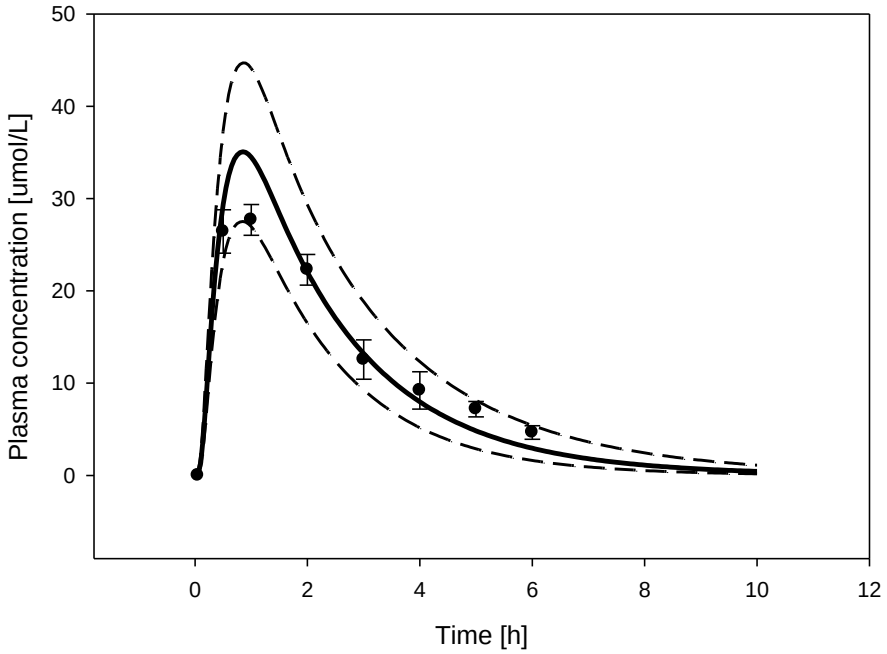

Figure 7. Simulated mean (solid line) and standard deviation (dotted lines) plasma concentration data in 100 individuals as compared to observed (symbols) mean and standard deviation plasma concentration data following a 500 mg oral dose of acetaminophen in adults Rawlins et al [43]. Observed SD has been calculated from standard error mean (SEM) reported by Rawlins et al.

Workflow 2 of acetaminophen

Development of the human PBPK model following IV administration

In contrast to the substituted nature of Workflow 1, Workflow 2 was constructed based on adult IV *in vivo* data as the base model. Similar to the development of the rat IV PBPK model in Workflow 1, the adult IV PBPK model incorporated relevant physicochemical drug data, observed mean drug CL, and dose. Since this workflow incorporates data from in-human studies, patient demographic data was also incorporated into this model. An IV PBPK model was simulated for the drug acetaminophen based on the dosing protocol from an adult IV study conducted by Rawlins et al [43]. Organism specific anatomy and physiology parameters incorporated into PK-Sim, pertaining to an average 30 year old European male were used. Physicochemical properties such as fu, lipophilicity (LogP), pKa, molecular weight, and observed total plasma CL were obtained from literature (Table 1). Once the PBPK adult IV base model had been simulated, following a 1000 mg IV dose administration, observed data was superimposed upon the simulated plasma concentration profile. Given that the simulated data points did not accurately reflect the curve shape of the observed data, model parameters influencing distribution (LogP) and CL (hepatic CL) were numerically optimized. LogP was optimized to 0.66 and the total hepatic plasma CL was optimized to 259 mL/h/kg, which resulted in a CL_{spec} of 0.316 1/min (Figure 8).

A mass balance study following IV administration was conducted by Clements et al [55]. From this study, it was determined that 4.3% of the dose was renally excreted unchanged. As a result, a renal component was added into the adult IV model. Both renal (GFR fraction) and hepatic specific CL were numerically optimized to fit observed data (Table 7; 0.194 1/min hepatic CL_{spec} and GFR fraction of 0.14). The hepatic component was further divided into the four enzymes responsible for hepatic CL (Table 7), as described in Workflow 1. Once all CL pathways had been quantified, the individual CL_{spec} values would serve as the final CL input for each subsequent model within Workflow 2.

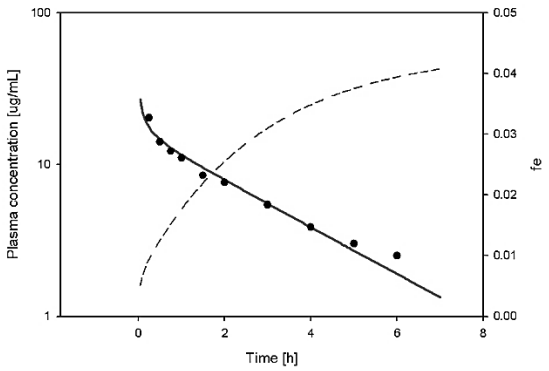

Figure 8. Simulated (line) and observed (symbols) plasma concentration data following an IV dose of acetaminophen in adults, including simulated fe (dotted line). IV profile was optimized for CL and distribution (i.e. LogP) based on data from Rawlins et al [43].

Table 7. Relative proportions of individual pathways of CL within the adult IV model in Workflow 2			
Enzyme	Percent contribution of overall CL (%)	CL_{spec} (1/min)	GFR fraction
UGT1A9	39.4	0.0703	n/a
UGT1A1	18.5	0.0299	
SULT1A1	33.7	0.0699	
CYP2E1	8.4	0.0242	
Total	**100.0**	**0.194**	**0.14**

Development of the acetaminophen adult PBPK model following oral administration

Three adult oral models were simulated following a 325 mg, 500 mg, and 1000 mg oral administration of acetaminophen respectively, similar to building the adult oral model in Workflow 1. Physicochemical input parameters such as pKa, molecular weight, optimized LogP, and optimized CL remained unchanged from the optimized adult IV model, with the addition of compound specific solubility at reference pH (Table 1). Organism specific anatomy and physiology parameters incorporated into PK-Sim, pertaining to an average 30 year old European male, were used. Once each PBPK adult oral model had been simulated, observed data [43-45] was superimposed upon the simulated plasma concentration profile. Given that the simulated data points did not fall within the range of observed data, the most uncertain model parameter influencing absorption, P_{int}, was numerically optimized respective to each simulation (Table 8, Figure 9 a-c). The arithmetic mean of the P_{int} value would serve as the final input within the adult oral model scaled to pediatrics.

Table 8. Numerically optimized P_{int} for each of three simulated profiles following oral dose administration in adults within Workflow 2	
Study group by oral dose	**P_{int} (cm/min)**
325 mg dose [43]	1.08 E-05
500 mg dose[44]	1.20 E-05
1000 mg dose [45]	1.13 E-05
Mean P_{int}	**1.13 E-05**

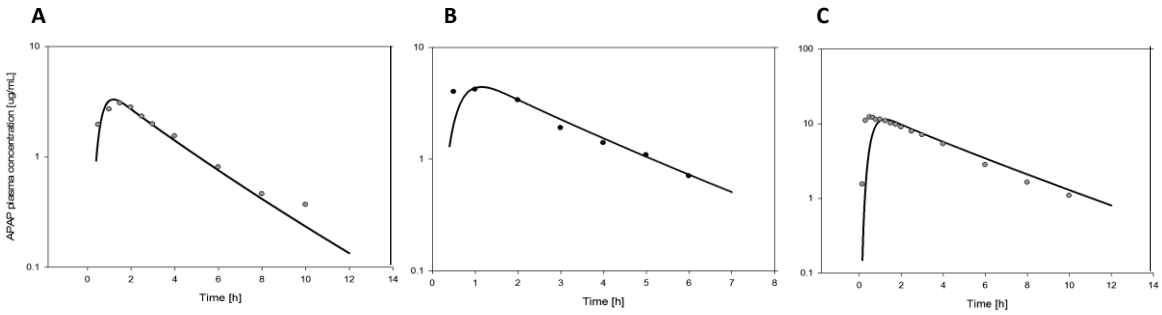

Figure 9. Simulated (line) and observed (symbols) plasma concentration data following a A) 325 mg B) 500 mg and C) 1000 mg oral dose of acetaminophen in adults, as well as simulated fe (dotted line). Simulated profiles are optimized for P_{int} and hepatic CL.

Development of an adult oral population PBPK model

Similar to Workflow 1, an adult population of 100 individuals was created within PK-Sim consisting of 18-55 year old males to reflect the demographics of the reference observed study participants [43]. The same nine aspects of population variability were factored into the adult oral model (Table 6); physicochemical and mean CL parameters remained consistent from the previous model. Once the population model had been simulated, accounting for the added variability, observed data obtained from Rawlins et al following a 500 mg oral dose was superimposed onto the model. Figure 10 presents the observed and simulated data. Observed data points fell towards the lower limit of the population curve. For similar reasons as discussed in Workflow 1, the model was deemed reasonable.

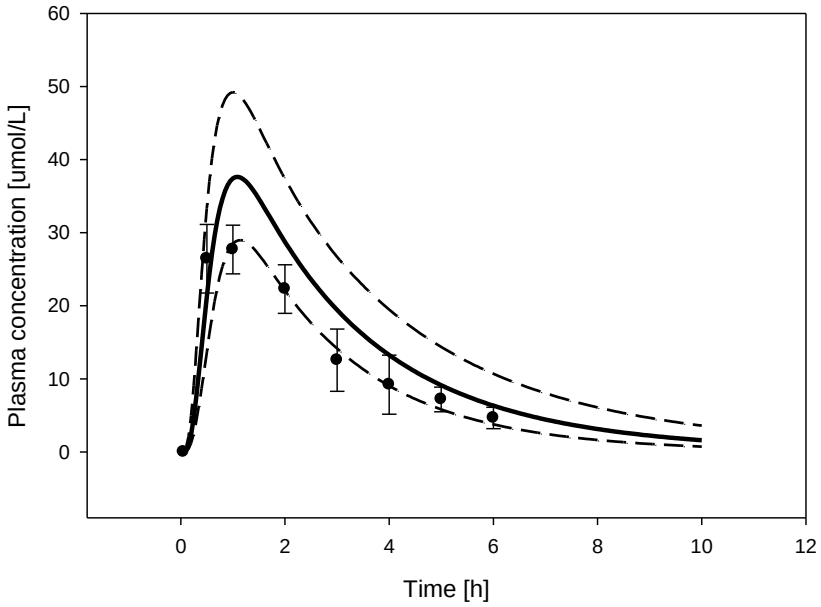

Figure 10. Simulated mean (central line) and standard deviation (dotted line) plasma concentration data in 100 individuals as compared to observed (symbols) mean and standard deviation plasma concentration data following a 500 mg oral dose of acetaminophen in adults Rawlins et al [43]. Observed SD have been calculated from standard error mean (SEM) reported by Rawlins et al.

Building the acetaminophen pediatric population model for Workflow 1 and 2

Scaling the adult oral model to children

The mean adult oral model created using either the rat IV or adult IV base models must be scaled down to pediatric populations to successfully create the pediatric PBPK model. The methods used for scaling are not dependent on the workflows used to derive the final adult oral model. As a result, scaling an adult model to a pediatric model is identical for Workflow 1 and Workflow 2. Many scaling factors from adults to children were considered.

Scaling anatomy and physiology

Age dependencies of relevant anatomical and physiological parameters (i.e. organ specific volumes, blood flows and tissue composition) were set as incorporated into PK-Sim. The values used in PK-Sim are presented in Edginton et al [18].

Scaling unbound fraction (fu)

Albumin is a highly abundant protein in plasma and interstitial fluid and it binds to a number of compounds at two distinct sites [12]. Alpha 1-acid glycoprotein is another plasma protein that binds drugs, such as lipophilic cations, and has considerable inter- and intra-patient variability in its concentration found in plasma [12]. The fraction of free drug concentration to total drug concentration is referred to as fraction unbound [12]. Predictions of fu relative to that in adults were estimated using equations presented by McNamara and Alcorn [12, 49]. Using knowledge of plasma protein binding characteristics in adults, and known age related differences in binding protein concentrations in plasma, the authors were able to successfully scale fu from adults to infant pediatric patients. The ratio of protein concentration in a child relative to adult serum albumin concentration [12], to a maximum of 100%, is:

$$level\ (\%\ of\ adult) = 0.005627 * Days + 76.7 \qquad (10)$$

The ratio of protein concentration in a child relative to adult glycoprotein concentration is:

$$level\ (\%\ of\ adult) = 0.01137 * Days + 53.4 \qquad (11)$$

This equation is represented by the variable $\frac{Pinf}{P\ adult}$ in the following equation for fraction unbound in infants relative to that in adults [12]:

$$fu, \text{inf} = \frac{1}{1+\frac{Pinf\ \ (1-fu,adult)}{Padult\ \ \ fu,adult}} \qquad (12)$$

Equation (12) is used to scale unbound fraction in adults to children of different ages during pediatric PBPK model development [12]. As plasma protein levels in infants begin to stabilize to adult levels, equation (10) and (11) begin to approach a ratio of 1; a maximum value of 1 was incorporated into the model. Knowledge of the binding partner and binding capacity in adults ($f_{up,\ adult}$) was determined from literature.

Scaling CL

Physiology-based CL scaling significantly relied upon methods from Edginton et al, 2006 [32]. For the purposes of scaling CL, it must be known how the drug is cleared in adults and the relative proportion of total plasma CL that is attributed to each pathway. This is because each pathway is scaled individually as each pathway has a unique maturation function. CL scaling operates under the assumption that CL pathways are the same in children as they are in adults, enzyme kinetics operates within the linear range, and well stirred model conditions apply.

Scaling Renal CL

Glomerular filtration rate is a measure of renal function in adults. Mature adult GFR values are well understood to be approximately 100-120mL/min. In children, Rhodin et al [31] quantified GFR maturation taking into account changes in both size and age. The model generated by Rhodin et al, defines GFR, in equation (13), as:

$$GFR = F(pma) \times F(size) \times GFR(mat) \qquad (13)$$

GFR (mat) is the mature value for GFR (mL/min). F(size) refers to allometric scaling for body size while incorporating weight of the *i*th individual (Wi), weight of a standard individual (W_{std} = 70kg), and an allometric power exponent of 0.75 (Pwr), which is denoted by equation (14):

$$F_{size} = \left(\frac{Wi}{W_{std}}\right)^{pwr} \qquad (14)$$

F(pma) in equation (13) denotes a sigmoid hyperbolic model that takes into account maturation half time (TM50), Hill coefficient, and Post Menstrual Age (pma) in weeks, to which 40 weeks was applied as the gestational time[31].

$$F_{pma} = \frac{PMA^{Hill}}{TM_{50}^{Hill} + PMA^{Hill}} \qquad (15)$$

In the pediatric PBPK model, adult GFR was scaled towards the estimated GFR of pediatric patients using the following equation (16) as proposed by Edginton et al, [32] in combination with Rhodin et al., [31]:

$$CL_{GFR(child)} = \frac{GFR_{child}}{GFR_{adult}} \times \frac{f_{u,p(child)}}{f_{u,p(adult)}} \times CL_{GFR,adult} \qquad (16)$$

TS in adults was scaled to pediatric patients by incorporating the effects of age and body weight on maturation and growth using the following equation (17) as proposed by Hayton, 2000[33]:

$$TS_{age,weight} = a * W^b e^{-k_{mat} * age} + cW^b(1 - e^{-k_{mat} * age}) \qquad (17)$$

Where W is body weight, b is body weight exponent, k_{mat} is the maturation rate constant, a and c refer to immature values of TS from birth, and mature values of TS based on influences of allometry and age as discussed in Hayton, 2000 [33].

Scaling Hepatic CL

The scaling of hepatic plasma CL from adults to children takes into account physiological factors such as organ size and blood flow, fu and ontogeny factors for hepatic enzymes that modify CL_{int}, and follows a perfusion rate limited model. Within the PBPK model framework, organ size, organ blood flow and fu are already considered. The perfusion rate limited model assumes instantaneous, well-stirred, drug

distribution across membranes into single compartment organs, whereas an added permeability rate limitation would introduce a far more complex multi-compartmental organ structure into the model [56]. Ontogeny factors for enzymes requires input if pediatric predictions of CL are to be made. An example will be demonstrated with UGT2B7, one of the most extensively studied glucuronidation enzymes in humans and a pathway of CL for acetaminophen. It is estimated that UGT2B7 enzyme activity reaches adult activity by 1 year of age in infants [57]. Intrinsic CL in adults (e.g. L/min/gram liver tissue) can be scaled to pediatric subjects using the equation [57]:

$$CL_{int\ UGT2B7_{(child)}} = OSF_{UGT2B7} \times CL_{int\ UGT2B7_{(adult)}} \quad (18)$$

where $CL_{int\ UGT2B7_{(child)}}$ is the intrinsic CL due to UGT2B7 scaled to children, $CL_{int\ UGT2B7_{(adult)}}$ is intrinsic CL due to UGT2B7 in adults, and OSF_{UGT2B7} is the Ontogeny Scaling Factor specific to age [57]. Intrinsic CL values specific to pediatric populations are directly incorporated into the PBPK model for each child while model parameters accounting for physiological and anatomical changes are already incorporated.

Population Derivation

Creation of pediatric populations was closely based on the algorithm and methods of Willmann et al, 2007 [21] as discussed previously. A reference pediatric population of 5000 individuals between the ages of 0-17 years, inclusive, was produced under a uniform distribution with a uniform distribution in each month of age within that range. Each child within the virtual population had parameter values scaled for age, with the starting point being the final mean adult male previously created from either Workflow 1 or Workflow 2. Virtual populations consisted of up to a maximum of 1000 kids isolated from the reference population to reflect patients within the age range established in the *in vivo* study being replicated. Age groups were uniformly distributed among a maximum of 1000 children depending on the lowest age denomination of the youngest patient defined in the study. For example, if a study is conducted among 20 children from 2 months to 17 years of age (204 months), the virtual population of up to a maximum of 1000 children in the virtual population were uniformly distributed from 2 months to 204 months of age, so as to allow a unbiased platform (e.g. equal year distribution would create a population of 0-1 year olds that have fewer children than all other years). Although we delineate a uniform distribution of age within the virtual population, this may not necessarily equate identically to the distribution of ages within the observed *in vivo* study. Due to ethical and logistical constraints and limitations of clinical studies, it is not always possible to have a uniform distribution of age groups within the sample population, which may make sample resolutions for statistical inferences difficult. The output from the pediatric population PBPK model was the same as that in the *in vivo* pediatric study to ensure comparisons can be made (e.g. AUC, Cmax).

Development of the pediatric population model for Workflow 1 and 2 of acetaminophen

A pediatric population of up to a maximum of 1000 individuals between the ages of 0.9-13 years, inclusive, was isolated from the reference pediatric population for acetaminophen. Drug-specific parameters were equal to those of the final adult oral acetaminophen simulation. Similar to methods discussed in section 1.4, nine aspects of population variability specific to pediatrics were factored into the pediatric population model, as obtained from literature (Table 9). Contrary to variability parameters incorporated into the adult population model, Table 9 includes gastric emptying time (GET), and small intestinal transit time (SITT) variability specific to pediatrics as obtained from Willmann et al [58], and was applied as such to each subsequent pediatric population simulation within this study. Once variability had been successfully incorporated into the pediatric population PK parameters of $AUC_{0\text{-}inf}$, Cmax, and Tmax following the observed study protocol dosing regimen were obtained for comparison to observed values for prediction accuracy assessment.

Table 9. Pediatric inter-individual variability factors applied to the pediatric population of acetaminophen

Pathway	**Value**	**Distribution**	**Notes and reference**
GET	CV % = 60%	Log normal	Gastric emptying time (GET) in the fasted state was obtained from Willmann et al [58], as derived from *in vitro* experiments.
SITT	CV = 60%	Log normal	Small intestinal transit time (SITT) was obtained from Willmann et al. [58], as derived from *in vitro* experiments.
Small intestinal surface area	9 fold variation in a uniform distribution (mean*3 – mean/3). Each individual had the same surface enhancement factor applied.	Uniform	As taken from Willmann et al [50]
GFR (specific)	CV = 25%	Normal	Determined from Van Biesen et al [51]
CYP2E1 (specific)	CV = 16 %	Log normal	CV of CYP2E1 protein activity Vmax was obtained from Bourrie et al., using human liver microsomal assays to assess protein activity and metabolite production for Aniline [52].
SULT1A1 (specific)	CV = 29%	Log normal	CV of sulfonation Vmax was obtained from Alhusainy et al. using human liver microsomal assays to assess protein activity and sulfonated metabolite production [53].
UGT1A1 (specific)	CV = 20%	Log normal	CV of glucuronidation by ugt1A1 Vmax was obtained from Borlak et al. using human liver microsomal assays to assess protein activity and glucuronide metabolite production [54].
UGT1A9 (specific)	CV = 50%	Log normal	CV of glucuronidation by ugt1A9 Vmax was obtained from Borlak et al. using human liver microsomal assays to assess protein activity and glucuronide metabolite production [54].

3.4.2 Levofloxacin

Workflow 1 of levofloxacin

Development of the rat PBPK model following IV administration

A rat PBPK model was created for the drug levofloxacin, based on a rat IV study (20 mg/kg) conducted by Fujieda et al [59]. Organism specific anatomy and physiology parameters, of a generic rat, were used. Physicochemical properties such as fu in rat, LogP, pKa, and molecular weight were obtained from various sources within literature (Table 10). Following simulation of the rat PBPK model, experimentally derived *in vivo* data was superimposed upon the simulated plasma concentration profile. Given that the simulated data points did not reflect the curve shape of the observed data, model parameters influencing distribution and CL were numerically optimized (Figure 11). The optimal LogP was 1.8, and plasma CL was optimized to a CL_{spec} value of 5.95 1/min (Table 10).

Table 10. Levofloxacin initial input, and optimized final model parameterization for Workflow 1 and Workflow 2

Initial input	Initial Value	Reference	Value in final model
fu (rat)	0.84	[60]	0.84
Fu (human)	0.7	[60]	0.7
LogP (experimental)	1.49	[61]	1.8
Molecular weight	370.4	[60]	370.4
pKa	5.5 (acid) 8.0 (base)	[61]	5.5 (acid) 8.0 (base)
Solubility	300 mg/ml at 6.5pH	[62]	300 mg/ml at 6.5pH
Dissolution	50% dissolved in 10 min	[61]	50% dissolved in 10 min

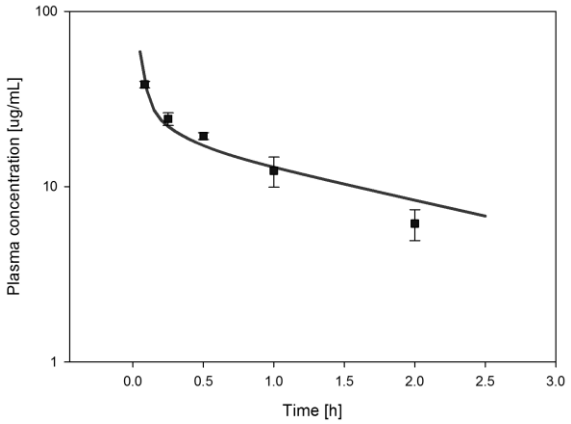

Figure 11. Simulated (line) and observed (symbols) plasma concentration data following 20 mg/kg levofloxacin to rats. Observed data was taken from Fujieda et al [59].

Development of the levofloxacin adult PBPK model following oral administration

Using the rat PBPK model as a base, all drug specific physicochemical input parameters such as pKa, molecular weight, and solubility at reference pH, and optimized LogP were maintained as in the optimized rat PBPK model (Table 10). Species specific inputs such as fu of levofloxacin in humans, anatomy, physiology as well as formulation solubility and dissolution parameters were applied to the model [60, 61]. Three experimental studies were obtained from literature, in which a sample group of participants were administered oral doses of 500, 750, and 1000 mg of levofloxacin [63, 64]. Since levofloxacin displays dose independent linear kinetics, plasma concentration data obtained from each study was dose-normalized to 500 mg [65]. Observed data was superimposed upon the simulated plasma concentration time profiles following 500 mg of levofloxacin, for an initial visual goodness of fit assessment. Given that the simulated data points did not fall within the range of observed data, model parameters influencing absorption (P_{int}) (Table 11) and total plasma CL were numerically optimized respective to each simulation (Figure 12a-c).

CL pathway partitioning

Within the initial adult PBPK model, CL input was compartmentalized as a superficial hepatic and renal component. The next step was to proportion this CL into individual pathways that are responsible for levofloxacin metabolism, as determined from mass balance studies [65]. Literature suggests 80% of oral levofloxacin is excreted via the urine unchanged, whereas >5% of the dose is recovered in urine as glucuronidated metabolite [65]. Experimentally, total renal CL was found to be greater than GFR_{max}, thereby indicating that a significant portion of levofloxacin is eliminated via active TS by renal transporters. GFR fraction was set to a maximum ratio of 1, and an additional TS component was added to the adult PBPK model in place of an overall renal plasma CL. The isoforms primarily responsible for the glucuronidation of levofloxacin are UGT1A1, UGT1A3, and UGT1A9; however *in vitro* studies show that *in vivo* glucuronidation of levofloxacin is mainly due to UGT1A1 [66]. As a result, UGT1A1 was considered the only glucuronidation enzyme responsible for levofloxacin metabolism. Once CL pathways had been defined within the model, UGT1A1 activity and TS were numerically optimized so that fe approximately reflected observed values (0.80) (Table 11, Figure 12 a-c). The final mean adult model was utilized for the subsequent adult population model.

Table 11. Numerically optimized P_{int}, TS and UGT1A1 parameters for the oral model of levofloxacin			
Study group dosing before dose normalization (mg)	**P_{int} (cm/min)**	**TS CL_{spec} (1/h)**	**UGT1A1 CL_{spec} (1/min)**
500 [63]	3.23 E-05	0.247	0.00377
750 [64]	1.17 E-05	0.251	0.00383
1000 [64]	0.93 E-05	0.265	0.0038
Mean	**1.77 E-05**	**0.255**	**0.0038**

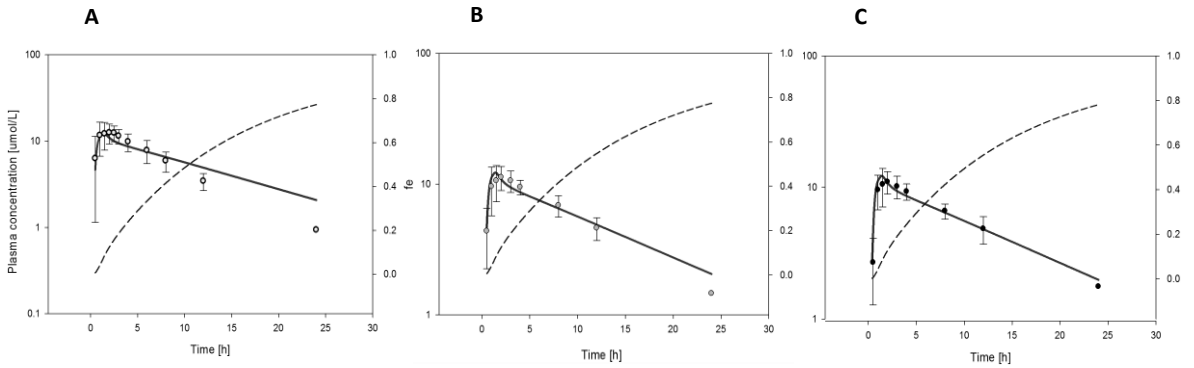

Figure 12. Simulated (line) and observed (symbols) plasma concentration profiles, and fe (dotted line) for a 500 mg oral levofloxacin administration. B) and C) have been dose normalized from 750 mg and 1000 mg respectively. All graphs were optimized for CL and P_{int}.

Development of the adult oral population PBPK model for levofloxacin

For the population model for levofloxacin, 100 virtual individuals were generated within an age range of 18-55 years. Additional variability was also included (Table 12) and followed variability estimates and distributions from literature. Six aspects of population variability were factored into the adult population model (Table 12), four of which were similarly incorporated within the acetaminophen model. Physicochemical parameters were not further modified from the optimized adult PBPK model. Once the population model had been simulated to generate an arithmetic standard deviation curve, observed data obtained from each of the experimental observed studies was superimposed onto the model [63] [64] (Figure 12). Given that a majority of observed data points fell within one standard deviation of the mean population simulation, the model was deemed sufficient to move forward to pediatric predictions.

Table 12. Population variability incorporated into the adult population model simulations in PK-Sim and MoBi for levofloxacin			
Pathway	**Value**	**Distribution**	**Notes and reference**
GET	CV = 24%	Log normal	Table 6
SITT	CV = 22.5%	Log normal	Table 6
Small intestinal surface area	9 fold variation in a uniform distribution (mean*3 – mean/3). Each individual had the same surface enhancement factor applied.	Uniform	Table 6
GFR (specific)	CV = 25%	Normal	Table 6
TS (specific)	CV = 30	Log normal	Determined Willmann et al., 2014, following log normal distribution [15].
UGT1A1 (specific)	CV = 20%	Log normal	CV of glucuronidation by ugt1A1 Vmax was obtained from Borlak et al. using human liver microsomal assays to assess protein activity and glucuronide metabolite production [54]

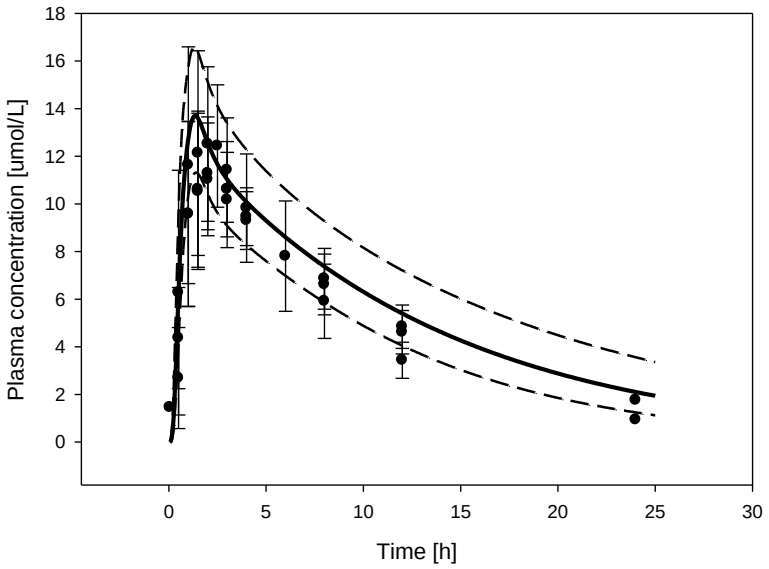

Figure 13. Simulated mean (central line) and standard deviation (dotted line) plasma concentration data in 100 individuals as compared to observed (symbols) mean and standard deviation plasma concentration data following a 500 mg oral dose of levofloxacin [61]

Workflow 2 of levofloxacin

Development of the human PBPK model following IV administration

An adult IV PBPK model was simulated for the drug levofloxacin based on the dosing protocol from an IV infusion study conducted in adults by Chien et al, in which 500 mg of levofloxacin was administered over a 1 hour period to 10 adults between the ages of 18-55 years [63]. Similar to the development of the rat PBPK model in Workflow 1, the adult IV PBPK model incorporated relevant organism, and drug specific physicochemical parameters (Table 10). Since the standard workflow incorporates data from human studies, patient demographic data was also incorporated into this model. Model parameters influencing distribution (LogP) and CL were numerically optimized.

Clearance pathways were derived based on a mass balance study, conducted by Fish et al, following an IV dose of levofloxacin to healthy volunteers [67]. Within the study, it was observed that 80-87% of the dose was recovered unchanged in urine, with approximately 5-10% of the dose recovered as glucuronidated metabolites of levofloxacin [67]. Within the model, renal CL was partitioned into GFR and TS since total renal CL of levofloxacin exceeded GFR_{max}. Hepatic metabolism and TS were optimized. As presented in Figure 14, LogP was numerically optimized to 1.78, TS and UGT1A1 were optimized to reflect observed fe (0.8-0.87) (Figure 14).

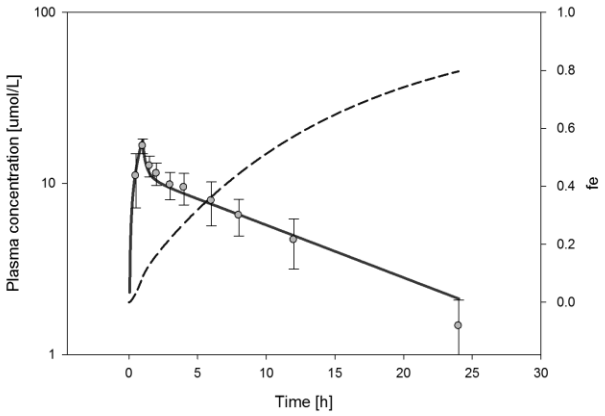

Figure 14. Simulated (line) and observed (symbols) plasma concentration data following a 500 mg IV infusion of levofloxacin in adults, including simulated fe (dotted line). IV profile was optimized for CL and distribution (i.e. LogP) Based on data from Chien et al [64]. Adult IV model optimized for LogP and CL.

Development of the levofloxacin adult PBPK model following oral administration

Three adult oral models were simulated following an oral dose of 500 mg levofloxacin, similar to building the adult oral PBPK model in Workflow 1. Physicochemical input parameters such as pKa, molecular weight, optimized LogP, and optimized CL remained unchanged from the optimized adult IV model, with the addition of compound specific solubility at reference pH (Table 10). Organism specific

anatomy and physiology parameters incorporated into PK-Sim, pertaining to an average 30 year old European male, were used. Once each PBPK adult oral model had been simulated, observed data [63, 64] was superimposed upon the simulated plasma concentration profile. P_{int} was numerically optimized respective to each simulation (Table 13, Figure 15 a-c). The arithmetic mean P_{int} value would serve as the final input within the adult oral model scaled to pediatrics.

Table 13. Numerically optimized P_{int}, TS, UGT1A1 CL_{spec}, LogP for the adult PBPK model of levofloxacin within the standard workflow

Study group dosing before dose normalization (mg)	**P_{int} (cm/min)**	**TS CL_{spec} (1/min)**	**UGT1A1 CL_{spec} (1/min)**	**LogP (log units)**
500 mg IV [63]		0.232	0.004	1.78
500 [63]	1.4 E-05			
750 [64]	1.1 E-05			
1000 [64]	1.2 E-05			
Mean	**1.23 E-05**			

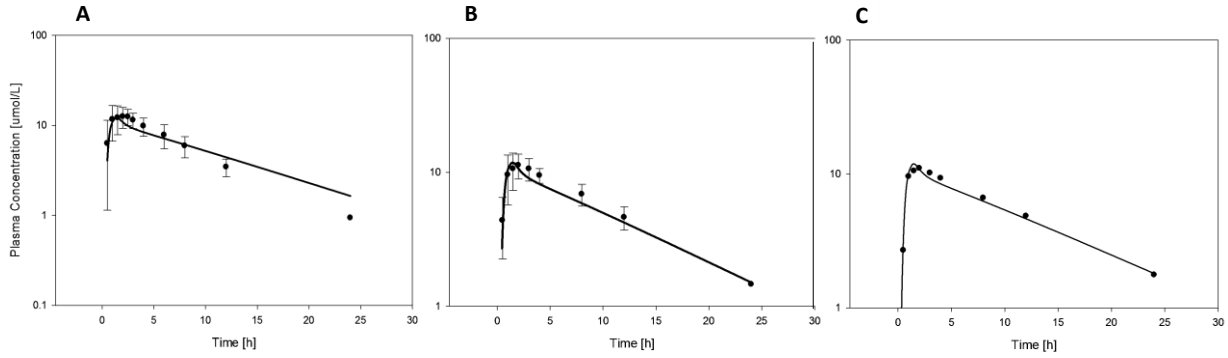

Figure 15. Simulated (line) and observed (symbols) plasma concentration profiles of 500 mg [63] oral levofloxacin. B) and C) have been dose normalized from 750 mg [64] and 1000 mg [64] respectively. All graphs were optimized for CL and P_{int}.

Development of an adult oral population PBPK model

An adult population of 100 individuals was created within PK-Sim consisting of 18-55 year old males to reflect the demographics of the reference observed study participants [63, 64]. Since CL pathways were different between workflows, the same seven aspects of population variability from Workflow 1 were factored into the Workflow 2 adult population model as obtained from literature (Table 12). Once the population model had been simulated to generate an arithmetic standard deviation curve, observed data obtained from each of the experimental observed studies was superimposed onto the model (Figure 16). Given that the majority of data points fell within one standard deviation of the mean population model, it was determined sufficient to progress to pediatric development.

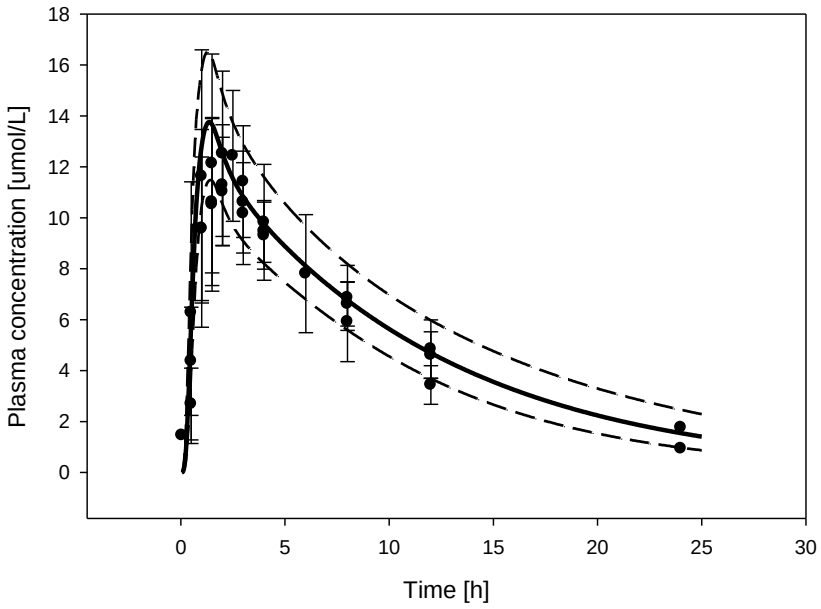

Figure 16. Simulated mean (central line) and standard deviation (dotted line) plasma concentration data in 100 individuals as compared to observed (symbols) mean and standard deviation plasma concentration data following data following a 500 mg oral dose of levofloxacin in adults

Development of the pediatric population model for Workflow 1 and 2 of levofloxacin

A pediatric study investigating the pharmacokinetics of levofloxacin in infants and children between the ages of 0.5-16 years was obtained from literature [68]. In the study, patients received a 7mg/kg dose to a maximum of, of oral levofloxacin (n = 8), and were subdivided into five groups based upon age. A pediatric population of up to a maximum of 1000 individuals between the ages of 0.5-16 years, inclusive, were isolated from the reference pediatric population to reflect the demographic of the observed pediatric study [68]. Similar to methods discussed previously, once population variability was included in the model, PK data was simulated for each child following the observed study protocol dosing regimen.

3.4.3 Lorazepam

Workflow 1 of lorazepam

Development of the rat PBPK model following IV administration

A rat PBPK model was created for the drug lorazepam, based on a rat IV study conducted by Atack et al. Three observed data sets were obtained from Atack et al, each of which wad dose normalized to a 0.05 mg/kg IV dose [69]. Observed data was dose normalized to reflect a 0.05 mg/kg IV dose of lorazepam. Organism specific anatomy and physiology parameters, of a generic rat, were used. Physicochemical properties such as fu in rat, LogP, pKa, and molecular weight were obtained from various sources within literature (Table 14). Following simulation of the rat PBPK model, experimentally derived *in vivo* data was superimposed upon the simulated plasma concentration profile. Given that the simulated data points did not reflect the curve shape of the observed data, model parameters influencing distribution and CL were numerically optimized (Figure 17); the optimal LogP was 2.6.

Table 14. Lorazepam initial input, and optimized final model parameterization for Workflow 1 and Workflow 2

Initial input	Initial Value	Reference	Value in final model
fu (rat)	0.091	[69]	0.091
fu (human)	0.11	[70]	0.11
LogP (experimental)	2.39	[71]	2.6
Molecular weight	321.16	[72]	321.16
pKa	1.3 (acid), 11.5 (base)	[72]	1.3 (acid), 11.5 (base)
Solubility	0.08 mg/ml	[70]	0.08 mg/ml
Dissolution	50% dissolved in 20 min	[73]	50% dissolved in 20 min

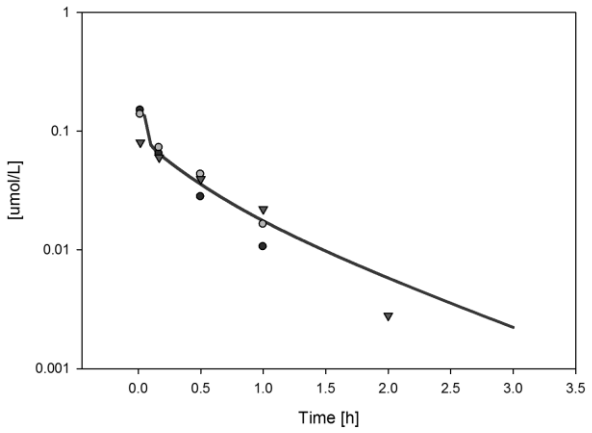

Figure 17. Simulated (line) and observed (symbols) plasma concentration data following 0.05 mg/kg mg lorazepam to rats. Observed data was taken from Atack et al[69]

Development of the lorazepam adult PBPK model following oral administration

Using the rat PBPK model as a base, all drug specific physicochemical input parameters such as pKa, molecular weight, and solubility at reference pH, and optimized LogP were maintained as in the optimized rat PBPK model. Species specific inputs such as fu of lorazepam in humans, anatomy, physiology as well as formulation solubility and dissolution parameters were applied to the model [70] [73]. Three experimental studies were obtained from literature, which were all dose normalized to reflect a 1.5 mg oral dose, due to dose dependant linear kinetics of lorazepam [74]. Observed data was superimposed upon the simulated plasma concentration time profiles following 1.5 mg of lorazepam, for an initial visual goodness of fit assessment. Given that the simulated data points did not fall within the range of observed data, model parameters influencing absorption (i.e. transcellular intestinal permeability) and total hepatic plasma CL were numerically optimized respective to each simulation (Table 15,Figure 18a-c).

CL pathway partitioning

Within the initial adult PBPK model, CL input was compartmentalized as superficial hepatic CL. In a mass balance study following oral administration of lorazepam conducted by Greenblatt et al, approximately 75-82% of total administered dose was excreted as a glucuronide metabolite, and less than 0.5% was excreted as unchanged parent compound [74]. *In vitro* studies suggest hepatic metabolism of lorazepam is primarily facilitated by hepatic UGT2B7 [75]. Due to the very low fe, CL was completely partitioned into hepatic UGT2B7 CL within the model. Once CL pathways had been defined within the model, UGT2B7 activity was optimized Table 15. Figures remained unchanged.

Table 15. Mean optimized P_{int} and hepatic UGT2B7 CL_{spec}

Study dosing before dose normalization (mg)	**P_{int} (cm/min)**	**UGT2B7 CL_{spec} (1/min)**
2 [74]	6.80 E-06	0.16
3 [74]	8.20 E-06	0.23
1.5 [74]	7.68 E-06	0.28
Arithmetic mean	**7.56 E-06**	**0.22**

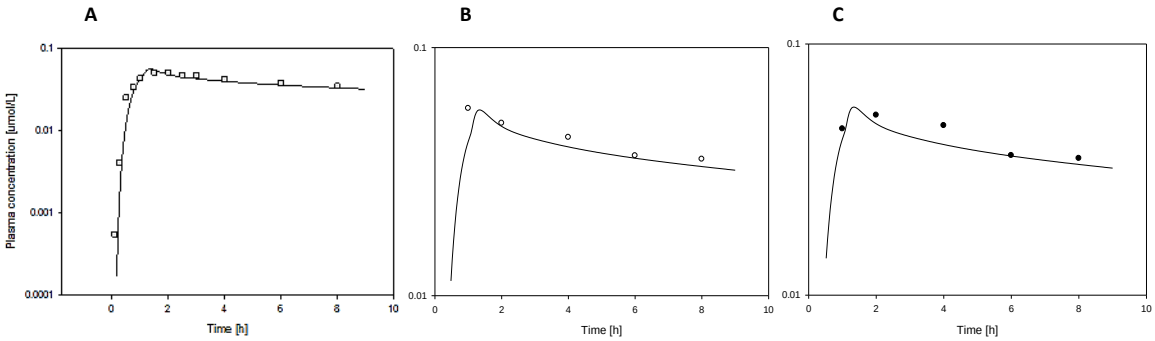

Figure 18. Simulated (line) and observed (symbols) plasma concentration profiles of 1.5 mg oral lorazepam. A-C have been dose normalized to reflect a 1.5 mg dose. All graphs were optimized for P_{int} and total CL

Development of the adult oral population PBPK model for lorazepam

For the population model of lorazepam, 100 virtual individuals were generated within an age range of 18-55 years. Additional variability was also included into the adult population model, with respect to UGT2B7 (Table 16). Physicochemical parameters were not further modified from the optimized adult PBPK model. Once the population model had been simulated to generate an arithmetic standard deviation curve, Observed data obtained from each observed study was superimposed on the model. Given that the majority of observed data points sufficiently fell within on standard deviation of the mean population simulation, the model was deemed adequate to more forward to pediatric predictions.

Table 16. Population variability incorporated into the adult population model simulations in PK-Sim for lorazepam

Pathway	**Value**	**Distribution**	**Notes and reference**
GET	CV % = 24%	Log normal	Table 6
SITT	CV = 22.5%	Log normal	Table 6
Small intestinal surface area	9 fold variation in a uniform distribution (mean*3 – mean/3). Each individual had the same surface enhancement factor applied.	Uniform	Table 6
UGTB7 (specific)	CV = 35%	Log normal	CV of glucuronidation by UGT2B7 Vmax was obtained from Upichat et al. using human liver microsomal assays to assess protein activity and glucuronide metabolite production [76]

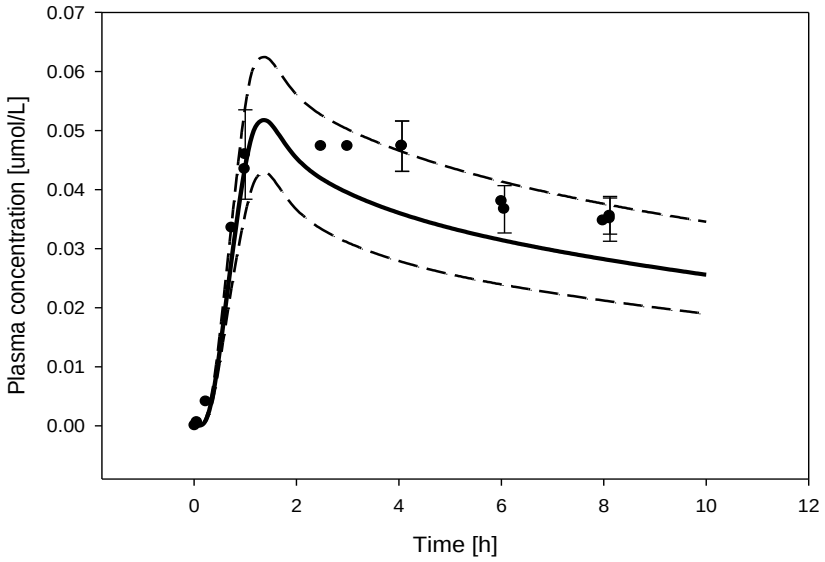

Figure 19. Simulated mean (central line) and standard deviation (dotted line) plasma concentration data in 100 individuals as compared to observed (symbols) mean and standard deviation plasma concentration data following a 1.5 mg oral dose of lorazepam

Workflow 2 of lorazepam

Development of the human PBPK model following IV administration

An adult IV PBPK model was simulated for the drug lorazepam based on the dosing protocol from an IV infusion study conducted in adults by Greenblatt et al, in which 2 mg of lorazepam was administered as an IV bolus [74]. Similar to the development of the rat PBPK model in Workflow 1, the adult IV PBPK model incorporated relevant organism, and drug specific physicochemical parameters (Table 10). Additionally, since this workflow incorporates data from in-human studies, patient demographic data was also incorporated into this model. Model parameters influencing distribution (LogP) and CL were numerically optimized (Table 17, Figure 20).

Clearance pathways were derived based on a mass balance study conducted by Greenblatt et al, following an IV dose of levofloxacin to healthy volunteers [74]. Within the study, it was observed that approximately 85-90% of the dose was recovered as a glucuronidated metabolite in the urine, with less than 0.5% of the dose recovered unchanged in urine. Within the model, CL was completely partitioned into hepatic UGT2B7 metabolism.

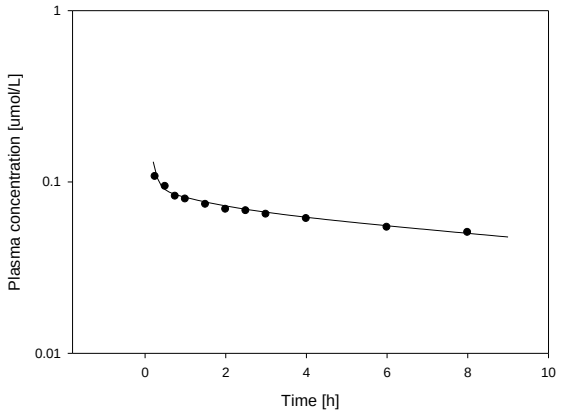

Figure 20. Simulated (line) and observed (symbols) plasma concentration data following a 2 mg IV bolus dose of levofloxacin in adults. IV profile was optimized for CL and distribution (i.e. LogP) Based on data from Greenblatt et al [74]

Development of the levofloxacin adult PBPK model following oral administration

Three adult oral models were simulated following an oral dose of 1.5 mg lorazepam, similar to building the adult oral PBPK model in Workflow 1. Physicochemical input parameters such as pKa, molecular weight, optimized LogP, and optimized CL remained unchanged from the optimized adult IV model, with the addition of compound specific solubility at reference pH. Organism specific anatomy and physiology parameters incorporated into PK-Sim, pertaining to an average 30 year old European male, were used. Once each PBPK adult oral model had been simulated, observed data [74] was superimposed upon the simulated plasma concentration profiles. P_{int} was numerically optimized respective to each simulation

(Table 17, Figure 21a-c). The arithmetic mean P_{int} value would serve as the final input within the adult oral model scaled to pediatrics.

Table 17. Numerically optimized P_{int}, LogP, UGT2B7 CL_{spec} for the standard workflow of lorazepam

Study dosing before dose normalization (mg)	**P_{int} (cm/min)**	**UGT2B7 CL_{spec} (1/min)**	**LogP (log units)**
2 mg IV dose [74]		0.39	2.45
2 [74]	7.65 E-06		
3 [74]	7.71 E-06		
1.5 [74]	7.35 E-06		
Arithmetic mean	**7.57 E-06**		

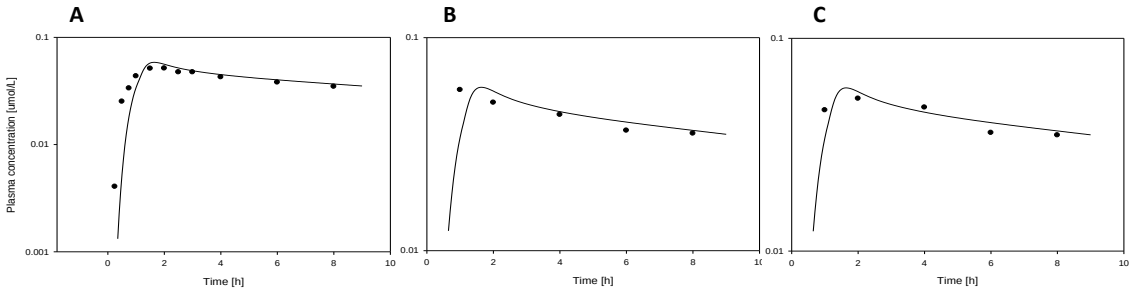

Figure 21. Simulated (line) and observed (symbols) plasma concentration profiles of 1.5 mg oral lorazepam. All graphs were optimized for CL and P_{int}

Development of an adult oral population PBPK model

Similar to Workflow 1, an adult population of 100 individuals was created within PK-Sim consisting of 18-55 year old males to reflect the demographics of the reference observed study participants [74]. The same aspects of variability were factored into the adult population model, as discussed in Workflow 1 (Table 16). Once the population model had been simulated to generate an arithmetic standard deviation curve, observed data obtained from each of the experimental observed studies was superimposed onto the model (Figure 22). Given that the majority of data points fell within one standard deviation of the mean population model, it was determined sufficient to progress to pediatric development.

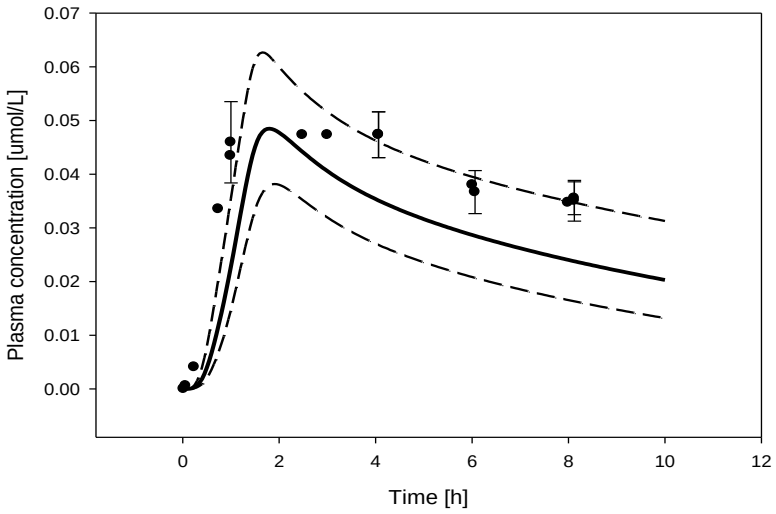

Figure 22. Simulated mean (central line) and standard deviation (dotted line) plasma concentration data in 100 individuals as compared to observed (symbols) mean and standard deviation plasma concentration data following a 1.5 mg oral dose of lorazepam

Development of the pediatric population model for Workflow 1 and 2 of lorazepam

Three observed studies for the investigation of lorazepam pharmacokinetics in pediatrics were obtained from literature. Since lorazepam is commonly administered to infants and pediatrics intravenously, each study follows a given IV bolus dose to each respective study group. A pediatric population of up to a maximum of 1000 individuals for each age group of 0.6-1 year, 2.7-7.6 years, and 3-17 years was isolated from the pediatric reference population for lorazepam. Drug-specific parameters were equal to dose of the final adult oral lorazepam simulation. Four aspects of population variability were factored into the pediatric population model. Once variability had been successfully incorporated into the pediatric population simulation of 1000 individuals following a 1 mg dose, PK parameters of $AUC_{0\text{-}inf}$, Cmax, and half-life ($T_{½}$) following the observed study protocol dosing regimen were obtained for comparison to observed values for prediction accuracy assessment.

3.5 Pediatric PK predictions for BCS class 2 compounds

3.5.1 Ofloxacin

Workflow 1 of ofloxacin

Development of the rat PBPK model following IV administration

A rat PBPK model was created to simulate a 40 mg/kg intravenous bolus dose administration of ofloxacin, based on the study conducted by Wang et al [77]. All rat specific physiology parameters incorporated within PK-Sim were applied to the PBPK model simulation. Various *in vitro* physicochemical properties required for initial input into the model, such as molecular weight, experimental LogP, plasma proteins binding, pKa, aqueous solubility and dissolution were obtained from literature and incorporated into the rat PBPK simulation (Table 18). An experimentally derived *in vivo* data set obtained from literature was superimposed upon the simulated plasma concentration profile to assess model prediction of distribution. Given that the simulated plasma concentration profile did not reflect the curve shape of the observed data, model goodness of fit was achieved via numerical optimization of LogP and CL (Figure 23). A numerical optimization of LogP determined 0.36 as the best value of input in order to achieve line shape (Table 18).

Table 18. Physicochemical initial parameter inputs for ofloxacin within Workflow 1

Input Parameter	Initial Value	Reference	Final applied to model
Molecular weight	361.37 C(18)H(20)FN0(3)	[78]	361.37 C(18)H(20)FN0(3)
LogP (log units)	0.35	[79]	0.36
Plasma protein	Albumin	[80]	Albumin
fu (rat)	0.77	[81]	0.77
fu (human)	0.75	[80]	0.75
pKa (acidic)	6.1	[82]	6.1
pKa (base)	8.2	[82]	8.2
Solubility in water (aqueous)	2.66 mg/mL	[78]	2.66 mg/mL
Dissolution	55% @ 10min	[78]	55% @ 10min

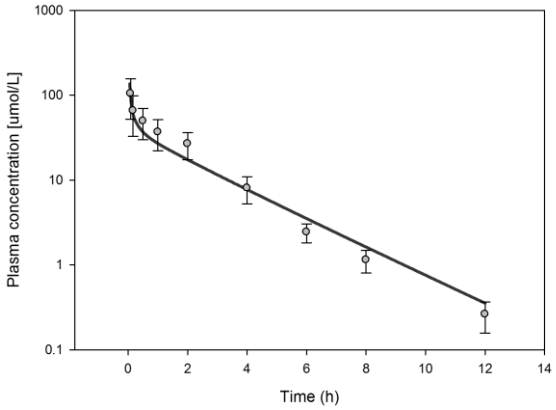

Figure 23. Simulated (line and observed (symbols) plasma concentration data following a 40 mg/kg IV bolus administration of ofloxacin to rats. IV profile optimized for LogP, based on data from Wang et al [90]

Development of the ofloxacin adult PBPK model following oral administration

Using the rat model as a base, three adult oral PBPK models were simulated for the drug ofloxacin. Physicochemical input parameters such as pKa, molecular weight, and optimized LogP remained consistent between the optimized rat IV model and the adult oral model (Table 18). Organism specific parameters were changed to reflect an average 30 year old European human male, with the addition of formulation specific dissolution time, solubility data at reference pH, and fu in humans. Dosing protocol for each simulation was based upon three existing *in vivo* adult pharmacokinetic studies following an oral 400 mg dose administration [80, 83, 84]. Each PBPK adult oral model was simulated and simulated data points did not fall within the range of observed data. Model parameters influencing absorption (P_{int}) and CL were numerically optimized respective to each simulation (Table 19, Figure 24a-c).

CL pathway partitioning

A mass balance study following oral dose administration of ofloxacin suggest the compound is minimally metabolized, approximately <4%, and excreted mainly unchanged by renal CL processes with an fe of 0.7 [80]. Much of the dose was also recovered in bile fluids unchanged. Renal CL was much greater than GFR_{max}, which suggests the involvement of TS. Due to the presence of TS; GFR fraction was set to a value of 1 within the PBPK model. Parameters pertaining to TS and biliary CL were numerically optimized using corresponding observed studies (Table 19). Mean values of the optimized CL and P_{int} parameters from the three optimized adult oral simulations (Figure 24a-c) were incorporated into a final mean adult model, which was utilized for the subsequent adult population model.

Table 19. Workflow 1- optimized CL parameters for adult oral model of ofloxacin			
Study	**P_{int} (cm/min)**	**TS specific (1/min)**	**Biliary CL_{spec}**
Lehto [83]	5.15 E-6	0.6853	3.1 E-3
Lode [80]	7.42 E-6	0.5744	3.1 E-3
Yuk [84]	5.57 E-6	0.6853	3.1 E-3
Mean	**6.04 E-6**	**0.647**	**3.1 E-3**

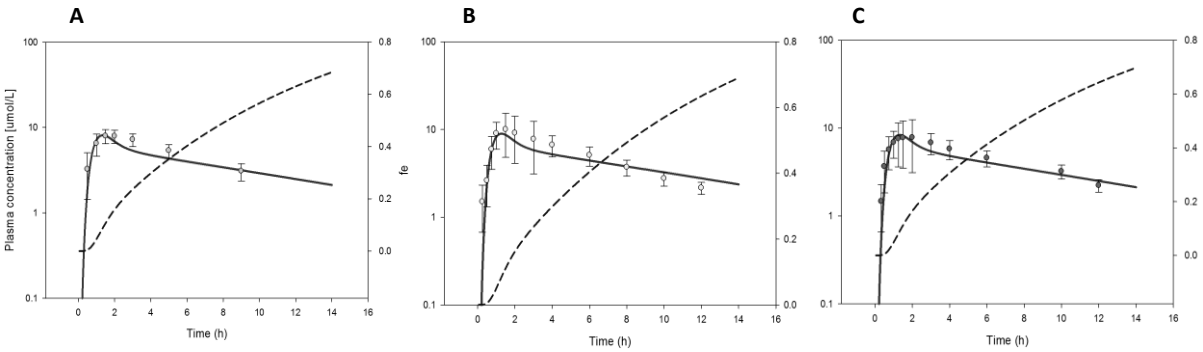

Figure 24. Simulated (line) and observed (symbols) plasma concentration data following a 400 mg oral dose administration of ofloxacin in humans, including fe (dotted). Data is taken from A) Lehto [87] B) Lode [84] C) Yuk [88]

Development of an adult oral population PBPK model

For the population model for ofloxacin, 100 virtual individuals were generated within an age range of 18-55 years. Six aspects of population variability were factored into the adult population model (Table 20). Biliary CL inter-individual variability was introduced into the model, and was assigned a standard CV of 30% following log normal distribution [32]. Observed data obtained from each of the experimental observed studies was superimposed onto the model to assess the model's ability to encompass observed data within one arithmetic standard deviation of the simulated population (Figure 25). Physicochemical parameters were not further modified from the optimized adult PBPK model. Once the population model had been simulated to generate an arithmetic standard deviation curve, observed data obtained from each of the experimental observed studies was superimposed onto the model [85, 86]. Given that the majority of data points fell within one standard deviation of the mean population model, it was determined sufficient to progress to pediatric model development (Figure 25).

Table 20. Population variability incorporated into the adult population model of ofloxacin			
Pathway	**Value**	**Distribution**	**Notes and reference**
GET	CV % = 24%	Log normal	Table 6
SITT	CV = 22.5%	Log normal	Table 6
Small intestinal surface area	9 fold variation in a uniform distribution (mean*3 – mean/3). Each individual had the same surface enhancement factor applied.	Uniform	Table 6
GFR (specific)	CV = 25%	Normal	Table 6
TS (specific)	CV = 30%	Log normal	Table 13
Biliary	CV = 30%	Log normal	Standard population variability attributed to Biliary CL in adults and children based on Edginton, 2006 [32]

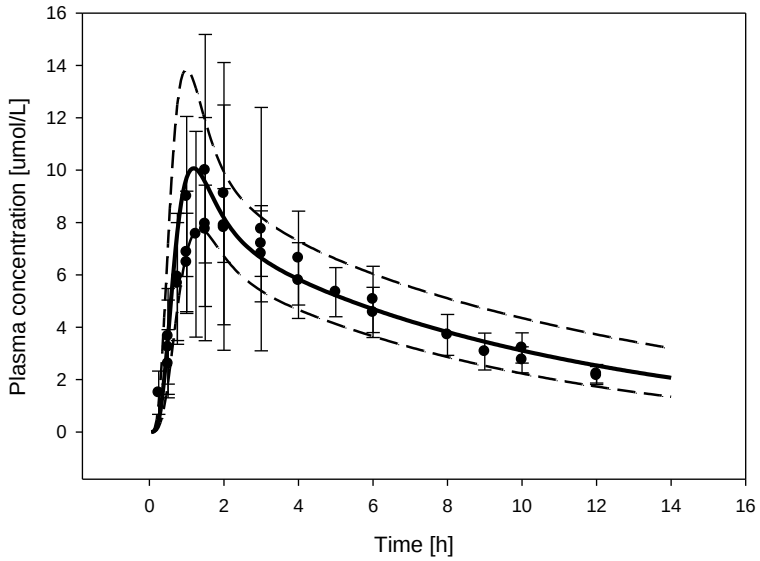

Figure 25. Simulated mean (central line) and standard deviation (dotted line) plasma concentration data in 100 individuals as compared to observed (symbols) mean and standard deviation plasma concentration data following data following a 400 mg oral dose of ofloxacin in adults

Workflow 2 of ofloxacin

Development of the human PBPK model following IV administration

An adult IV PBPK model was simulated for the drug ofloxacin based on the dosing protocol from an IV study conducted in adults by Lode et al, in which 100 mg of ofloxacin was administered as an IV bolus to 18 healthy adult participants [80]. Organism specific input parameters pertaining to anatomy and physiology were incorporated within PK-Sim, reflecting an average 30 year old European male were applied to the model. Physicochemical primary input parameters such as fu, lipophilicity (LogP), pKa, molecular weight, and solubility at reference pH were obtained from literature (Table 18).

A mass balance study conducted by Lode et al suggests fe of ofloxacin was approximately 0.7-0.8 following an IV dose; ofloxacin metabolites accounted for <4% of recovery [80]. The remaining dose was recovered in bile fluids unchanged [80]. Similarly to Workflow 1, a biliary component, TS, and GFR were incorporated within the model.

Once the PBPK adult IV base model had been simulated following a 100 mg IV bolus, experimentally derived *in vivo* data from Lode et al [80], was superimposed upon the simulated plasma concentration profile. Model parameters influencing distribution (i.e. LogP) and CL were numerically optimized, and the simulated AUC matched the observed AUC within ±10%. Log P was optimized to 1.6 log units. TS_{spec} was optimized to reflect the observed fe of 0.7-0.8; the optimized value was 0.617 1/min (Table 21**,** Figure 26).

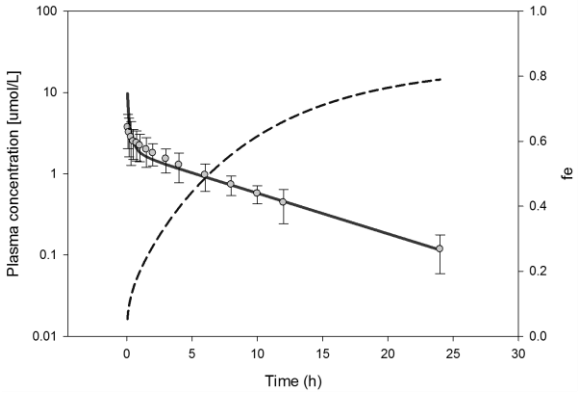

Figure 26. Simulated (line) and observed (symbols) plasma concentration profile of ofloxacin following a 100 mg IV bolus. Observed data was taken from Lode et al [80].

Development of the adult oral model for ofloxacin

Similarly to Workflow 1, three adult oral models were simulated to reflect demographic and dosing regimen of three observed obtained from literature [80, 83, 84]. Subsequently, each PBPK model was numerically optimized against the corresponding experimental study [80, 83, 84]. All physicochemical input parameters such as pKa, molecular weight, solubility, optimized LogP and CL remained consistent between the optimized adult IV model and each adult oral model (Table 18).

Once all three PBPK adult oral models had been simulated following a 400 mg oral dose, experimentally derived *in vivo* data was superimposed upon the simulated plasma concentration profiles [80, 83, 84]. Model parameters influencing absorption (P_{int}) were numerically optimized (Table 21**,** Figure 27). The mean P_{int} and CL values calculated from the optimized oral and IV PBPK models, were incorporated into a final mean adult simulation, which was further utilized in building the subsequent adult population model.

Table 21. Optimized P_{int}, TS, and Hepatic CL for the standard workflow of ofloxacin

Study	**P_{int} (cm/min)**	**TS CL_{spec} (1/min)**	**Hepatic CL_{spec} (1/min)**	**LogP (log units)**
Lehto [83]	6.37 E-06	0.617	0.038	1.6
Lode [80]	8.37 E-06			
Yuk [84]	6.28 E-06			
Mean	**7.01 E-06**			

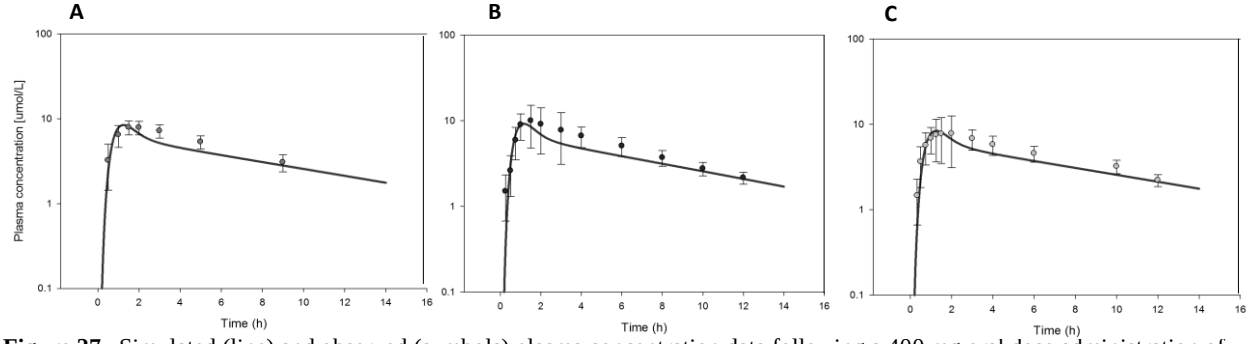

Figure 27. Simulated (line) and observed (symbols) plasma concentration data following a 400 mg oral dose administration of ofloxacin in humans, including fe (dotted). Data is taken from A) Lehto [87] B) Lode [84] C) Yuk [88]

Development of an adult oral population PBPK model

An adult population of 100 individuals was created within PK-Sim to assess variability of ofloxacin exposure in adults following a 400 mg oral dose administration to 100 adults. Observed data obtained from each of the experimental observed studies was superimposed onto the model to assess whether observed data would be successfully encompassed within one standard deviation of the population model

simulation (Table 20, Figure 28). Given that the majority of data points fell within one standard deviation of the mean population model, it was determined sufficient to progress to pediatric model development.

Table 22. Population variability incorporated into the adult population model simulations in MoBi for ofloxacin

Pathway	**Value**	**Distribution**	**Notes and reference**
GET	CV = 24%	Log normal	Table 6
SITT	CV = 22.5%	Log normal	Table 6
Small intestinal surface area	9 fold variation in a uniform distribution (mean*3 – mean/3). Each individual had the same surface enhancement factor applied.	Uniform	Table 6
GFR (specific)	CV = 25%	Normal	Table 6
TS (specific)	CV = 30%	Log normal	Table 13
Biliary	CV = 30%	Log normal	Table 27

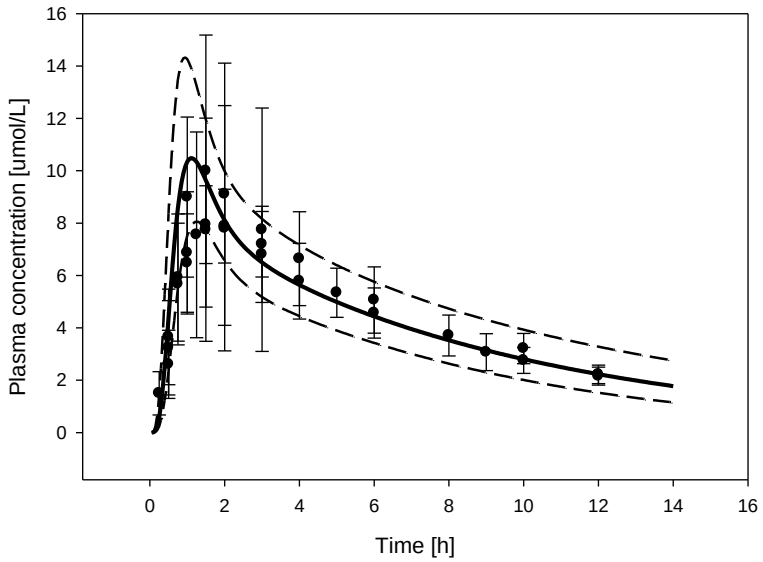

Figure 28. Simulated mean (central line) and standard deviation (dotted line) plasma concentration data in 100 individuals as compared to observed (symbols) mean and standard deviation plasma concentration data following data following a 400 mg oral ofloxacin in adults

Development of the pediatric population model for Workflow 1 and 2 of ofloxacin

A pediatric study investigating the pharmacokinetics of ofloxacin in infants and children between the ages of 0.25-2years, 2-6 years, and 6-8 year olds was obtained from literature [87]. In the study, patients received a 20 mg/kg dose of oral ofloxacin. This experimental study served as the comparative reference for the assessment of the utility of Workflow 1 in predicting the PK profile in pediatrics for CL, as compared to the standard workflow.

A population of up to a maximum of 1000 individuals were randomly selected from the reference pediatric population, to reflect the age demographic of each observed study for ofloxacin. Drug-specific inputs were equal to those of the final adult oral ofloxacin simulation. All relevant inter-individual population variability parameters were applied to the pediatric models (Table 23). Once variability had been successfully incorporated into the pediatric population simulation, population PK parameters of $AUC_{0\text{-}inf}$, Cmax, and Tmax following the observed study protocol dosing regimen were obtained for comparison to corresponding observed values and further data analysis.

Table 23. Population variability incorporated into the pediatric population model for ofloxacin

Pathway	**Value**	**Distribution**	**Notes and reference**
GET	CV = 60%	Log normal	Table 6
SITT	CV = 60%	Log normal	Table 6
Small intestinal surface area	9 fold variation in a uniform distribution (mean*3 – mean/3). Each individual had the same surface enhancement factor applied.	Uniform	Table 6
GFR (specific)	CV = 25%	Normal	Table 6
TS (specific)	CV = 61%	Log normal	Table 13
Biliary	CV = 30%	Log normal	Table 27

3.5.2 Ciprofloxacin

Workflow 1 of ciprofloxacin

Development of the rat PBPK model following IV administration

A rat PBPK model was created for the drug ciprofloxacin, based on a rat IV study (5 mg/kg) conducted by Naora et al [88]. Organism specific parameters pertaining to anatomy and physiology of a generic rat (e.g. 275 g) were applied. Physicochemical properties such as fu in rat, LogP, pKa, and molecular weight were obtained from various sources within literature (Table 24); ciprofloxacin binds primarily to albumin within rat and humans. Following simulation of the rat PBPK model, experimentally derived *in vivo* data was superimposed upon the simulated plasma concentration profile. Given that the simulated data points did not reflect the curve shape of the observed data, model parameters influencing distribution and CL were numerically optimized (Table 25, Figure 29). Numerical optimization suggested an optimal LogP value of 1.99 log units.

Table 24. Ciprofloxacin physicochemical input parameters for the rat and adult models within Workflow 1

Initial Input	Initial Value	Reference	Value in final model
fu (rat)	0.70	[88]	0.70
fu (human)	0.70	[88]	0.70
LogP (log units)	1.32	[89]	1.99
Molecular weight	331.34	[89]	331.34
pKa	pKa1: 6.09 pKa2: 8.73	[90-93]	pKa1: 6.09 pKa2: 8.73
Solubility	0.17mg/mL at 6.8pH	[89]	0.17mg/mL at 6.8pH
Dissolution	>75% at 45 min	[94]	>75% at 45 min

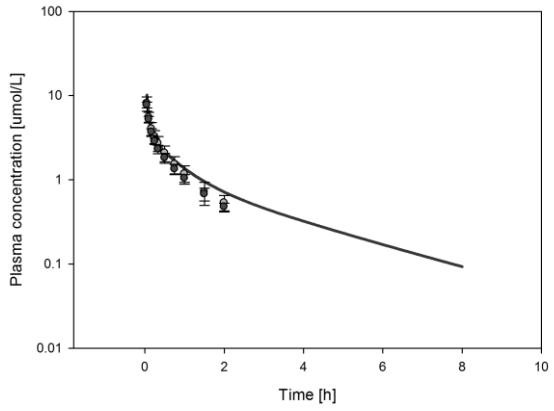

Figure 29. Rat IV PBPK model following 5 mg/kg of ciprofloxacin, optimized for LogP, based on observed data.

Development of the ciprofloxacin adult PBPK model following oral administration

Using the rat model as a base, all species specific inputs were changed to reflect an average 30 year old European human male. This included anatomical and physiological inputs. All drug-specific inputs were maintained as in the rat PBPK model (Table 24) with the addition of compound specific solubility and dissolution data (Table 18). Three adult PBPK models were simulated, and were based upon three oral studies following doses of 100 mg [86], 250 mg [85], and 750 mg [86] of ciprofloxacin. Observed data was superimposed upon the simulated plasma concentration time profiles for an initial visual goodness of fit assessment. Given that the simulated data points did not fall within the range of observed data, model parameters influencing absorption (P_{int}) (Table 25) and total plasma CL were numerically optimized respective to each simulation (Figure 30a-c).

CL pathway partitioning

CL was characterized in the initial adult PBPK model by generic renal and generic hepatic components. The next step was to proportion this CL into individual pathways that are responsible for ciprofloxacin clearance. Ciprofloxacin undergoes the renal CL processes of GFR, TS as well as having hepatic, and CYP1A2 metabolism. According to literature, approximately 40-50% of orally administered ciprofloxacin is excreted in the urine [86, 95, 96] with approximately 15-20% of the oral dose recovered as biologically active metabolites in feces and urine [97]. Additionally, total renal plasma CL had been found to exceed GFR_{max}, therefore literature suggests a significant portion of ciprofloxacin is eliminated via active TS [85, 97]. As a result, GFR and TS were added to the adult oral model in place of an overall generic renal CL component, as well as CYP1A2, in place of a generic hepatic component within the naïve adult oral model.

Once CL pathways had been defined within the oral model, parameters pertaining to TS, CYP1A2 CL activity were numerically optimized using the respective observed studies (Figure 30a-c). Although there are many uncertainties with respect to bioavailability estimates within an oral model when lacking IV data, renal CL input parameters were fixed to reflect an observed fe of 40% as closely as possible. The mean value of the optimized TS, hepatic CL and P_{int} (Table 25) from each of the three simulated PBPK models was incorporated into a final mean adult model, which was applied to the subsequent adult population model.

Table 25. Optimized total hepatic CL_{spec}, P_{int} for three simulated adult oral profiles			
Study dosing before dose normalization	**P_{int} (cm/min)**	**CYP1A2 CL_{spec} (1/min)**	**TS CL_{spec} (1/min)**
100 [86]	1.04 e-04	0.127	2.86
250 [85]	2.11e-03	0.191	2.88
750 [86]	5.87e-05	0.184	3.43
Mean	**3.01 E-4**	**0.167**	**3.05**

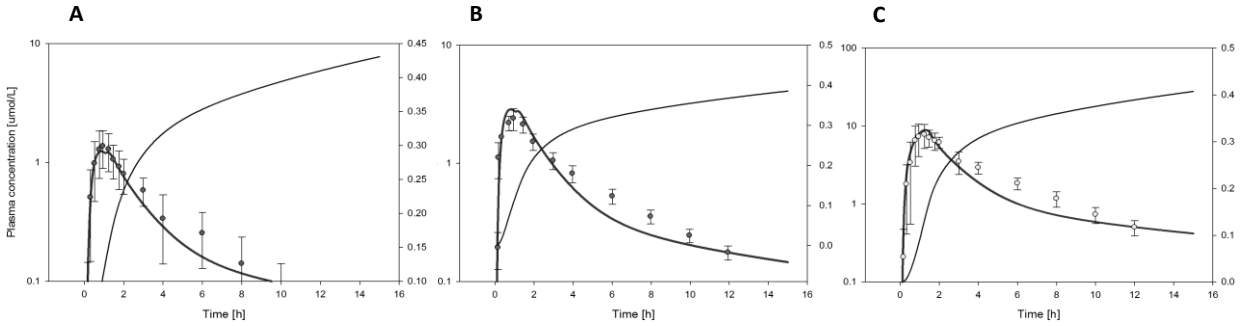

Figure 30. Simulated (line) and observed (symbols) plasma concentration profiles, including fe (dotted), of ciprofloxacin following A) 100 mg [86] B) 250 mg [85] and C)750 mg [86] or oral ciprofloxacin.

Development of an adult oral population PBPK model

For the population model for ciprofloxacin, 100 virtual individuals were generated within an age range of 18-55 years. Six aspects of population variability were factored into the adult population model (Table 26), each of which was similarly incorporated within the previously described models. Physicochemical parameters were not further modified from the optimized adult PBPK model. Once the population model had been simulated to generate an arithmetic standard deviation curve, observed data was superimposed [85, 86] (Figure 31). Given that the majority of data points fell within one standard deviation of the mean population model, it was determined sufficient to progress to pediatric model development.

Table 26. Population variability incorporated into the adult population model simulations of ciprofloxacin			
Pathway	**Value**	**Distribution**	**Notes and reference**
GET	CV = 24%	Log normal	Table 6
SITT	CV = 22.5%	Log normal	Table 6
Small intestinal surface area	9 fold variation in a uniform distribution (mean*3 – mean/3). Each individual had the same surface enhancement factor applied.	Uniform	Table 6
GFR (specific)	CV = 25%	Normal	Table 6
TS (specific)	CV = 30%	Log normal	Table 13
CYP1A2 (specific)	CV = 30%	Log normal	Table 19

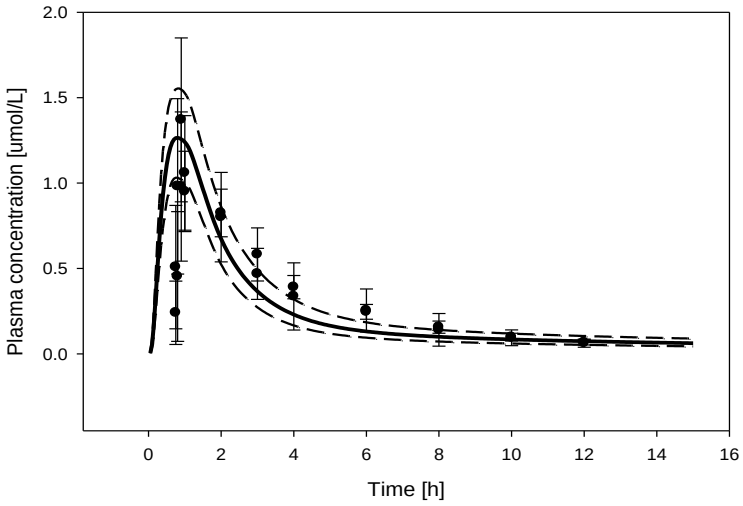

Figure 31. Simulated mean (central line) and standard deviation (dotted line) plasma concentration data in 100 individuals as compared to observed (symbols) mean and standard deviation plasma concentration data following data following a 100 mg oral dose of ciprofloxacin in adults [85, 86]

Workflow 2 of ciprofloxacin

Development of the human PBPK model following IV administration

An adult IV PBPK model was simulated for the drug ciprofloxacin based on the dosing protocol from an IV study conducted in adults by Wise et al, in which a 100 mg IV bolus was administered to six healthy adults [98]. Similar to Workflow 1, organism specific input parameters pertaining to anatomy and physiology were incorporated within PK-Sim, reflecting an average 30 year old European male. Physicochemical parameters such as fu, LogP, pKa, and molecular weight were applied to the model, as obtained from literature (Table 24). Once the PBPK adult IV base model had been simulated following a 100 mg IV bolus, experimentally derived *in vivo* data from Wise et al, was superimposed upon the simulated plasma concentration profile to allow for a goodness of fit assessment [98]. Model parameters influencing distribution (LogP) and CL were optimized (Figure 32). LogP was optimized to 1.85 log (Table 27).

A study by Hoffken et al suggests approximately 40-60% of the IV administered dose was recovered as parent compound excreted unchanged in urine [86], with approximately 20-30% of the dose recovered in urine and feces as metabolites [86], and the remainder was recovered in feces unchanged; this was characterized as both a CYP1A2 and generic biliary CL component within the model (Table 27).

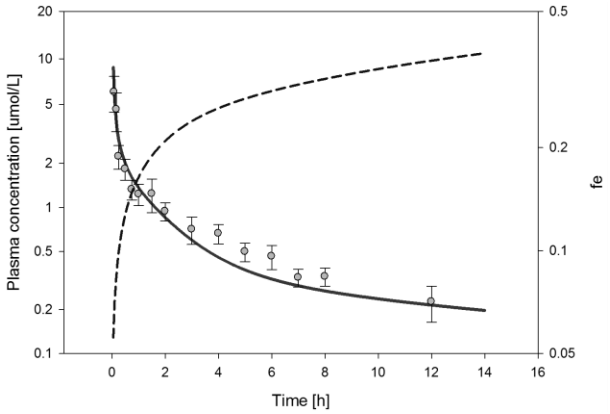

Figure 32. Simulated (line) and observed (symbols) plasma concentration data following a 100 mg IV bolus of ciprofloxacin in adults, including simulated fe (dotted line). IV profile was optimized for CL and distribution (i.e. LogP) Based on data from Wise et al[98]. Adult IV model optimized for LogP and CL

Development of the ciprofloxacin adult PBPK model following oral administration

Three adult oral models were simulated following 100 mg, 250 mg, and 750 mg oral doses of ciprofloxacin respectively. Physicochemical input parameters such as pKa, molecular weight, optimized LogP, and optimized CL remained unchanged from the final adult IV model, with the addition of compound specific solubility at reference pH (Table 24). Organism specific anatomy and physiology parameters incorporated into PK-Sim, pertaining to an average 30 year old European male, were used.

Once each PBPK adult oral model had been simulated, observed data [85, 86] was superimposed upon the simulated plasma concentration profile. Given that the simulated data points did not fall within the range of observed data, the most uncertain model parameter influencing absorption, P_{int}, was numerically optimized respective to each simulation (Table 27, Figure 33a-c). The arithmetic mean P_{int} value would serve as the final input within the adult oral model scaled to pediatrics.

Table 27. Numerically optimized parameters of P_{int}, TS, CYP1A2 CL and LogP for the standard workflow of ciprofloxacin

Study group by dose administered (mg)	**P_{int} (cm/min)**	**TS CL_{spec} (1/min)**	**CYP1A2 CL_{spec} (1/min)**	**Biliary CL_{spec} (1/min)**	**LogP (log units)**
100 mg IV bolus [98]		1.01	0.59	0.6	1.85
100 [86]	0.0134 E-02				
250 [85]	0.0175 E-02				
750 [86]	0.0375 E-02				
Mean	**2.28 E-02**				

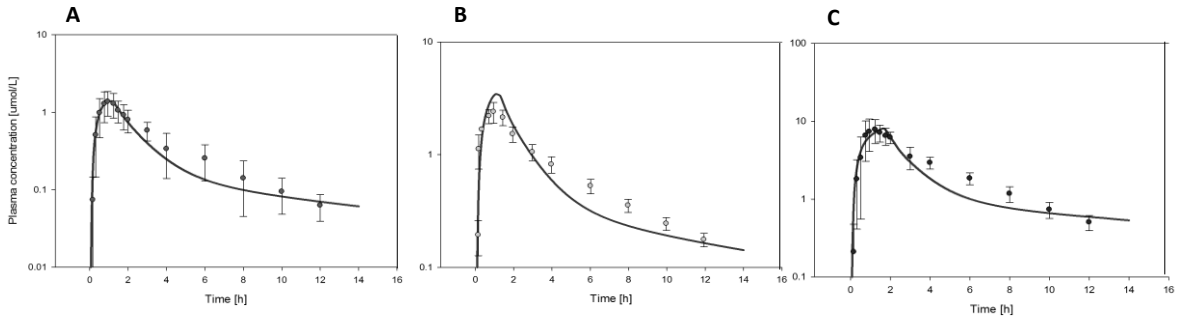

Figure 33. Simulated (line) and observed (symbols) plasma concentration profiles of ciprofloxacin following A) 100 mg B)250 mg and C)750 mg oral dose administration within Workflow 2

Development of an adult oral population PBPK model

Similar to the population model of ciprofloxacin in Workflow 1, 100 virtual individuals were generated within an age range of 18-55 years. Seven aspects of population variability were factored into the adult population model, six of which was similarly incorporated within Workflow 1 (Table 26), with the addition of a 30% CV of Biliary CL (Table 26), as described in previous models. Physicochemical parameters were not further modified from the optimized adult PBPK model. Once the population model had been simulated, following a 100 mg oral dose administration, observed data obtained from each study was dose normalized to reflect a 100 mg dose, and superimposed onto the model [85, 86] (Figure 34). Observed data points successfully fell approximately within the arithmetic standard deviation limits of the population model.

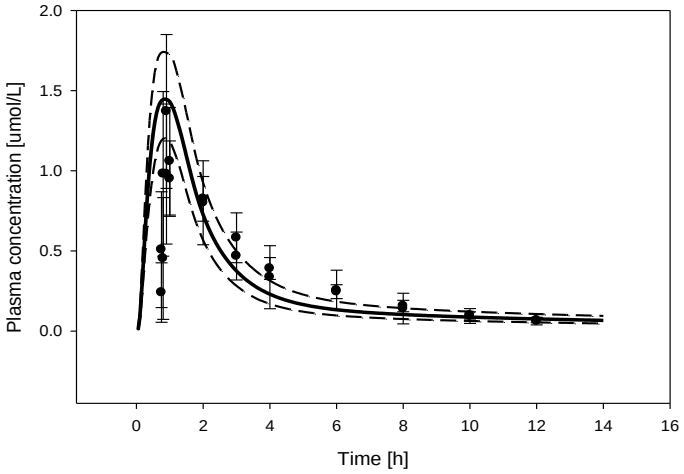

Figure 34. Simulated mean (central line) and standard deviation (dotted line) plasma concentration data in 100 individuals as compared to observed (symbols) mean and standard deviation plasma concentration data following data following a 100 mg oral dose of ciprofloxacin in adults.

Development of the pediatric population model for Workflow 1 and 2 of ciprofloxacin

A pediatric study investigating the pharmacokinetics of ciprofloxacin in infants and children between the ages of 5-14 weeks and 1-5 years was obtained from literature [99]. In the study, patients received a 15 mg/kg dose or oral ciprofloxacin. This experimental study served as the comparative reference for the assessment of the utility of Workflow 1 in predicting the PK profile in pediatrics for CL, as compared to the standard workflow.

A pediatric population of up to a maximum of 1000 individuals reflecting the observed study were isolated from the reference pediatric population for ciprofloxacin. Drug-specific parameters were equal to those of the final adult oral ciprofloxacin simulation. Six aspects of population variability were factored into both pediatric population models as obtained from literature (Table 28). Once variability had been successfully incorporated into the pediatric population simulations, PK parameters of $AUC_{0\text{-inf}}$, Cmax, and Tmax following the observed study protocol dosing regimen were obtained for comparison to corresponding observed values and further data analysis.

Table 28. Population variability incorporated into the pediatric population model simulations for Ciprofloxacin

Pathway	**Value**	**Distribution**	**Notes and reference**
GET	CV = 60%	Log normal	Table 6
SITT	CV = 60%	Log normal	Table 6
Small intestinal surface area	9 fold variation in a uniform distribution (mean*3 – mean/3). Each individual had the same surface enhancement factor applied.	Uniform	Table 6
GFR (specific)	CV = 25%	Normal	Table 6
TS (specific)	CV = 61%	Log normal	Table 13
CYP1A2 (specific)	CV = 30%	Log normal	Table 19

3.5.3 Valsartan

Workflow 1 of valsartan

Development of the Rat PBPK model following IV administration

A PBPK model simulation was created to simulate a 1 mg/kg IV bolus of valsartan in rats. Drug specific physicochemical were obtained from literature and incorporated into the rat PBPK simulation (Table 29). A study by Yamashiro et al [87] suggests that valsartan metabolism in the rat is due primarily to hepatic mechanisms, which was reflected in the rat PBPK model CL processes. Observed *in vivo* data following 1 mg/kg valsartan IV bolus administration to rats was obtained from literature [87]. Once the initial, or naïve, PBPK rat model had been simulated, both experimentally derived *in vivo* data sets were superimposed upon the simulated plasma concentration profile. Given that the simulated data points did not reflect the curve shape of the observed data, model parameters influencing distribution (LogP) and CL were numerically optimized (Figure 35); LogP was optimized to 3.09. Although the terminal phase within the rat model in Figure 35 did not match observed line-shape, the objective of the optimized model was to define the distribution phase of the plasma concentration profile which is ideally captured by the initial time points.

Table 29. Physicochemical initial parameter inputs for valsartan in the Rat and adult model

Input Parameter	Initial Value	Reference	Final value in model
Molecular weight	435.52	[100]	435.52
LogP (experimental)	1.5	[100]	3.09
Fu rat	0.05	[101]	0.05
Fu human	0.05	[101]	0.05
pKa (acidic) x 2	3.9 and 4.73	[100]	3.9 and 4.73
Aqueous solubility	0.18 g/L	[100]	0.18 g/L
Dissolution	50% in 50 min	[102]	50% in 50 min

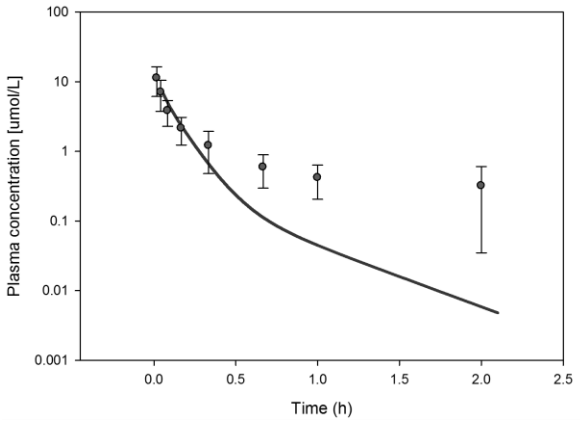

Figure 35. Simulated (line) and observed (symbols) valsartan Rat IV profile optimized for LogP, following 1 mg/kg IV bolus dose administration based on data from Yamashiro et al [87]

Development of the valsartan adult PBPK model following oral administration

Three adult oral PBPK models were simulated for the drug valsartan in which all physicochemical input parameters such as pKa, molecular weight, and solubility at reference pH, as well as optimized LogP remained consistent between the optimized rat IV model and the adult oral model (Table 29). Organism specific anatomy and physiology parameters such as fu in humans, as well as solubility and dissolution data were applied to the model. Dosing guidance for each simulation was based upon three existing *in vivo* adult pharmacokinetic studies following and 80 mg oral dose administration [100, 103, 104]. CL of valsartan was designated completely within generic hepatic and renal systems.

Once each PBPK adult oral model had been simulated following an oral dose of 80 mg of valsartan, experimentally derived *in vivo* data [100, 103, 104], was superimposed upon the simulated plasma concentration profile. Model parameters influencing absorption (P_{int}) and CL were numerically optimized (Table 30).

CL pathway partitioning

Pharmacokinetic studies following oral dose administration suggest approximately 10% recovery of unchanged compound in the urine, approximately 70% of the compound was recovered in bile fluids and feces unchanged, and approximately 9% was released as a hepatic CYP2D6 metabolite [105]. CYP2D6 metabolism, biliary CL, GFR, and TS CL processes were applied to the adult oral model [105]. CYP2D6 metabolizing enzyme was localized completely within the liver. All CL parameters were numerically optimized (Table 31, Figure 36a-c). Arithmetic mean values of the optimized CL and P_{int} parameters from the adult PBPK models were incorporated into a final adult PBPK model. Despite poor fit of the simulated rat PBPK model to observe data in the terminal phase (Figure 35), the adult oral model was not impeded by the large deviation in line shape.

Table 30. Optimized distribution and CL parameters of valsartan				
Study	**P_{int} (cm/min)**	**CYP 2D6 CL_{spec} (1/min)**	**Biliary CL_{spec} (1/min)**	**TS specific (1/min)**
Flesch [103]	3.70 E-06	0.315	0.194	0.457
Criscione [100]	3.70 E-06	0.331	0.189	0.343
Macek [104]	3.90 E-06	0.254	0.188	0.229
Mean	**3.77 E-06**	**0.300**	**0.190**	**0.343**

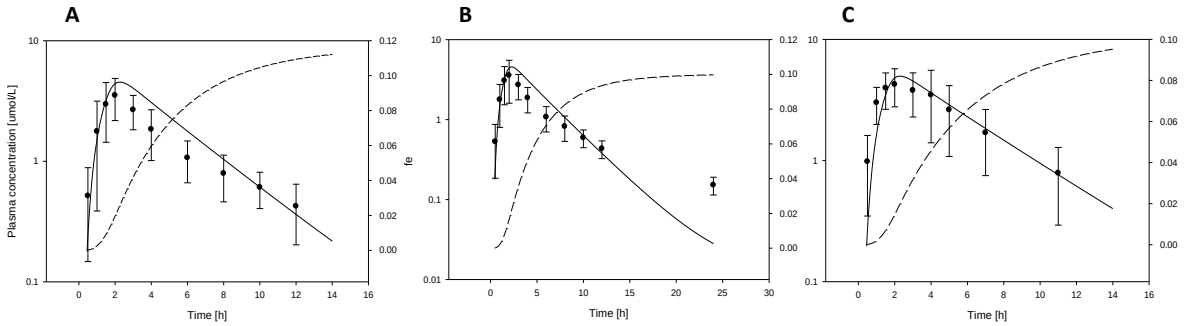

Figure 36. Simulated (line) and observed (symbols) plasma concentration profiles of valsartan following 80 mg oral dose administration, based on data from A) Flesch et al [103] B) Criscione et al [100] C) Macek et al [104] including fe (dotted)

Development of an adult oral population PBPK model

For the population model for valsartan, 100 virtual individuals were generated within an age range of 18-55 years. Once the population had been generated, the population was administered a 80 mg oral dose to reflect the observed studies [100, 103, 104]. Six aspects of population variability were factored into the adult population model (Table 31) as obtained from literature. CYP2D6 variability was incorporated into the model as obtained from Dorne et al [106] following a log normal distribution with CV of 66% in adults. Physicochemical parameters were not further modified from the optimized adult PBPK model. Once the population model had been simulated to generate an arithmetic standard deviation curve, observed data obtained from each of the experimental observed studies was superimposed onto the model (Figure 37). Given that the majority of data points and/or their respective observed standard deviations fell within one standard deviation of the mean population model, it was determined sufficient to progress to pediatric development.

Table 31. Population variability incorporated into the adult population model simulations for valsartan			
Pathway	**Value**	**Distribution**	**Notes and reference**
GET	CV % = 24%	Log normal	Table 6
SITT	CV = 22.5%	Log normal	Table 6
Small intestinal surface area	9 fold variation in a uniform distribution (mean*3 – mean/3). Each individual had the same surface enhancement factor applied.	Uniform	Table 6
GFR (specific)	CV = 25%	Normal	Table 6
TS (specific)	CV = 30%	Log normal	Table 13
CYP2D6	CV = 66%	log normal	Determined from Dorne et al [106] in which the inter-individual variability for various phase I, II and renal metabolic processes was assessed with various probe substrates.
Biliary	CV = 30%	Log normal	Table 27

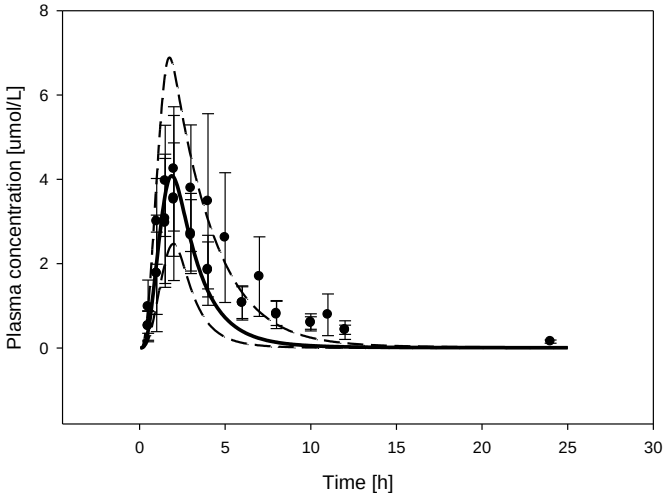

Figure 37. Simulated mean (central line) and standard deviation (dotted line) plasma concentration data in 100 individuals as compared to observed (symbols) mean and standard deviation plasma concentration data following data following a 80 mg oral dose of valsartan in adults

Workflow 2 of valsartan

Development of the human PBPK model following IV administration

An adult PBPK model was simulated for the drug valsartan based on the dosing protocol from an IV study conducted in adults by Flesch et al, in which 20 mg of valsartan was administered as an IV bolus to 12 healthy adult participants [103]. Organism specific input parameters pertaining to anatomy and physiology were incorporated within PK-Sim, reflecting an average 30 year old European male were applied to the model. Physicochemical primary input parameters such as fu, LogP, pKa, molecular weight, and solubility were obtained from literature (Table 29).

A mass balance study of valsartan suggests fe was 0.30 following an IV dose. Biliary CL is an important route of elimination for valsartan, as a greater concentration of valsartan was found in bile fluids unchanged, as compared to plasma samples [103]. Similar to Workflow 1, biliary, CYP2D6, GFR, and TS pathways of CL were defined within the model.

Once the PBPK adult IV base model had been simulated following a 20 mg IV bolus dose administration, experimentally derived *in vivo* data from Flesch et al [103], was superimposed upon the simulated plasma concentration profile (Figure 38). Given that the simulated data points did not reflect curve shape and exposure of the experimental data, LogP and CL were numerically optimized (Table 32).

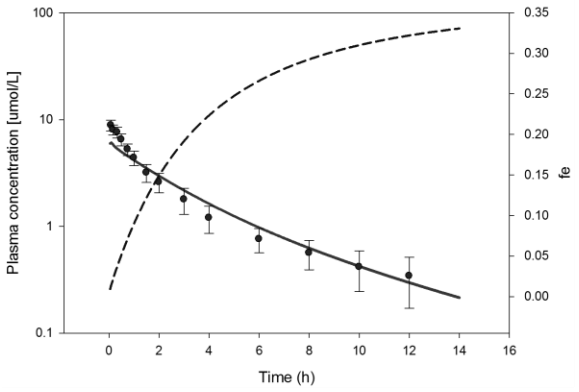

Figure 38. Simulated (line) and observed (symbols) plasma concentration data of a 20 mg IV bolus of valsartan in humans, including fe (dotted) optimized for distribution and CL. Observed data taken from Flesch et al [103]

Development of the valsartan adult PBPK model following oral administration

Similarly to Workflow 1, three adult oral PBPK models were simulated to reflect the dosing protocol of three observed obtained from literature, 80 mg oral valsartan. In addition to the physicochemical input parameters, optimized LogP and CL remained unchanged from the optimized adult IV model. Organism

specific anatomy and physiology input parameters were incorporated into PK-Sim, for a mean European 30 year old male. Once all three PBPK adult oral models had been simulated, experimentally derived *in vivo* data was superimposed upon the simulated plasma concentration profiles [100, 103, 104]. Model parameters influencing absorption (P_{int}) were numerically optimized (Table 32, Figure 39a-c). The arithmetic mean of each optimized parameter was incorporated into a final mean adult simulation, which was further utilized in building an adult population model.

Table 32. Optimized absorption and CL parameters of valsartan

Study	**P_{int} (cm/min)**	**CYP 2D6 (1/min)**	**Biliary (1/min)**	**TS specific (1/min)**	**LogP (log units)**
Flesch IV [103]		0.967	0.626	0.366	0.36
Flesch [103]	1.30 E-6				
Criscione [100]	1.32 E-6				
Macek [104]	1.70 E-6				
Mean	**1.44 E-6**				

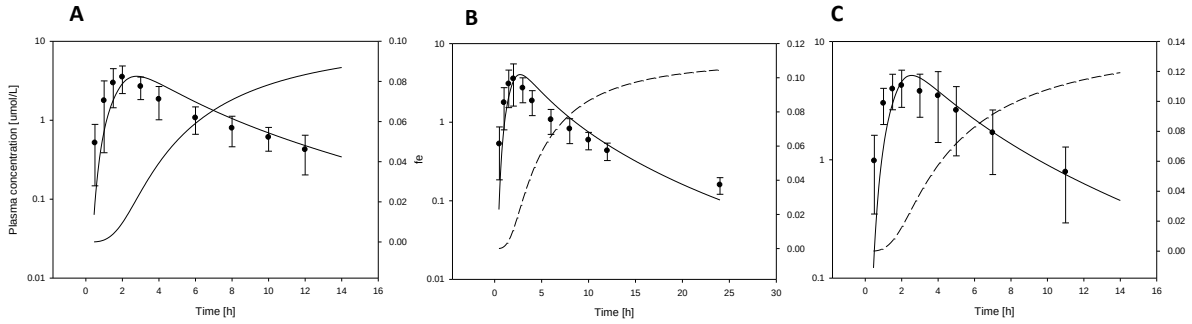

Figure 39. Simulated (line) and observed (symbols) plasma concentration profiles of valsartan following 80 mg oral dose administration, based on data from A) Flesch et al [93] B)Criscione et al [90] C) Macek et al [94]

Development of an adult oral population PBPK model

An adult population of 100 individuals was created within PK-Sim to assess variability of valsartan exposure in adults following an 80 mg oral dose (Figure 40). Eight aspects of population variability were factored into the adult population model (Table 33) as obtained from literature. CYP2D6 variability was incorporated into the model as obtained from Dorne et al [106] following a log normal distribution with CV of 66% in adults. Physicochemical parameters were not further modified from the optimized adult PBPK model. Once the population model had been simulated to generate an arithmetic standard deviation curve, observed data obtained from each of the experimental observed studies was superimposed onto the model for an assessment of the models ability to appropriately characterize population variability (Figure 40). Given that the majority of data points fell within one standard deviation of the mean population model, it was determined sufficient to progress to pediatric model development.

Table 33. Population variability incorporated into the adult population model simulations of valsartan			
Pathway	**Value**	**Distribution**	**Notes and reference**
GET	CV = 24%	Log normal	Table 6
SITT	CV = 22.5%	Log normal	Table 6
Small intestinal surface area	9 fold variation in a uniform distribution (mean*3 – mean/3). Each individual had the same surface enhancement factor applied.	Uniform	Table 6
GFR (specific)	CV = 25%	Normal	Table 6
TS (specific)	CV = 60.7%	Log normal	Table 13
CYP2D6	CV = 66%		Determined from Dorne et al [106] in which the inter-individual variability for various phase I, II and renal metabolic processes was assessed with various probe substrates.
Biliary	CV = 30%	Log normal	Table 27

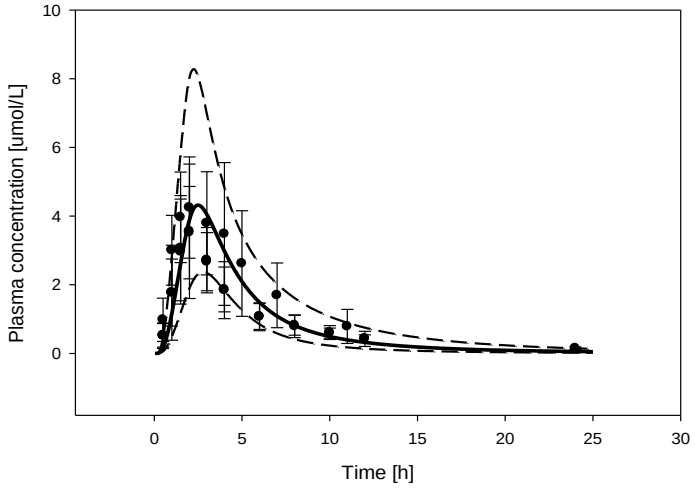

Figure 40. Simulated mean (central line) and standard deviation (dotted line) plasma concentration data in 100 individuals as compared to observed (symbols) mean and standard deviation plasma concentration data following data following a 80 mg oral valsartan in adults

Development of the pediatric population model for Workflow 1 and 2 of valsartan

A pediatric study investigating the pharmacokinetics of valsartan in infants and children after a 2 mg/kg oral dose administration, with a maximum single dose of 80 mg, was obtained from literature [107]. Subjects were stratified into four age groups; 1-4 years, 4-6 years, 6-12 years, and 12-16 year olds. This experimental study served as the comparative reference for the assessment of the utility of Workflow 1 in predicting the PK profile in pediatrics for CL, as compared to the standard workflow.

A pediatric population of up to a maximum of 1000 individuals reflecting the observed study were isolated from the reference pediatric population for valsartan. Similar to methods discussed previously, seven aspects of population variability were factored into the pediatric population model, as obtained from literature (Table 34). Once variability had been successfully incorporated into the pediatric population, PK parameters of $AUC_{0\text{-}inf}$, Cmax, and Tmax following the observed study protocol dosing regimen were obtained for comparison to corresponding observed values and further data analysis.

Table 34. Population variability incorporated into the pediatric population model simulations in PK-Sim and MoBi for Workflow 1 and 2

Pathway	**Value**	**Distribution**	**Notes and reference**
GET	CV = 60%	Log normal	Table 6
SITT	CV = 60%	Log normal	Table 6
Small intestinal surface area	9 fold variation in a uniform distribution (mean*3 – mean/3). Each individual had the same surface enhancement factor applied.	Uniform	Table 6
GFR (specific)	CV = 25%	Normal	Table 6
TS (specific)	CV = 61%	Log normal	Table 13
CYP2D6	CV = 66%		Determined from Dorne et al [106] in which the inter-individual variability for various phase I, II and renal metabolic processes was assessed with various probe substrates.
Biliary	CV = 30%	Log normal	Table 27

3.6 Pediatric PK predictions for BCS class 3 compounds

3.6.1 Acyclovir

Workflow 1 of acyclovir

Development of the rat PBPK model following IV administration

A rat PBPK model simulation was created for the drug acyclovir, based on rat IV studies conducted by Ogiso et al [108], and Ye et al [109], in which rats were administered a 1 mg/kg IV bolus. All rat specific physiological parameters incorporated within PK-Sim were applied to the PBPK model simulation. Various *in vitro* physicochemical properties required for initial input into the model, such as fu in rat, LogP, pKa, and molecular weight, were obtained from literature and incorporated into the rat model simulation (Table 35). Once the initial, or naïve, PBPK rat model had been simulated, both experimentally derived *in vivo* data sets were superimposed upon the simulated plasma concentration profile (Figure 41). Given that the simulated plasma concentration profile did not reflect the curve shape of the observed data, model goodness of fit was achieved via numerical optimization (Figure 41). A numerical optimization of LogP determined -0.75 as the best value of input in order to match line shape.

Table 35. Physicochemical initial parameter inputs for acyclovir

Initial Input	**Initial Value**	**reference**	**Final value in model**
Fu (rat)	0.67	[110]	0.67
Fu (human)	0.85	[111]	0.85
LogP (experimental)	-0.95	[111, 112]	-0.75
Molecular weight	225.21	[12, 113]	225.21
pKa	9.5 (acid) 2.16 (base)	[114]	9.5 (acid) 2.16 (base)
Solubility	2.62 mg/ml	[62]	2.62 mg/ml
Dissolution profile	50% dissolved in 10min	[115]	50% dissolved in 10min

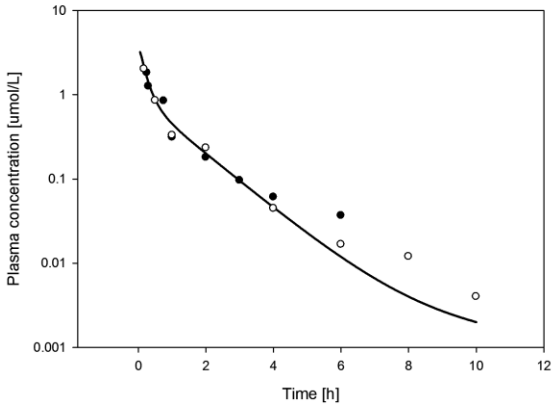

Figure 41. Simulated (line) and observed (symbols) plasma concentration data following a 1 mg/kg IV bolus of acyclovir in rats. Observed data taken from Ogiso et al [108], and YE et al [109]

Development of the acyclovir adult PBPK model following oral administration

Three adult oral PBPK models were simulated for the drug acyclovir. Three experimental studies were obtained from literature following a 400 mg oral dose of acyclovir [116-118]. For each adult oral PBPK model simulation, physicochemical input parameters and optimized LogP remained unchanged from the optimized rat IV model (Table 35). Organism specific anatomy and physiology parameters incorporated into PK-Sim, pertaining to an average 30 year old European male, free fraction of acyclovir in humans, solubility and dissolution data were applied to the human oral model. CL of acyclovir was designated completely as a renal process, as there was not any literature reference found to identify metabolite excreted via urine or feces following an oral dose administration. For this workflow, it was therefore assumed there was no significant contribution of hepatic CL pathways towards the metabolism of acyclovir. Once each PBPK adult oral model had been simulated, *in vivo* data from the three observed studies were superimposed upon the simulated plasma concentration profile (Figure 42a-c) [116-118]. Model parameters influencing absorption (i.e. P_{int}) (Table 36), and total renal plasma CL were numerically optimized respective to each simulation, to match observed AUC within ±10%.

CL pathway partitioning

Within the adult PBPK model, CL was input as a renal process only, as there was not any literature available to support hepatic metabolism of acyclovir following an oral dose. Subsequently, renal CL was proportioned into individual pathways responsible for acyclovir CL as understood from literature. In a mass balance study conducted by Vergin et al, 24 patients received a 400 mg oral dose of acyclovir. Approximately 15.4% ± 4.7 of the total acyclovir dose administered was recovered as unchanged in urine [118]. There were no significant data found to support metabolites of acyclovir recovered following an oral dose administration only. In the study, total renal CL was greater than GFR, thereby indicating that a

significant portion of acyclovir is eliminated via active TS by renal transporters; as a result, GFR and TS CL compartments were incorporated into the PBPK model. Although there are many uncertainties with respect to bioavailability estimates within an oral model when lacking IV data, renal CL input parameters were fixed to reflect an observed fe of 15.4% ± 4.7 as closely as possible. The optimization of P_{int}, and CL to match observed AUC, may alter the final fe value based on the model's ability to predict bioavailability. The arithmetic mean of optimized CL and absorption parameters were incorporated into a final adult model.

Table 36. Numerically optimized P_{int}, TS CL_{spec} for each of three simulated profiles following oral dose administration in adults

Oral dose administration simulation	**P_{int} (cm/min)**	**TS CL_{spec} (1/min)**
Bangaru et al. [116]	3.50 E-07	0.659
Vergin et al. [118]	3.04 E-07	0.527
Yuen et al. [117]	2.76 E-07	0.654
Mean	**3.1 E-07**	**0.613**

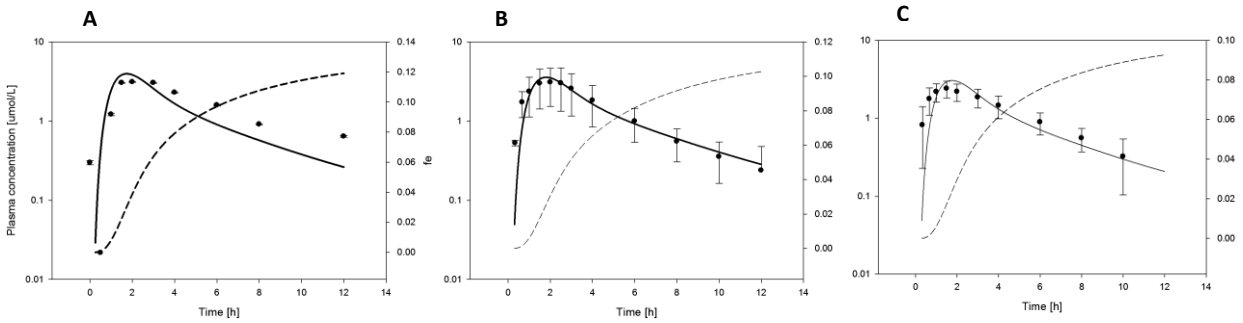

Figure 42. Simulated (line) and observed (symbols) plasma concentration data following a 400 mg oral dose of acyclovir, including fe (dotted). Observed data taken from A) Bangaru et al [116] B) Vergin et al [118] C) Yuen et al [117]

Development of an adult oral population PBPK model

For the population model of acyclovir, 100 virtual individuals were generated within an age range of 18-55 years. Once the population model had been generated, the population was administered a 400 mg oral dose to reflect the dosing protocol in observed studies [116] [117] [118]. Five aspects of population variability were factored into the adult population model as obtained from literature (Table 37). Physicochemical parameters were not further modified from the optimized adult PBPK model. Once the population model had been simulated to generate an arithmetic standard deviation curve, observed data obtained from each of the experimental observed studies was superimposed onto the model (Figure 43). Given that the majority of data points fell within one standard deviation of the mean population model, it was determined sufficient to progress to pediatric development.

Table 37. Population variability incorporated into the adult population model simulations of acyclovir			
Pathway	**Value**	**Distribution**	**Notes and reference**
GET	CV % = 24%	Log normal	Table 6
SITT	CV = 22.5%	Log normal	Table 6
Small intestinal surface area	9 fold variation in a uniform distribution (mean*3 – mean/3). Each individual had the same surface enhancement factor applied.	Uniform	Table 6
GFR (specific)	CV = 25%	Normal	Table 6
TS (specific)	CV = 30%	Log normal	Table 13

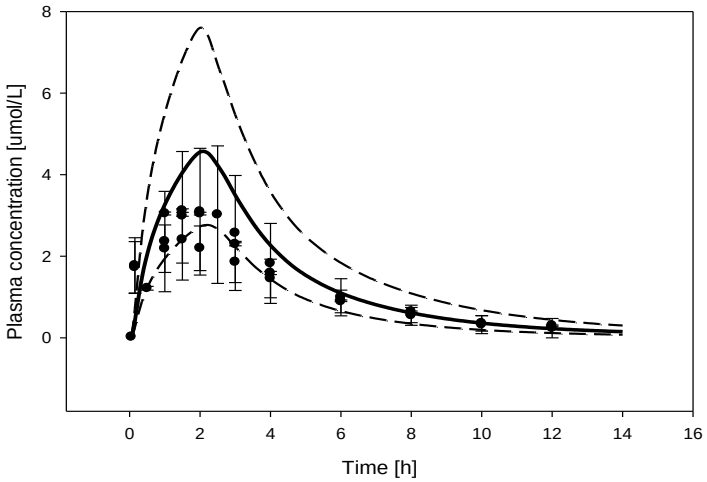

Figure 43. Simulated mean (central line) and standard deviation (dotted line) plasma concentration data in 100 individuals as compared to observed (symbols) mean and standard deviation plasma concentration data following data following a 400 mg oral dose of acyclovir in adults.

Workflow 2 of acyclovir

Development of the human PBPK model following IV administration

An adult IV PBPK model was simulated for acyclovir based on the dosing protocol from an IV infusion study conducted in adults by Soul-Lawton et al, in which 350 mg of acyclovir was administered over a 1 hour period to 12 healthy participants [119]. Similar to the rat IV PBPK model, organism specific and drug specific physicochemical parameters (Table 35) were applied to the model.

Study findings by Soul-Lawton et al suggest acyclovir has an fe of 0.87 ± 0.19 following an IV dose, with an additional 13.78% ± 4.2% of the dose recovered as 9-(carboxymethoxymethyl)guanine (CMMG), as well as <2% of the dose recovered as 8-hydroxy-9-[(2-hydroxyethoxy)methyl]guanine (8-OHACV) acyclovir metabolites [119]. Since the recovery of 8-OHACV was <2%, it was not included within the model, as it will not provide a significant contribution towards clearance. Due to the recovery of acyclovir metabolite CMMG, a hepatic component was incorporated into the IV model. Due to a lack of knowledge regarding the exact enzyme responsible for acyclovir metabolism into CMMG, the specific ontogeny of said enzyme was not incorporated into the model. This may affect the models ability to accurately quantify the variability of CL in adults and pediatrics as the model progresses. Since renal CL far exceeded creatinine CL within the observed IV study, it is apparent much of the compound undergoes TS [118]. Due to multiple tandem processes of renal CLs, GFR fraction was set to a fixed value of 1 within the simulation, whereas TS was subject to further optimization to reach a fe value close to 0.87. Once the PBPK adult IV base model had been simulated following a 350 mg IV infusion, experimentally derived *in vivo* data from Soul-Lawton et al [119] was superimposed upon the simulated plasma concentration profile (Figure 44). Given that the simulated data points did not reflect curve shape and exposure of the experimental data, model parameters influencing distribution (LogP) and CL were numerically optimized (Table 37).

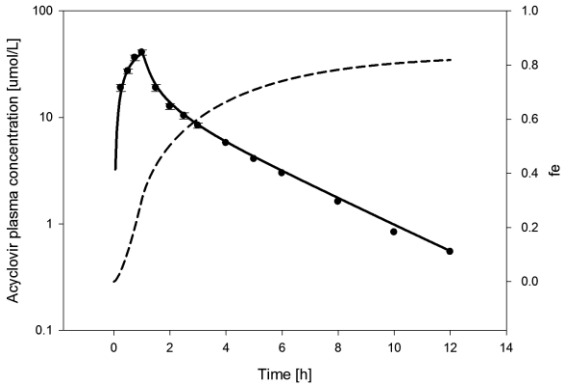

Figure 44. Simulated (line) and observed (symbols) plasma concentration data in adults following a 350 mg IV infusion of acyclovir. Observed data taken from [119].

Development of the acyclovir adult PBPK model following oral administration

Similarly to Workflow 1, three adult oral PBPK models were simulated to reflect the dosing protocol of three observed obtained from literature. All physicochemical input parameters, optimized LogP and CL remained unchanged from the optimized adult IV model. Organism specific anatomy and physiology input parameters were incorporated into PK-Sim, for a mean European 30 year old male. CL parameters were not changed from the adult IV model. Each PBPK model was numerically optimized for absorption (P_{int}) against the corresponding experimental study (Table 38, Figure 45 a-c) [116-118]. The mean P_{int}, TS_{spec}, and hepatic CL_{spec} values obtained from the IV and oral models were incorporated into a final mean adult simulation, which was further utilized in building an adult population model.

Table 38. Numerically optimized P_{int}, TS, and hepatic CL parameters for acyclovir within the standard workflow

Simulation specific adult oral Study	**P_{int} (cm/min)**	**TS_{spec} (1/min)**	**Hepatic CL_{spec} (1/min)**	**LogP (log units)**
Soul-Lawton et al [119]		0.779	0.0397	-0.68
Bangaru et al. [116]	1.73 E-04			
Vergin et al. [118]	1.70 E-04			
Yuen et al. [117]	1.67 E-04			
Mean	**1.70 E-04**			

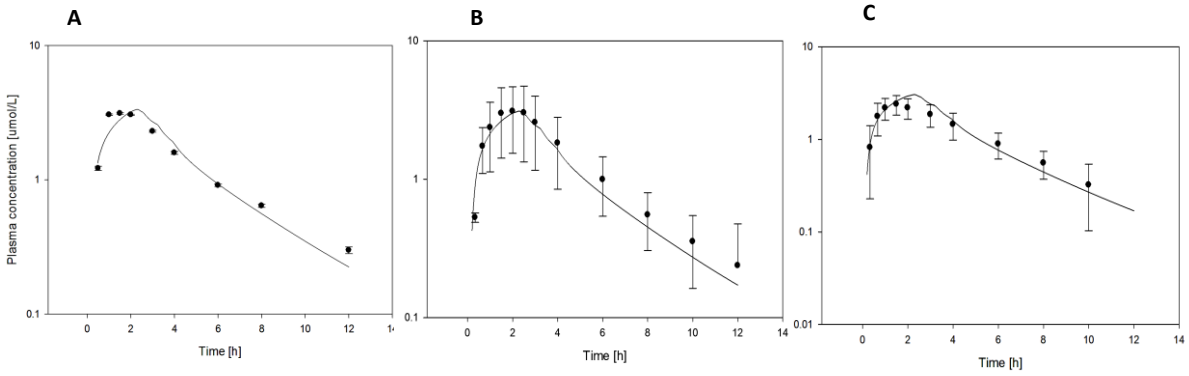

Figure 45. Simulated (line) and observed (symbols) plasma concentration data following a 400 mg oral dose of acyclovir. Observed data taken from A) Bangaru et al [116] B) Vergin et al [118] C) Yuen et al [117]

Development of an adult oral population PBPK model

Similarly to Workflow 1, 100 virtual individuals were created within an age range of 18-55 years. Once the population was created, a 400 mg oral dose was applied to the model, as well as six aspects of population variability as obtained from literature (Table 39). A hepatic CL CV of 30% was added to the population model, based on CMMG recovery reported in Soul-Lawton et al [119]. Once the population model had been generated, observed data from each of the three observed studies were superimposed onto the population model (Figure 46). Given that the majority of data points fell within one standard deviation of the mean population model, it was determined sufficient to progress to pediatric development.

Table 39. Population variability incorporated into population model simulations for acyclovir			
Pathway	**Value**	**Distribution**	**Notes and reference**
GET	CV = 24%	Log normal	Table 6
SITT	CV = 22.5%	Log normal	Table 6
Small intestinal surface area	9 fold variation in a uniform distribution (mean*3 – mean/3). Each individual had the same surface enhancement factor applied.	Uniform	Table 6
GFR (specific)	CV = 25%	Normal	Table 6
TS (specific)	CV = 30%	Log normal	Table 13
Hepatic CL_{spec}	CV = 30%	Log normal	Table 19

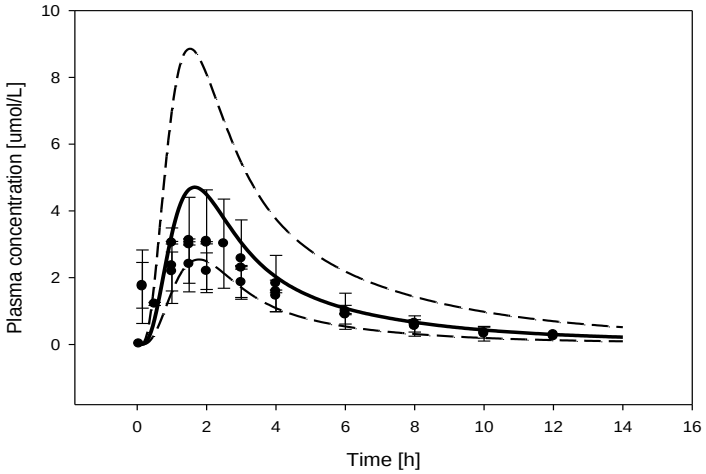

Figure 46. Simulated mean (central line) and standard deviation (dotted line) plasma concentration data in 100 individuals as compared to observed (symbols) mean and standard deviation plasma concentration data following data following a 400 mg oral dose of acyclovir in adults. Observed data taken from Bangaru et al [116], Vergin et al [118], Yuen et al [117]

Development of the pediatric population model for Workflow 1 and 2

A pediatric study investigating the pharmacokinetics of acyclovir in infants and children, conducted by Sullender et al [120] was obtained from literature. In the study, a 600 mg/m^2 dose of acyclovir was administered to 13 children, divided into two groups based on age. The first group consisted of 0.5-4 year olds with a mean body surface area (BSA) of 0.6 m^2, whereas the second group consisted of 4-7 year olds with a mean BSA of 0.8 m^2. As a result, the two groups of participants received an approximate mean dose of 1000 mg, and 750 mg respectively. This experimental study served as the comparative reference for the assessment of the utility of Workflow 1 in predicting the PK profile in pediatrics for acyclovir, as compared to the standard workflow. 1000 pediatric individuals were randomly selected from the reference population to reflect the age demographic of the observed studies. Variability with respect to Anatomy, physiology, physicochemical data, absorption, distribution and CL were incorporated within the model

(Table 40). The lack of ontogeny and variability information pertaining to the enzyme responsible for acyclovir metabolism may lead to inaccurate clearance predictions by the model.

Table 40. Population variability parameters incorporated into the pediatric population model for Workflow 1 and 2

Pathway	**Value**	**Distribution**	**Notes and reference**
GET	CV = 60%	Log normal	Table 6
SITT	CV = 60%	Log normal	Table 6
Small intestinal surface area	9 fold variation in a uniform distribution (mean*3 – mean/3). Each individual had the same surface enhancement factor applied.	Uniform	Table 6
GFR (specific)	CV = 25%	Normal	Table 6
TS (specific)	CV = 61%	Log normal	Table 15
Hepatic CL_{spec}	CV = 30%	Log normal	Table 19

3.6.2 Cimetidine

Workflow 1 of cimetidine

Development of the Rat PBPK model following IV administration

A rat PBPK model was created to simulate a 40 mg/kg IV bolus dose administration of cimetidine, based on the observed study conducted by Adedoyin et al [121]. All rat specific physiology parameters incorporated within PK-Sim were applied to the PBPK model. Various drug specific physicochemical properties required for initial input into the model were obtained from literature and applied to the model (Table 41). Once the PBPK rat model had been simulated, experimentally derived *in vivo* data was superimposed upon the simulated plasma concentration profile, as obtained from Adedoyin et al (Figure 47) [121]. A numerical optimization of LogP determined 1.84 as the best value of input in order to achieve observed line shape.

Table 41. Physicochemical parameters of cimetidine for initial input into Workflow 1 and 2

Input	Value	Reference	Value in final model
fu_{human}	0.8	[121]	0.8
fu_{rat}	0.8	[121]	0.8
Molecular weight	252.34	[39, 122]	252.34
pKa	6.8 (base)	[39, 122]	6.8 (base)
Solubility	11.3 mg/ml @ pH 9.8	[39, 122]	11.3 mg/ml @ pH 9.8
Dissolution profile	50% in 15 min	[123]	50% in 15 min
Dose administration	IV 40 mg /kg	[121]	IV 40 mg /kg
LogP (log units)	0.4	Optimized	1.84

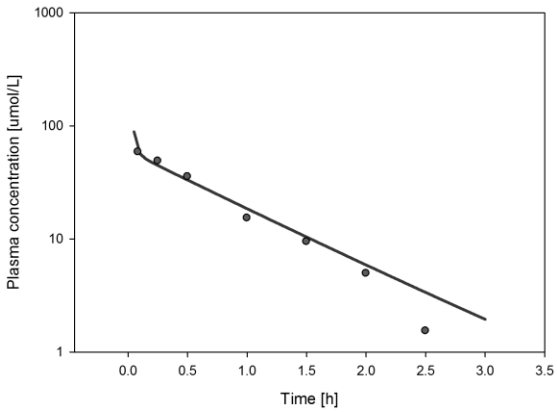

Figure 47. Simulated (line) and observed (symbols) plasma concentration data following a 40 mg/kg IV dose of cimetidine in rats; based on observed data from Adedoyin et al [121].

Development of the cimetidine adult PBPK model following oral administration

Using the rat IV model as a base, all species specific inputs were changed to reflect an average 30 year old European human male. This included anatomical and physiological inputs. All drug specific inputs were maintained as in the rat PBPK model with the addition of compound specific solubility and dissolution dat. Two adult oral PBPK models were simulated for the drug cimetidine, following a 200 mg oral dose of cimetidine, and were based on two experimental studies obtained from literature, in which a sample group of participants were administered oral doses of 200 and 400 mg cimetidine respectively [122, 124]. cimetidine has been observed to follow dose dependent kinetics when dosing within the therapeutic range, as a result, observed data from the study following a 400 mg oral dose of cimetidine was dose normalized to 200 mg [122]. Observed derived data was superimposed upon the simulated profile to allow for goodness-of fit assessment. The simulated profile was optimized numerically for parameters of absorption (P_{int}), and renal and hepatic CL (Table 42, Figure 48a-b).

CL pathway partitioning

Once the adult oral PBPK model had been optimized, CL pathways were further refined. Experimentally, total renal CL was found to be greater than GFR, thereby indicating that a significant portion of cimetidine is eliminated via active TS by renal transporters. As a result, GFR and TS were added to the adult oral model in place of an overall renal CL as identified from the naïve adult oral model. Basic drugs are generally attributed to greater hepatic metabolism, however studies suggest the very low LogP of cimetidine may contribute to its unusually high level of renal CL [125]. Only, 10-20% of the administered oral dose was excreted in urine as sulfide metabolites due to various hepatic enzymes [122, 124]. As a result, the generic hepatic component applied initially was unchanged within the model. Due to a lack of knowledge regarding the exact enzyme responsible for cimetidine metabolism into sulfide metabolites, the specific ontogeny of said enzyme(s) was not incorporated into the model. This may affect the models ability to accurately quantify the variability of CL in adults and pediatrics as the model progresses. CL parameters were optimized for each study and an arithmetic mean was obtained and applied to a final mean adult oral PBPK model (Table 42, Figure 48).

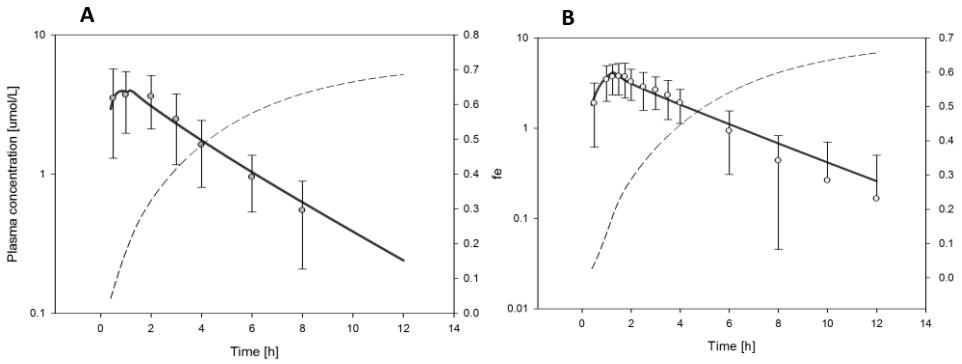

Figure 48. Simulated (line) and observed (symbols) plasma concentration data following a 200 mg oral dose of cimetidine in adults. Observed data taken from A) Yamasaki et al [124] B) Jantratid et al [122] fe (dotted) included

Table 42. Numerically optimized P_{int}, TS CL_{spec}, and hepatic CL parameters based on observed data			
Study dose before dose normalization (mg)	**P_{int} (cm/min)**	**TS CL_{spec} (1/h)**	**hepatic CL_{spec} (1/min)**
200 [124]	1.75 E-04	2.285	0.0827
400 [122]	1.05 E-04	2.125	0.0922
Mean	**1.40 E-04**	**2.205**	**0.0875**

Development of an adult oral population PBPK

For the population model of cimetidine, 100 virtual individuals were generated within an age range of 18-55 years. A 200 mg oral dose was administered to each individual within the population to reflect dosing protocol from the observed studies [124] [122]. Six aspects of population variability were factored into the adult population model (Table 43) as obtained from literature. The lack of ontogeny and variability information pertaining to the enzyme(s) responsible for cimetidine metabolism may lead to inaccurate clearance predictions by the model. Physicochemical parameters were not further modified from the optimized adult PBPK model. Once the population model had been simulated, an arithmetic mean and standard deviation curve was generated to assess the characterization of inter-individual variability. Observed data was superimposed onto the model (Figure 49). Given that the majority of data points fell within one standard deviation of the mean population model, it was determined sufficient to progress to pediatric model development.

Table 43. Population variability incorporated into the adult population model simulation of cimetidine			
Pathway	**Value**	**Distribution**	**Notes and reference**
GET	CV = 24%	Log normal	Table 6
SITT	CV = 22.5%	Log normal	Table 6
Small intestinal surface area	9 fold variation in a uniform distribution (mean*3 – mean/3). Each individual had the same surface enhancement factor applied.	Uniform	Table 6
GFR (specific)	CV = 25%	Normal	Table 6
TS (specific)	CV = 30%	Log normal	Table 15
Hepatic (specific)	CV = 30%	Log normal	Table 19

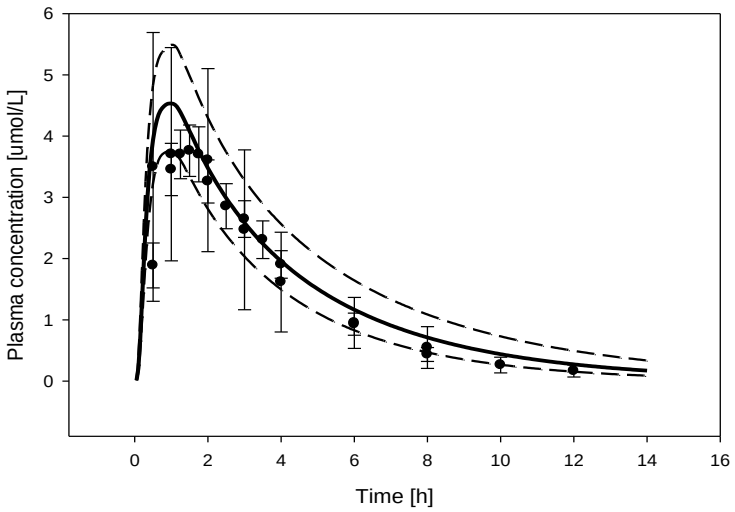

Figure 49. Simulated mean (central line) and standard deviation (dotted line) plasma concentration data in 100 individuals as compared to observed (symbols) mean and standard deviation plasma concentration data following data following a 200 mg oral dose of cimetidine in adults.

Workflow 2 of cimetidine

Development of the human PBPK model following IV administration

An adult IV PBPK model was simulated for the drug cimetidine based on the dosing protocol from an adult IV study conducted by Jantratid et al, in which 300 mg of cimetidine was administered as an IV bolus [122]. Organism specific anatomy and physiology parameters incorporated into PK-Sim, pertaining to an average 30 year old European male were used. Physicochemical primary input parameters such as fu, LogP, pKa, and molecular weight were obtained from literature (Table 41). Once the PBPK adult IV base model had been simulated, experimentally derived *in vivo* data was superimposed upon the simulated plasma concentration profile [122]. LogP was numerically optimized to 0.2 log units. (Figure 50, Table 44).

Mass balance studies following IV administration of cimetidine, conducted by Jantratid et al and Somogyi et al, found that approximately 50-80% of intravenously administered cimetidine had been recovered in urine as unchanged drug, approximately 20-40% recovered as a sulfide metabolite, and the remainder recovered unchanged in feces [122, 125]. A hepatic CL component, TS renal component, and fixed GFR fraction of 1 were applied to the PBPK model. There was no biliary CL component included in the model, as multiple hepatic processes may lead to an over-prediction of CL within the PBPK model, thereby generating erroneous AUC estimates.

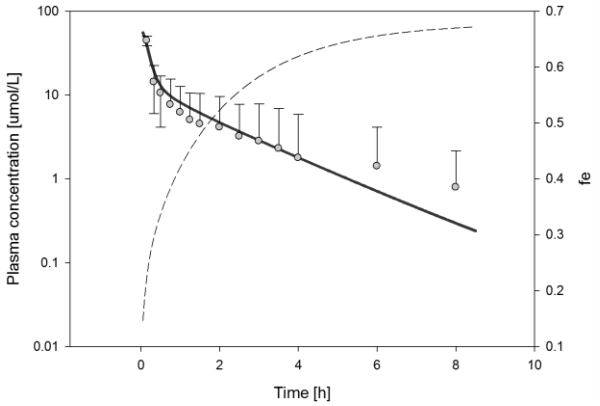

Figure 50. Simulated (line) and observed (symbols) plasma concentration data following an IV dose of cimetidine in adults. Observed data was taken from Jantratid et [122].

Development of the adult PBPK model following oral administration

An adult oral model was simulated to reflect demographic and dosing regimen of two observed obtained from literature [122, 124]. All physicochemical input parameters such as pKa, molecular weight, solubility, and optimized LogP remained consistent between the optimized adult IV model and each adult oral model. Once the adult oral PBPK model had been simulated following a 200 mg oral dose,

experimentally derived *in vivo* data was superimposed upon the simulated plasma concentration profiles [122, 124]; model parameters influencing absorption (P_{int}) were numerically optimized (Table 44, Figure 51a-b). A mean P_{int} value was calculated from each of the optimized adult oral PBPK models, and was incorporated into a final mean adult simulation, which was further utilized in building an adult population model.

Table 44. Numerically optimized parameters of LogP, P_{int}, TS, and hepatic CL spec

Study dosing before dose normalization (mg)	**P_{int} (cm/min)**	**TS_{spec}**	**Hepatic CL_{spec}**	**LogP (log units)**
300 mg IV bolus [121]		1.83	0.124	0.2
200 [124]	2.75 E-06			
400 [122]	2.25 E-06			
Mean	**2.50 E-06**			

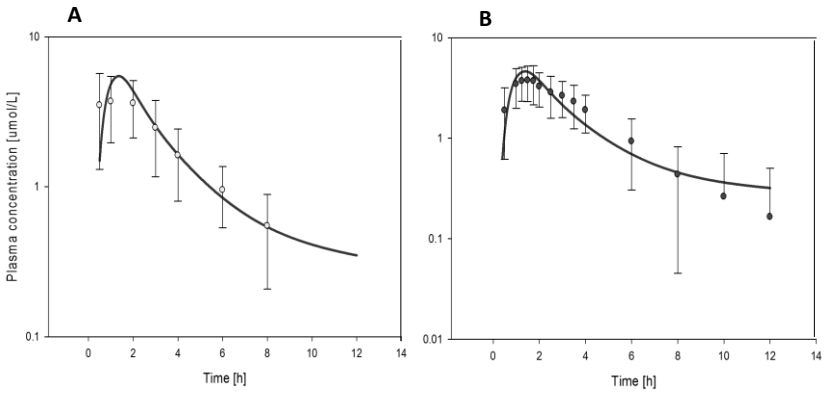

Figure 51. Simulated (line) and observed (symbols) plasma concentration data following a 200 mg oral dose of cimetidine in adults. Observed data taken from A) Yamasaki et al [124]B) Jantratid et al [122]

Development of an adult oral population PBPK model

An adult population simulation was generated within PK-Sim to assess the inter-individual variability of cimetidine exposure in adults following a 200 mg oral dose administration to 100 adults. Since there were no additional CL compartments added to Workflow 2, identical aspects of population variability were factored into the Workflow 2 adult population model as in Workflow 1 (Table 43).Once the population model had been simulated to generate an arithmetic standard deviation curve, observed data obtained from each of the experimental observed studies was superimposed onto the model (Figure 52). Given that the majority of data points fell within one standard deviation of the mean population model, it was determined sufficient to progress to pediatric development.

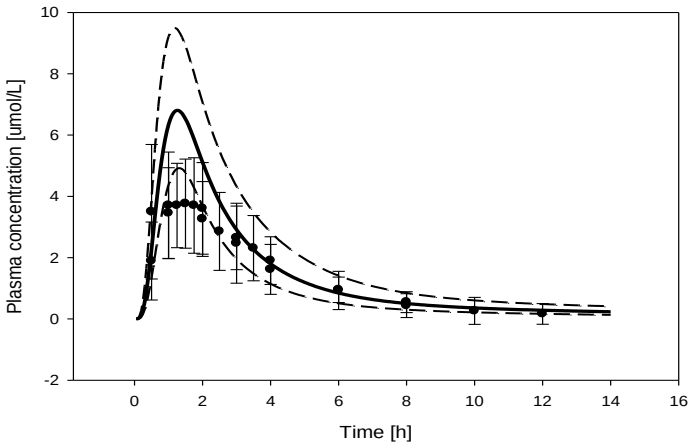

Figure 52. Simulated mean (central line) and standard deviation (dotted line) plasma concentration data in 100 individuals as compared to observed (symbols) mean and standard deviation plasma concentration data following data following a 200 mg oral dose of cimetidine in adults.

Development of the pediatric population model for Workflow 1 and 2 of cimetidine

A pediatric study investigating the pharmacokinetics of cimetidine in infants and children between the ages of 4-16 years was obtained from literature. In the study, patients received a 20 mg/kg dose, of oral cimetidine (n = 11) [126]. This experimental study served as the comparative reference for the assessment of the utility of Workflow 1 in predicting the PK profile in pediatrics for cimetidine, as compared to the standard workflow.

Up to a maximum of 1000 individuals within the specified age range of the observed study were randomly selected from the reference pediatric population for cimetidine. All drug-specific parameters were equal to those of the final cimetidine simulation. Similar to methods discussed previously, six aspects of population variability were factored into the pediatric population model, for workflows 1 and 2, as obtained from literature (Table 45). Once variability had been successfully incorporated into the pediatric population following a 20 mg/kg dose, PK parameters of $AUC_{0\text{-end}}$, Cmax, and Tmax following the observed study protocol dosing regimen were obtained for comparison to corresponding observed values and further data analysis.

Table 45. Population variability parameters incorporated into the pediatric model for Workflow 1 and 2 of cimetidine

Pathway	**Value**	**Distribution**	**Notes and reference**
GET	CV = 60%	Log normal	Table 6
SITT	CV = 60%	Log normal	Table 6
Small intestinal surface area	9 fold variation in a uniform distribution (mean*3 – mean/3). Each individual had the same surface enhancement factor applied.	Uniform	Table 6
GFR (specific)	CV = 25%	Normal	Table 6
TS (specific)	CV = 61%	Log normal	Table 15
Hepatic(specific)	CV = 30%	Log normal	Table 19

3.6.3 Azithromycin

Workflow 1 of azithromycin

Development of the Rat PBPK model following IV administration

A rat PBPK model simulation was created to simulate a 20 mg/kg intravenous bolus dose administration of azithromycin based on two observed studies obtained from literature [81, 127], [128]. Physicochemical properties were obtained from literature and incorporated into the rat PBPK simulation (Table 46). Studies by Shepard et al [128], as well as Tananika et al [127] suggest that azithromycin metabolism in the rat is due primarily to hepatic mechanisms. Although rat CL is not utilized within the workflow as a model predictor, hepatic CL was reflected in the rat PBPK model CL processes for model fitting purposes.

Once rat PBPK model had been simulated, both experimentally derived *in vivo* data sets were superimposed upon the simulated plasma concentration profile. Model goodness of fit was achieved via numerical optimization of LogP (Figure 53). A numerical optimization of LogP determined 0.36 as the best value of input in order to achieve optimal line shape in the rat model.

Table 46. Physicochemical initial parameter inputs for azithromycin in the Rat and adult model

Parameter	**Value**	**Reference**	**Final value**
Molecular weight (g/mol)	748.98	[129]	748.98
LogP (log units)	3	[129]	0.36
Plasma protein	Albumin	[130]	Albumin
Fu rat	0.84	[128]	0.84
Fu human	0.88	[130]	0.88
pKa (acidic)	12.43	[129]	12.43
pKa (base)	9.57	[129]	9.57
Solubility in water (aqueous)	50 mg/mL @ pH 7	[131]	50 mg/mL @ pH 7
Dissolution	80% in 50 minutes	[132]	80% in 50 minutes

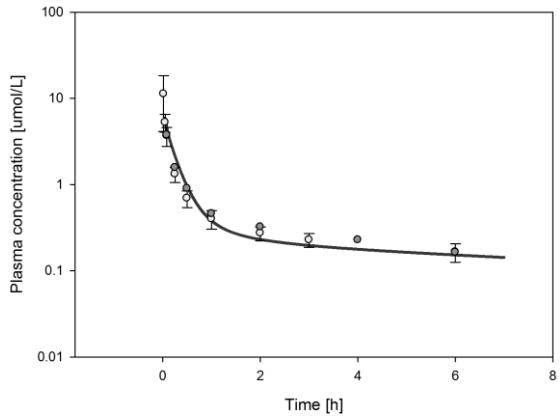

Figure 53. Simulated (line) and observed (symbols) azithromycin Rat IV plasma concentration profile optimized for LogP, following 20 mg/kg IV bolus dose administration of azithromycin

Development of the azithromycin adult PBPK model following oral administration

Using the rat IV model as a base, all species specific inputs were changed to reflect an average 30 year old European human male. This included anatomical and physiological inputs. All drug specific inputs were maintained as in the rat PBPK model with the addition of compound specific solubility and dissolution data. Three adult oral PBPK models were simulated for the drug azithromycin based on dosing protocol of three existing observed studies, in which participants received a 500 mg oral dose [133-135]. CL of azithromycin was designated completely within generic hepatic and renal systems.

Once each PBPK adult oral model had been simulated following a 500 mg, oral dose administration, experimentally derived *in vivo* data from three observed studies [133-135], were superimposed upon the simulated plasma concentration profile. Model parameters influencing absorption (P_{int}) and CL were numerically optimized respective to each simulation (Table 47, Figure 54 a-c).

CL pathway partitioning

Pharmacokinetic studies following oral dose administration suggest azithromycin is a substrate of CYP3A4 and is primarily recovered in bile fluid unchanged and in feces as metabolites [136], whereas 4.5% of the dose is excreted in urine unchanged (i.e. fe=0.045) [130]. In a pharmacokinetic study conducted by Fould et al [136], biliary CL was determined to be the primary route of elimination as concentration in bile fluids was greater than plasma concentrations [136]. Within the observed study, total renal CL was greater than GFR, thereby indicating that a portion of azithromycin is eliminated via active TS by renal transporters. As a result, CL was modeled as 57.3% biliary CL, 38.2% CYP3A4 CL and 4.5% as renal CL. Parameters pertaining to biliary CL, CYP3A4 CL_{spec}, and TS were numerically optimized so that model CL could reflect dose exposure as closely to the observed studies as possible (Table 47). Due to limitations of bioavailability estimates within the Workflow 1, fe values within the

model did not truly reflect observed data. The mean value of the optimized TS and P_{int} parameters from of three adult oral simulations (Table 47, Figure 54a-c), were incorporated into a final mean adult model, which was utilized for the subsequent adult population model.

Table 47. Optimized parameters of P_{int}, biliary CL, CYP 3A4 CL and TS within Workflow 1 of azithromycin

Study	P_{int} (cm/min)	Biliary CL_{spec} (1/min)	CYP 3A4 CL_{spec} (1/min)	TS spec (1/min)
Najib [135]	9.6 E-5	0.65	0.5	0.228
Matzneller [133]	1.45 E-4	0.73	0.65	0.251
Iqbal [134]	1.05 E-4	0.72	0.3	0.297
Mean	**1.15 E-4**	**0.7**	**0.48**	**0.26**

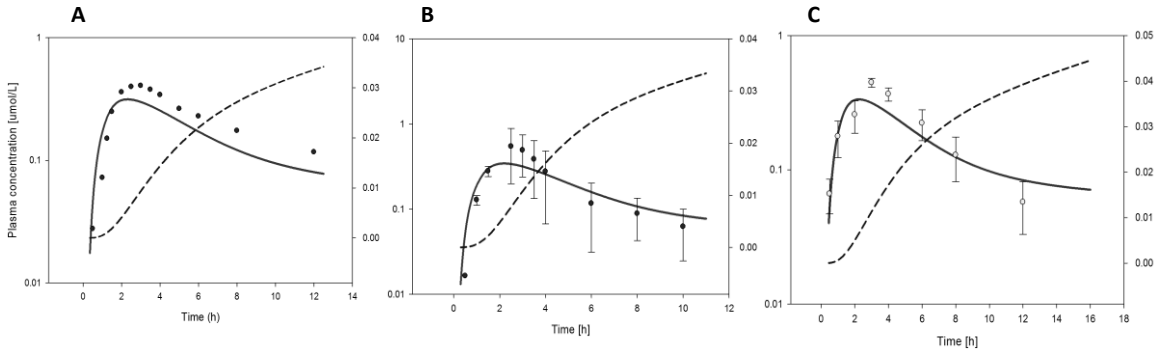

Figure 54. Simulated (line) and observed (symbols) plasma concentration data following 500 mg of oral azithromycin. Observed data obtained from A) Najib et al [126] B) Matzneller et al [124] C) Iqbal et al[125]. Fe (dotted) included

Building the mean adult population model

Similar to methods discussed previously, an adult population of 100 adult individuals was generated, following a 500 mg oral dose of azithromycin. Seven aspects of population variability were factored into the adult population model (Table 48) as obtained from literature. CYP3A4 variability was obtained from Dorne et al [106] following a log normal distribution with CV of 46% in adults. Once the population model had been simulated to generate an arithmetic standard deviation curve, observed data obtained from each of the experimental study was superimposed onto the simulated population profile (Figure 55). Given that the majority of data points fell within one standard deviation of the mean population model, it was determined sufficient to progress to pediatric development.

Table 48. Population variability incorporated into the adult population model simulations of azithromycin			
Pathway	**Value**	**Distribution**	**Notes and reference**
GET	CV = 24%	Log normal	Table 6
SITT	CV = 22.5%	Log normal	Table 6
Small intestinal surface area	9 fold variation in a uniform distribution (mean*3 – mean/3). Each individual had the same surface enhancement factor applied.	Uniform	Table 6
GFR (specific)	CV = 25%	Normal	Table 6
TS (specific)	CV = 30%	Log normal	Table 15
CYP3A4	CV = 46%	log normal	Determined from Dorne et al [106] in which the inter-individual variability for various phase I, II and renal metabolic processes was assessed with various probe substrates.
Biliary	CV = 30%	Log normal	Table 27

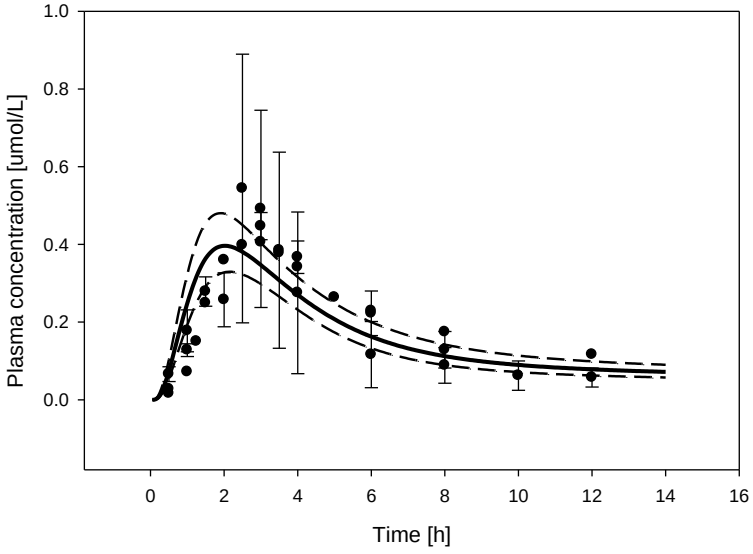

Figure 55. Simulated mean (central line) and standard deviation (dotted line) plasma concentration data in 100 individuals as compared to observed (symbols) mean and standard deviation plasma concentration data following data following a 500 mg oral dose of azithromycin in adults.

Workflow 2 of azithromycin

Development of the human PBPK model following IV administration

An adult PBPK model was simulated for the drug azithromycin based on the dosing protocol from an IV infusion study conducted in adults by Foulds et al, in which 500 mg of azithromycin was administered over 20 minutes to ten healthy male participants [130]. Organism specific input parameters pertaining to anatomy and physiology were incorporated within PK-Sim, reflecting an average 30 year old European male were applied to the model. Physicochemical primary input parameters such as fu, lipophilicity (LogP), pKa, molecular weight, and solubility at reference pH were obtained from literature (Table 46).

Study findings by Foulds et [130] al suggest the fe of azithromycin was approximately 0.12. Biliary CL is an important route of elimination for azithromycin, as majority of the administered dose is found in bile fluids as unchanged compound [136]. Similar to Workflow 1, a biliary CL component, GFR, and TS pathways of CL were defined within the model. Once the PBPK adult IV base model had been simulated following a 500 mg IV infusion, experimentally derived *in vivo* data from Foulds et al., was superimposed upon the simulated plasma concentration profile (Figure 56). Given that the simulated data points did not reflect curve shape and exposure of the experimental data, model parameters influencing distribution (i.e. LogP) and CL were numerically optimized (Table 49); Log P was numerically optimized to 2.8 log units.

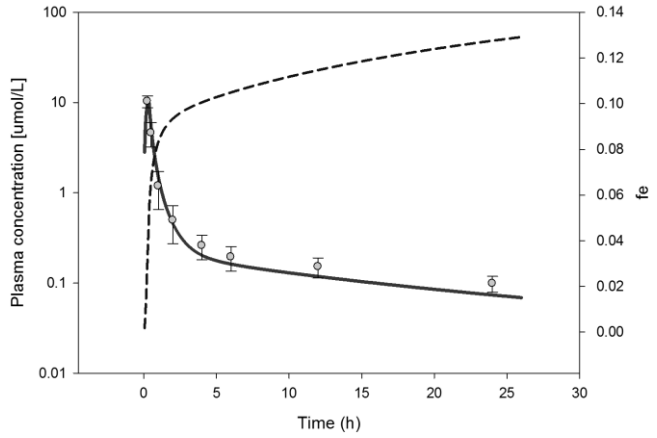

Figure 56. Simulated (line) and observed (symbols) plasma concentration data, and fe (dotted), following a 500 mg IV infusion study. Workflow 2 adult iv model optimized for distribution and CL. Observed data taken from Foulds et al[130]

Development of the azithromycin adult PBPK model following oral administration

Similarly to methods discussed in Workflow 1, three adult oral models were simulated to reflect demographic and 500 mg oral dose described in three observed studies obtained from literature [133-135]. All physicochemical input parameters such as pKa, molecular weight, optimized LogP and CL remained consistent between the optimized adult IV model and each adult oral model. Organism specific

anatomy and physiology input parameters incorporated into PK-Sim, for a mean European 30 year old male were applied to the model. Once all three PBPK adult oral models had been simulated following a 500 mg oral dose, experimentally derived *in vivo* data was superimposed upon the simulated plasma concentration profiles [133-135]. Model parameters such as P_{int} were numerically optimized until a quantitative goodness of fit was achieved (Table 49, Figure 57a-c). The mean of the optimized P_{int}, Ts_{spec}, and CYP3A4 CL_{spec} values were incorporated into a final mean adult simulation, which was further utilized in building an adult population model.

Table 49. Optimized P_{int}, CYP3A4 CL, Biliary CL, TS and Log P for cimetidine within the standard workflow

Study	**P_{int} (cm/min)**	**CYP 3A4 (1/min)**	**Biliary CL (1/min)**	**TS specific (1/min)**	**LogP (log units)**
Foulds IV [130]		6.36	7.81	0.228	2.8
Najib [135]	3.6 E-6				
Matzneller [133]	4.4 E-6				
85Iqbal [134]	3.73 E-6				
Mean	**3.91 E-6**				

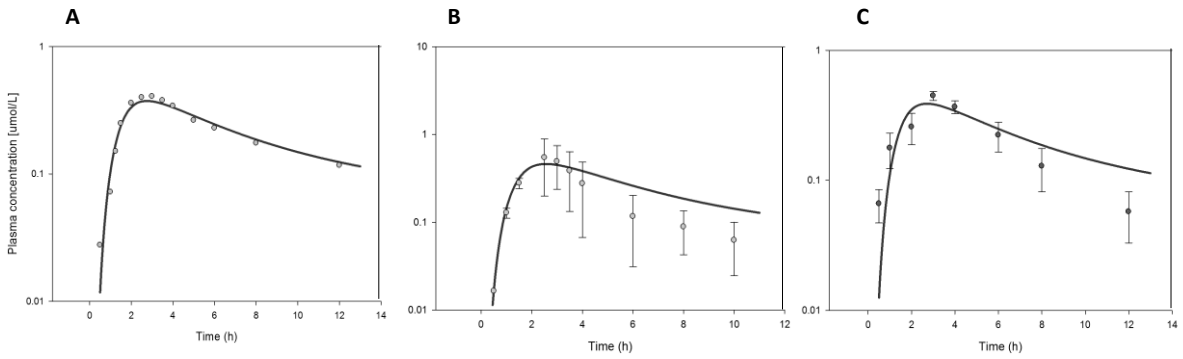

Figure 57. Simulated (line) and observed (symbols) plasma concentration data following 500 mg of oral azithromycin. Observed data obtained from A) Najib et al [126] B) Matzneller et al [124] C) Iqbal et al [125]

Development of an adult oral population PBPK model

Similar to Workflow 1, an adult population of 100 individuals was created within PK-Sim consisting of 18-55 year old males to reflect the demographics of the reference observed study participants [126] [124] [125]. Population variability factors incorporated within the model were identical to Workflow 1 (Table 43). Once the population model had been simulated to generate an arithmetic standard deviation curve, observed data obtained from each of the experimental observed studies was superimposed onto the model (Figure 58). Given that the majority of data points fell within one standard deviation of the mean population model, it was determined sufficient to progress to pediatric development.

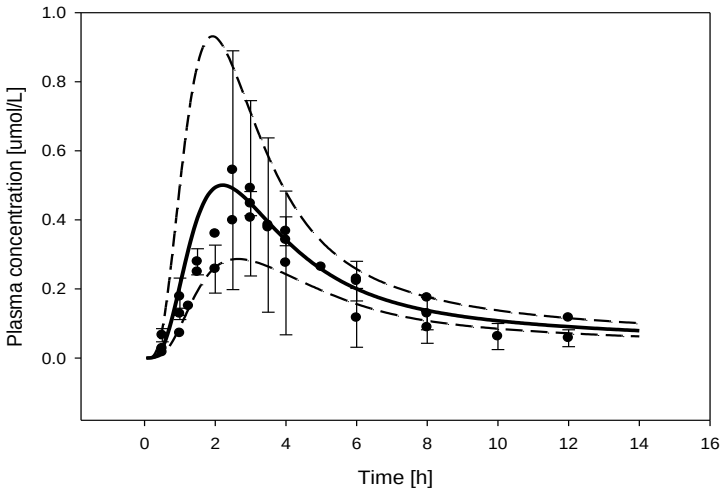

Figure 58. Simulated mean (central line) and standard deviation (dotted line) plasma concentration data in 100 individuals as compared to observed (symbols) mean and standard deviation plasma concentration data following data following a 500 mg oral dose of azithromycin in adults.

Development of the pediatric population model for Workflow 1 and 2 of azithromycin

Two pediatric studies conducted by Nahata et al were obtained from literature [137, 138]. Both studies aimed to investigate the pharmacokinetics of azithromycin in infants and children between the ages of 0.5-6 and 6-15 years of age. In the study, patients received a 5 mg/kg dose of oral azithromycin. Up to a maximum of 1000 individuals, reflecting the age range of each observed study patient population, were randomly selected from the reference pediatric population. Population variability for various parameters was factored into the pediatric population model, for workflows 1 and 2, as obtained from literature (Table 50). PK parameters of $AUC_{0\text{-end}}$, Cmax, and Tmax following the observed study protocol dosing regimen were obtained for comparison to corresponding observed values and further data analysis.

Table 50. Population variability parameters incorporated into the pediatric model for Workflow 2 of azithromycin

Pathway	**Value**	**Distribution**	**Notes and reference**
GET	CV = 60%	Log normal	Table 6
SITT	CV = 60%	Log normal	Table 6
Small intestinal surface area	9 fold variation in a uniform distribution (mean*3 – mean/3). Each individual had the same surface enhancement factor applied.	Uniform	Table 6
GFR (specific)	CV = 25%	Normal	Table 6
TS (specific)	CV = 60.7%	Log normal	Table 15
CYP3A4	CV = 50%	Log normal	Table 78
Biliary	CV = 30%	Log normal	Table 27
Hepatic	CV = 30%	Log normal	Table 19

3.7 Comparison of model predictive performance

3.7.1 Post-hoc ANOVA based tests (Aim 1 & 2)

AUC, Cmax, and Tmax for each virtual pediatric population derived from Workflow 1 and Workflow 2 were used to test the differences between parameters means from Workflow 1, Workflow 2 and observed data using analysis of variance (ANOVA) statistical methods (ie. F-test) in SAS 9.2. The F test was implemented to evaluate the null hypothesis that the three group means (Workflow 1, Workflow 2 and observed) were not statistically different. The level of siginificance for this study was chosen to be 5%, that is, differences between all three group means were considered significant if the corresponding p value was less than 0.05. The F-test was used for exploratory purposes, since the sample size of observed pediatric studies are limited, compared to a greater resolution achieved by the virtual population (i.e. 1000+ individuals per population). Subsequently, a post-hoc multiple comparisons test (ie. Tukey-Kramer test) was conducted to assess differences between means. The multiple comparison test produced corresponding p values. A $p>0.05$ suggests group means are not significantly different from each other. Inversely, a $p<0.05$ suggests it is unlikely that differences in group means are due to random sampling, and therefore we must reject the null hypothesis and conclude the means are significantly different. Unbalanced sample sizes while comparing simulated vs. observed data may potentially compromise the validity of the underlying statistical assumptions of the F-test. While the employed post-hoc test adjusts for this limitation, results from largely unbalanced cases (1000+ vs 10+) should be taken cautiously and in an exploratory manner.

The null hypotheses for aim 1 (H1), states that Workflow 1 and Workflow 2 derived predictions of pediatric PK data will not be significantly different from observed data at a significance level of 5%. Similarly, the null hypothesis for aim 2 (H2), states that PK predictions derived from Workflow 1 will not be statistically significant from Workflow 2. The primary driver for acceptance of H1 and H2 was AUC as it serves as a quantitative measure of exposure in children. In the event that H1 is accepted for both workflows and H2 is also accepted, in that both workflow derived predictions were not different from observed and were not statistically different from one another, the conclusion is that IV data is not a necessary component of the workflow for model development and models were accurate. In the event that only H1 is accepted for both workflows, workflow derived means were not different from observed, and H2 is rejected, Workflow 1 means were not equal to those of Workflow 2, we conclude that IV data is not a necessary component of the workflow for model development, and models were accurate. Similarly, if we must reject H1 either workflow, but accept H2, we may still conclude that IV data is not a necessary component for pediatric PK model development. However, if we must reject H1 for Workflow 1 but accept H1 for Workflow 2; the conclusion is that IV data is a necessary component of the workflow for model development but models were not accurate. Lastly, in the event that H1, for either workflow, as well as H2 are rejected, then it is unknown if IV data is a necessary component of model development.

3.7.2 Assessing precision and bias of model derived predictions (Aim 3)

An objective of this study was to assess the ability of pediatric PBPK models, developed under Workflow 1 and Workflow 2, to predict observed PK parameters and to assess the implications to model accuracy when there is a lack of adult IV data. This was completed in addition to Aim 1 such that differences noted in Workflow 1 or Workflow 2 vs. observed using the above mentioned statistics may note statistical differences that are not necessarily relevant. As a result, the model's ability to effectively estimate mean AUC, Tmax and Cmax within the population, was subsequently evaluated using fold error (FE), absolute average fold error (AAFE) for a measure of model precision, and average fold error (AFE) for bias as in equations (19), (20) and (21) respectively [1;2] :

$$fold\ error = \frac{predicted}{observed} \quad (19)$$

$$AAFE = 10^{\frac{1}{n}\sum \log|fold\ error|} \quad (20)$$

$$AFE = 10^{\frac{1}{n}\sum \log(fold\ error)} \quad (21)$$

The measure of AAFE quantifies the overall magnitude of predictive deviation from observed data, irrespective of over- or under-prediction. Alternately, AFE indicates over prediction (AFE>1) or under prediction (AFE<1) of model derived predictions as compared to observed data; an AFE value closest to 1 indicates greater predictive performance of a model. AUC will be the most significantly considered parameter over all others for inference of model predictive performance, as it is drives dosing estimates. Predictions from Workflow 1 and Workflow 2 will be considered reasonable if AAFE is less than 2 meaning that the prediction is within two fold of the observed data. Root mean square error (RMSE) was calculated as expressed in equation (22), to rank the overall precision of the model. A smaller RMSE value would indicate an overall better model predictive performance, as a result of smaller error in comparison to observed means:

$$RMSE = \sqrt{\left(\frac{1}{n}\sum\left(LOG\ obsi - LOG\ pred_i\right)^2\right.} \quad (22)$$

A Chi square test was calculated to compare the overall predictive performance of each workflow based on the number of model derived estimates that were <2 fold AAFE, out of a possible 25 observed studies. The Chi square test would evaluate whether Workflow 1 performed differently than Workflow 2, and if either workflow performed with an overall greater predictive performance. A resulting p-value>0.05 would indicate that Workflow 1 did not perform differently than Workflow 2 based on overall predictive performance.

3.7.3 Assessing how BCS level influences pediatric model accuracy (Aim 4)

A Chi square test was calculated to compare the workflow performance based on BCS classification. The number of pediatric PK parameters that were accurately predicted within 2 fold (i.e. AAFE<2) using Workflow 1, within each BCS class, out of a possible 25 observed study comparisons, were compared to the corresponding number of model derived PK parameters within Workflow 2. The Chi squared test allows for an inference to be made as to whether Workflow 1 or Workflow 2 has greater overall predictive performance within individual BCS classes, or if they perform similarly. If the p-value from each Chi square test is >0.05, we may infer that overall Workflow 1 did not perform differently than Workflow 2, within the respective BCS level.

4 Results

4.1 Results for BCS class I compounds

Acetaminophen

Three clinical pediatric studies were compared to simulated data. In one study, conducted by Romsing et al, a sample group of 7-13 year old patients received a 22.5 mg/kg oral dose administration of acetaminophen [139]. In another study, conducted by Walson et al, a group of 2-11 year old children received a 10 mg/kg oral dose administration of aceaminophen [140]. Lastly, in a study conducted by Hopkins et al, pediatric patients ages 0.9-3.7 years of age received a 15 mg/kg oral dose administration of acetaminophen [141]. While 1000 individuals were simulated within the age range of each study, due to the narrow age range of 0.9-3.7 years as reported by Hopkins et al [141], only 874 individuals within the simulated population fell within this criteria.

All F-tests resulted in statistically significant differences at a 5% level. Table 51 shows the corresponding p values. The subsequent post-hoc tests show that Workflow 1 and Workflow 2 AUC estimates were not significantly different from observed, in reference to the 2-11 and 0.9-3.7 yr studies, whereas all Workflow 1 means were significantly different from those derived from Workflow 2 (Table 52). There was a significant difference between all three means of Workflow 1, Workflow 2 and observed for the 7-13 years study.

As Table 53a shows, for AUC, Workflow 1 predicted less bias (AFE) and more precise (AAFE) estimates for the 7-13 yr study and Workflow 2 predicted AUC with better precision than Workflow 1 for the 0.9-3.7 yr study. Statistically, as can be seen on Table 52, Cmax was different from observed in both Workflow 1 and Workflow 2 for the 7-13 and 0.9-3.7 yr studies. Predicted Tmax was not significant for 0.9-3.7 year olds. For the exposure metrics of AUC and Cmax, Workflow 1 and Workflow 2 predictions were within the 2 fold criteria for accuracy as previously set (Table 53a). There was no clear trend with regards to bias of AUC and Cmax predictions (Table 53a). For Tmax, precision was study specific however there was a bias towards underprediction in all studies for both workflows. Observed data is shown in Table 53b.

Table 51. ANOVA F-test summary comparing model derived vs. observed means of acetaminophen

Parameter	Age (yr.)	F value	N: Observed, Workflows	p-value
$AUC_{0\text{-}inf}$	7-13 [139]	28.09	10, 1000	<0.0001
	2-11 [140]	6.96	7, 874	0.0010
	0.9-3.7 [141]	18.34	16, 1000	<.0001
Cmax	7-13 [139]	29.61	10, 1000	<.0001
	2-11 [140]	4.19	7, 874	0.0154
	0.9-3.7 [141]	12.67	16, 1000	<.0001
Tmax	7-13 [139]	33.51	10, 1000	<.0001
	2-11 [140]	103.00	7, 874	<.0001
	0.9-3.7 [141]	4.03	16, 1000	0.0180

Differences not significant at a 5% level, shown in bold.

Table 52. P-values from post-hoc multiple comparison tests, of model derived PK predictions of observed data for acetaminophen.

Workflow 1 vs. Observed			
Study group age (yr.)	$AUC_{0\text{-}inf}$	Cmax	Tmax
7-13 [139]	0.0010	<.0001	<.0001
2-11 [140]	**0.0811**	**0.3056**	<.0001
0.9-3.7 [141]	**0.9527**	<.0001	**0.1119**
Workflow 2 vs. Observed			
7-13 [139]	<.0001	<.0001	<.0001
2-11 [140]	**0.167**	**0.1953**	<.0001
0.9-3.7 [141]	**0.7169**	<.0001	**0.2395**
Workflow 1 vs Workflow 2			
7-13 [139]	<.0001	**0.0657**	**0.2938**
2-11 [140]	0.0045	0.0424	0.0251
0.9-3.7 [141]	<.0001	**0.0534**	**0.0746**

Differences not significant at a 5% level, shown in bold.

Table 53a. Precision and bias measurements for Workflow 1 and Workflow 2 derived PK estimates based on observed studies of acetaminophen

	acetaminophen Workflow 1, 7-13yr			acetaminophen Workflow 2, 7-13yr		
	$AUC_{0\text{-}inf}$	Cmax	Tmax	$AUC_{0\text{-}inf}$	Cmax	Tmax
Mean	62.6	18.8	0.83	69.9	19.1	0.84
SD	24.5	2.72	0.22	27.2	2.62	0.22
AFE	1.79	1.47	0.57	1.99	1.49	0.58
AAFE	1.80	1.47	1.76	2.00	1.49	1.72
RMSE	0.29	0.18	0.27	0.33	0.18	0.26
	acetaminophen Workflow 1, 2-11yr			acetaminophen Workflow 2, 2-11yr		
Mean	25.1	8.12	0.79	28.0	8.25	0.81
SD	10.2	1.24	0.20	11.42	1.20	0.21
AFE	0.91	1.18	0.85	1.02	1.20	0.87
AAFE	1.32	1.21	1.27	1.30	1.23	1.26
RMSE	0.15	0.10	0.12	0.15	0.10	0.12
	acetaminophen Workflow 1, 0.9-3.7yr			acetaminophen Workflow 2, 0.9-3.7yr		
Mean	32.1	11.3	0.75	35.8	11.5	0.77
SD	23.5	2.02	0.18	26.3	1.94	0.17
AFE	0.53	1.06	0.38	0.59	1.08	0.39
AAFE	1.93	1.17	2.61	1.75	1.17	2.52
RMSE	0.32	0.08	0.43	0.28	0.08	0.41

Table 53b. Observed pediatric pharmacokinetic data for acetaminophen

Study	$AUC_{0\text{-}inf}$ ± SD (ug*h/mL)	Cmax ± SD (ug/mL)	Tmax ± SD (h)
7-13 [139]	33.13 ± 10.14	12.7 ± 3.8	1.4 ± 0.5
2-11 [140]	25.9 ± 6.34	6.8 ± 1.9	0.9 ± 0.4
0.9-3.7 [141]	56 ± 13.85	10.5 ± 1.21	1.9 ± 0.54

Levofloxacin

A pediatric pharmacokinetic study conducted by Chien et al [142] was selected for comparison of simulated pediatric PK results. Children and infants who participated in the study were subdivided into five groups based on age; 0-2, 2-5, 5-10, 10-12, 12-16 years [142]. All participants received an oral dose of 7 mg/kg of levofloxacin; up to a maximum dose of 500 mg. Up to a maximum of 1000 kids per age group were simulated to reflect the demographics of the study.

F-tests for Cmax predictions in 2-5 and 5-10 year olds, and Tmax predictions for 5-10 year old children were not significant at a 5% level (Table 54) To assess which workflow was a better predictor of observed PK data in children, Workflow 1 and Workflow 2 model derived estimates were compared (Table 55). Workflow 1 and Workflow 2 did not generate significantly different Cmax and Tmax estimates (Table 55). AUC was significantly different than observed for both Workflow 1 and Workflow 2 for 2-5 year olds, and Cmax was different than observed for 0.5-2 yr and 10-12 year old subjects.

With regards to the PK metrics, all predictions were within the 2 fold criteria for accuracy as previously designated (Table 56a). There was a bias towards over-prediction of AUC by both workflows; however there was no clear trend of bias for Cmax and Tmax predictions (Table 56a). For AUC estimates, Workflow 2 consistently predicted less bias and more precise estimates. Model derived Tmax estimates were predicted with similar precision between models (Table 56a), and not significantly different from observed. Observed data is shown in Table 56b.

Table 54. ANOVA F-test summary between model derived vs. observed means of levofloxacin

Parameter	Age (yr.)	F value	N: Observed, workflows	p-value
$AUC_{0\text{-inf}}$	0.5-2	7.50	8, 297	0.0006
	2-5	29.95	8,911	<.0001
	5-10	26.67	8,1000	<.0001
	10-12	15.55	8, 581	<.0001
	12-16	20.22	8,1000	<.0001
Cmax	0.5-2	5.23	8, 297	0.0056
	2-5	0.82	8,911	**0.4387**
	5-10	0.15	8,1000	**0.8628**
	10-12	15.06	8, 581	<.0001
	12-16	2.00	8,1000	0.1361
Tmax	0.5-2	5.71	8, 297	0.0035
	2-5	19.41	8,911	<.0001
	5-10	2.53	8,1000	**0.0803**
	10-12	64.83	8, 581	<.0001
	12-16	20.55	8,1000	<.0001

Differences not significant at a 5% level, shown in bold.

Table 55. P-values from post-hoc multiple comparison tests, of model derived PK predictions of observed data of levofloxacin			
Workflow 1 vs. Observed			
Study group age (yr.)	$AUC_{0\text{-}inf}$	Cmax	Tmax
0.5-2	0.0219	0.0067	**0.1057**
2-5	0.0021	**0.4636**	<.0001
5-10	0.0051	**1**	**0.6607**
10-12	**0.0508**	<.0001	<.0001
12-16	**0.0536**	**0.9878**	<.0001
Workflow 2 vs. Observed			
0.5-2	**0.1108**	0.004	0.0294
2-5	0.0399	**0.5101**	<.0001
5-10	**0.0597**	**0.9977**	**0.5009**
10-12	**0.3023**	<.0001	<.0001
12-16	**0.2659**	**0.9942**	<.0001
Workflow 1 vs. Workflow 2			
0.5-2	0.0052	**0.7677**	0.041
2-5	<.0001	**0.8326**	**0.0729**
5-10	<.0001	**0.8504**	**0.109**
10-12	<.0001	**0.6493**	**0.358**
12-16	<.0001	**0.1129**	**0.2993**
Differences not significant at a 5% level, shown in bold.			

Table 56a. Precision and bias measurements for Workflow 1 and Workflow 2 derived PK estimates based on observed studies for levofloxacin						
levofloxacin Workflow 1 – 0.5-2yr				levofloxacin Workflow 2 – 0.5-2yr		
	$AUC_{0\text{-}inf}$	Cmax	Tmax	$AUC_{0\text{-}inf}$	Cmax	Tmax
Mean	40.1	4.80	1.33	35.9	4.83	1.31
SD	16.0	0.49	0.14	13.3	0.50	0.15
AFE	1.46	1.14	0.95	1.31	1.14	0.93
AAFE	1.50	1.14	1.10	1.41	1.15	1.11
RMSE	0.22	0.07	0.05	0.19	0.07	0.06
levofloxacin Workflow 1 – 2-5yr				levofloxacin Workflow 2 – 2-5yr		
Mean	43.7	4.73	1.31	38.7	4.71	1.30
SD	15.9	0.40	0.16	13.6	0.42	0.15
AFE	1.59	1.03	0.81	1.42	1.03	0.80
AAFE	1.61	1.07	1.24	1.47	1.08	1.25
RMSE	0.25	0.04	0.10	0.20	0.04	0.11
levofloxacin Workflow 1 – 5-10yr				levofloxacin Workflow 2 – 5-10yr		
Mean	46.9	4.64	1.29	42.0	4.65	1.28
SD	17.4	0.37	0.14	14.8	0.39	0.14
AFE	1.53	1.00	0.99	1.37	1.00	0.98
AAFE	1.56	1.07	1.08	1.44	1.07	1.08
RMSE	0.23	0.03	0.04	0.20	0.04	0.05
levofloxacin Workflow 1 – 10-12yr				levofloxacin Workflow 2 – 10-12yr		
Mean	52.9	4.69	1.28	47.2	4.71	1.26
SD	20.5	0.37	0.15	16.9	0.38	0.15
AFE	1.33	1.17	0.67	1.20	1.18	0.66
AAFE	1.41	1.17	1.50	1.33	1.18	1.52
RMSE	0.19	0.08	0.18	0.16	0.08	0.19
levofloxacin Workflow 1 – 12-16yr				levofloxacin Workflow 2 – 12-16yr		
Mean	59.7	4.74	1.28	53.6	4.77	1.27
SD	24.1	0.38	0.15	20.3	0.39	0.15
AFE	1.36	0.99	0.79	1.23	1.00	0.79
AAFE	1.43	1.06	1.27	1.34	1.07	1.28
RMSE	0.20	0.03	0.11	0.17	0.04	0.12

Table 56b. Observed pediatric pharmacokinetic data for levofloxacin			
Study	$AUC_{0\text{-}inf}$ ± SD (ug*h/mL)	Cmax ± SD (ug/mL)	Tmax ± SD (h)
0.5-2	25.80 ± 9.2	4.23 ± 1.5	1.44 ± 0.41
2-5	25.93 ± 4.75	4.55 ± 0.84	1.64 ± 0.5
5-10	28.97 ± 10.1	4.64 ± 0.4	1.33 ± 0.4
10-12	37.29 ± 9.83	3.97 ± 0.87	1.95 ± 0.88
12-16	41.36 ± 6.8	4.76 ± 0.85	1.63 ± 0.99

Lorazepam

Three clinical pediatric studies were compared to simulated data. In one study, conducted by McDermott et al, a sample group of infants ages 0.6-1 year received a mean 0.8 mg/kg IV dose administration of lorazepam [143]. In another study, conducted by Muchohi et al, a group of 2.7-7.6 year old children received a 0.1 mg/kg oral dose administration of lorazepam [144]. Lastly, in a study conducted by Chamberlain et al, pediatric patients ages 3-17 years of age received a 0.05 mg/kg oral dose administration of lorazepam [145]. While 1000 individuals were simulated within the age range of each study, due to the narrow age range of 0.6-1 years as reported by Mcdermott et al [143], only 100 individuals within the simulated population fell within this criteria.

All F-tests resulted in statistically significant differences at a 5% level. Table 57 shows the corresponding P values. Workflow 1 and Workflow 2 model derived estimates were compared to assess which workflow was a better predictor of observed PK data in children (Table 58). Workflow 1 and Workflow 2 did not generate significantly different AUC estimatesfrom observed, aside from the infant age group within Workflow 1. All Cmax estimates were significant at a level of 5%. Two of three age group predictions of $T_{½}$ within Workflow 1 were not significant from observed.

With regards to the PK metrics, all AUC and Cmax predictions were within the 2 fold criteria for accuracy as previously determined (Table 59a). There was a noticable bias towards over prediction of infant AUC estimates within both workflows, and underprediction of $T_{½}$ estimates within all age groups. Observed data is shown in Table 59b.

Table 57. ANOVA F-test summary between model derived vs. observed means of lorazepam

Parameter	Age (yr.)	F value	N: Observed, Workflows	p-value
$AUC_{0\text{-inf}}$	0.6-1 [143]	8.39	10, 100	0.0003
	0.7-7.6 [144]	26.51	11, 1000	<.0001
	3-17 [145]	70.94	15, 1000	<.0001
Cmax	0.6-1 [143]	18.07	10, 100	<.0001
	0.7-7.6 [144]	853.15	11, 1000	<.0001
	3-17 [145]	23202.8	15, 1000	<.0001
$T_{½}$	0.6-1 [143]	99.77	10, 100	<.0001
	0.7-7.6 [144]	122.84	11, 1000	<.0001
	3-17 [145]	278.02	15, 1000	<.0001
Differences significant at a 5% level, shown in bold				

Table 58. P-values from post-hoc multiple comparison tests, of model derived PK predictions of observed data for lorazepam			
Workflow 1 vs. Observed			
	$AUC_{0\text{-}inf}$	Cmax	$T_{½}$
0.6-1	0.0093	<.0001	<.0001
2.7-7.6	**0.8307**	<.0001	**0.1434**
3-17	**0.3647**	<.0001	**0.9973**
Workflow 2 vs. Observed			
0.6-1	**0.2805**	<.0001	<.0001
2.7-7.6	**0.2284**	<.0001	<.0001
3-17	**0.7685**	<.0001	0.0002
Workflow 1 vs. Workflow 2			
0.6-1	0.0024	0.0139	<.0001
2.7-7.6	<.0001	<.0001	0.0002
3-17	<.0001	<.0001	<.0001
Differences not significant at a 5% level, shown in bold.			

Table 59a. Precision and bias measurements for Workflow 1 and Workflow 2 derived PK estimates based on observed studies of lorazepam

	lorazepam Workflow 1 – 0.6-1 yr.			lorazepam Workflow 2 – 0.6-1 yr.		
	$AUC_{0\text{-}inf}$	Cmax	$T_{½}$	$AUC_{0\text{-}inf}$	Cmax	$T_{½}$
Mean	11903	206.47	14.93	9419	183.66	8.59
SD	872.8	20.69	7.63	456.7	12.49	4.35
AFE	1.61	0.70	0.4	1.28	0.63	0.72
AAFE	1.67	1.43	2.95	1.4	1.6	5.01
RMSE	0.27	0.16	0.49	0.2	0.2	0.72
	lorazepam Workflow 1 – 2.7-7.6 yr.			lorazepam Workflow 2 – 2.7-7.6 yr.		
Mean	1870.4	241.80	17.32	1479.10	212.04	10.10
SD	1405.1	21.36	13.2	995.86	15.37	7.80
AFE	0.82	1.85	0.25	0.65	1.62	0.45
AAFE	1.45	1.85	1.64	1.65	1.62	2.60
RMSE	0.2	0.27	0.25	0.26	0.21	0.45
	lorazepam Workflow 1 – 3-17 yr.			lorazepam Workflow 2 – 3-17 yr.		
Mean	972.94	112.57	20.79	775.11	94.76	12.31
SD	409.47	11.85	9.84	323.92	12.58	5.73
AFE	1.09	1.99	0.2	0.87	1.67	0.37
AAFE	1.37	1.99	1.4	1.39	1.67	1.89
RMSE	0.17	0.3	0.18	0.18	0.23	0.32

Table 59b. Observed pediatric pharmacokinetic data for lorazepam

Study	$AUC_{0\text{-}inf}$ ± SD (ng*h/mL)	Cmax ± SD (ug/mL)	Tmax ± SD (h)
0.6-1	6793.4 ± 3071.5	292.8 ± 260.8	40.2 ± 16.5
2.7-7.6	2062.5 ± 792.7	130.2 ± 19.6	23.7 ± 6.95
3-17	822.5 ± 706.1	56.1 ± 44.9	20.5 ± 10.2

4.2 Results for BCS class II compounds

Ciprofloxacin

A pediatric pharmacokinetic study conducted by Peltola et al in children 5-14 weeks and 1-5 years, was selected for comparison of simulated pediatric PK results, with those obtained from literature [146].All participants received a single oral dose of 15 mg/kg of ciprofloxacin. Once pediatric populations following similar dosing regimen as in the study had been simulated, up to a maximum of 1000 kids per age group were isolated to reflect the demographics of the study. Due to limitations in age resolution within the standard 5000 simulated population of children between ages 0-17, only 58 infants between ages 5-14 weeks were created and incorporated into the comparative analysis of ciprofloxacin pharmacokinetics.

All F-tests resulted in statistically significant differences at a 5% level (Table 60). Workflow 1 and Workflow 2 model derived estimates were compared to assess which workflow was a better predictor of observed PK data in children (Table 61). AUC, Cmax and Tmax estimates were significant between Workflow 1 and Workflow 2 for both study groups. Model derived AUC and Cmax estimates were statistically significant from observed PK means for the study group consisting of 1-5 year old participants.

Workflow 1 and Workflow 2 derived predictions of Cmax, and Tmax were within the designated 2 fold criteria of accuracy for both study groups, whereas AUC predictions for 1-5 year olds were not contained within 2 fold of accuracy. There was no clear trend towards bias of PK predictions (Table 62a). With regards to AUC and Cmax, Workflow 1 predictions were more precise and less bias in correspondence to the study of 5-14 week old participants, whereas Workflow 1 AUC estimates were less precise than those of Workflow 2 for the study of 1-5 year old participants. Precision of Tmax estimates was study specific. Observed data is shown in Table 62b.

Table 60. ANOVA F-test summary between model derived vs. observed means for ciprofloxacin

Parameter	Age	F value	N: Observed, workflows	p-value
$AUC_{0\text{-}inf}$	5-14 weeks	8.99	7,58	<.0001
	1-5 yrs.	46.43	10,1000	<.0001
Cmax	5-14 weeks	11.81	7,58	**0.5042**
	1-5 yrs.	33.93	10,1000	<.0001
Tmax	5-14 weeks	89.95	7,58	<.0001
	1-5 yrs.	133.69	10,1000	<.0001
Differences not significant at a 5% level, shown in bold.				

Table 61. P-values from post-hoc multiple comparison tests, of model derived PK predictions of observed data for ciprofloxacin			
Workflow 1 vs. Observed			
Study group	$AUC_{0\text{-}inf}$	Cmax	Tmax
5-14 weeks	**0.0906**	**0.9448**	**0.9737**
1-5 yr.	<.0001	<.0001	**0.4612**
Workflow 2 vs. Observed			
5-14 weeks	0.0016	**0.8939**	<.0001
1-5 yr.	<.0001	**0.4378**	<.0001
Workflow 1 vs. Workflow 2			
5-14 weeks	0.0071	**0.5112**	<.0001
1-5 yr.	<.0001	<.0001	<.0001
Differences not significant at a 5% level, shown in bold.			

Table 62a. Precision and bias measurements for Workflow 1 and Workflow 2 derived PK estimates based on observed studies of ciprofloxacin						
	ciprofloxacin Workflow 1 – 5- 14 weeks			ciprofloxacin Workflow 2 – 5-14 weeks		
	$AUC_{0\text{-}inf}$	Cmax	Tmax	$AUC_{0\text{-}inf}$	Cmax	Tmax
Mean	11.45	3.15	1.20	30.51	3.10	2.26
SD	4.18	0.52	0.06	12.54	1.16	0.36
AFE	0.68	0.94	1.01	1.94	0.96	1.84
AAFE	1.54	1.15	1.04	1.97	1.40	1.84
RMSE	0.21	0.08	0.03	0.34	0.18	0.28
	ciprofloxacin Workflow 1 – 1-5 yr.			ciprofloxacin Workflow 2 – 1-5 yr.		
Mean	8.71	2.77	0.89	13.95	2.18	2.07
SD	2.37	0.48	0.17	6.17	0.99	0.22
AFE	1.67	1.33	0.90	2.41	0.94	2.06
AAFE	1.68	1.34	1.22	2.43	1.44	2.06
RMSE	0.26	0.15	0.09	0.42	0.20	0.32

Table 62b. Observed pediatric pharmacokinetic data for ciprofloxacin [146]			
Study	$AUC_{0\text{-}inf}$ ± SD (mg*h/L)	Cmax ± SD (mg/L)	Tmax ± SD (h)
5-14 weeks	16.14 ± 7.4	3.26 ± 1.35	1.18 ± 0.46
1-5 yrs.	5.34 ± 3.27	2.11 ± 1.4	1 ± 0.25

Ofloxacin

A pediatric pharmacokinetic study conducted by Thee et al was selected for comparison of simulated pediatric PK results; study participants consisted of infants and children between the ages of 0.25-2, 2-6, and 6-8 years [147]. All participants received a single oral dose of 20 mg/kg of ofloxacin. Up to a maximum of 1000 kids per age group were simulated to reflect the demographics and dosing regimen of the study.

The F-test comparing the AUC predictions of Workflow 1 vs Workflow 2 to observed data for 6-8 year olds was not significant at a 5% level (Table 64). To assess which workflow was better, Workflow 1 and Workflow 2 derived PK predictions were compared (Table 64). For Cmax, model derived estimates were statistically different between workflows and observed data. Model derived AUC was not statistically different for ages the study group consisting of 6-8 year olds. Tmax predictions were statistically different for all age groups, as compared to observed data. Model comparisons of Tmax were not significant corresponding to 0.25-2 year old study participants.

All AUC and Cmax Workflow 1 and Workflow 2 model derived predictions were within 2 fold accuracy of observed data; there was a tendency for over-prediction bias within both workflows (Table 65a). Only Tmax estimates corresponding to 0.25-2 year olds was contained within the 2 fold accuracy benchmark. Workflow 2 produced less bias and slightly more precise AUC and Cmax estimates. There was a strong trend towards an under-prediction bias of Tmax estimates, which is likely due to the highly variable nature of this parameter (Table 65a). Observed data is shown in Table 65b.

Table 63. ANOVA F-test summary between model derived vs. observed means of ofloxacin

Parameter	Age (yr.)	F value	N: Observed, workflows	p-value
$AUC_{0\text{-inf}}$	0.25-2	7.94	10, 508	0.0004
	2-6	9.11	10, 1000	0.0001
	6-8	2.27	5, 584	**0.1041**
Cmax	0.25-2	15.91	10, 508	<.0001
	2-6	78.87	10, 1000	<.0001
	6-8	53.53	5, 584	<.0001
Tmax	0.25-2	109.94	10, 508	<.0001
	2-6	196.02	10, 1000	<.0001
	6-8	271.21	5, 584	<.0001

Differences not significant at a 5% level, shown in bold.

Table 64. P-values from post-hoc multiple comparison tests, of model derived PK predictions of observed data for ofloxacin			
Workflow 1 vs. observed			
Study group	$AUC_{0\text{-}inf}$	Cmax	Tmax
0.25-2	0.0016	<.0001	<.0001
2-6	0.0044	<.0001	<.0001
6-8	**0.137**	<.0001	<.0001
Workflow 2 vs. Observed			
0.25-2	0.0067	0.0003	<.0001
2-6	0.0161	<.0001	<.0001
6-8	**0.1754**	<.0001	<.0001
Workflow 1 vs Workflow 2			
0.25-2	**0.0603**	0.0008	**0.0547**
2-6	0.0063	<.0001	<.0001
6-8	**0.5416**	<.0001	0.0021
Differences not significant at a 5% level, shown in bold.			

Table 65a. Precision and accuracy measurements for workflow 1 and workflow 2 derived PK estimates based on observed studies of ofloxacin						
	ofloxacin Workflow 1 – 0.25-2yr			ofloxacin Workflow 2 – 0.25-2yr		
	$AUC_{0\text{-}inf}$	Cmax	Tmax	$AUC_{0\text{-}inf}$	Cmax	Tmax
Mean	66.7	13.9	0.80	63.7	13.6	0.78
SD	20.4	1.66	0.11	21.9	1.66	0.11
AFE	1.37	1.27	0.65	1.30	1.24	0.64
AAFE	1.42	1.27	1.54	1.40	1.24	1.57
RMSE	0.19	0.12	0.20	0.18	0.11	0.20
	ofloxacin Workflow 1 – 2-6yr			ofloxacin Workflow 2 – 2-6yr		
Mean	69.7	13.7	0.77	66.7	13.2	0.75
SD	19.4	1.35	0.11	23.5	1.42	0.10
AFE	1.51	1.56	0.49	1.42	1.49	0.47
AAFE	1.53	1.56	2.05	1.49	1.49	2.11
RMSE	0.22	0.20	0.32	0.21	0.18	0.33
	ofloxacin Workflow 1 – 6-8yr			ofloxacin Workflow 2 – 6-8yr		
Mean	71.0	13.7	0.75	69.6	13.2	0.73
SD	19.3	1.19	0.11	24.1	1.25	0.10
AFE	1.76	1.78	0.30	1.69	1.71	0.29
AAFE	1.76	1.78	3.38	1.71	1.71	3.48
RMSE	0.27	0.25	0.53	0.27	0.24	0.54
Differences not significant at a 5% level, shown in bold.						

Table 65b. Observed pediatric pharmacokinetic data for ofloxacin			
Study	$AUC_{0\text{-}inf}$ ± SD (ug*h/mL)	Cmax ± SD (ug/mL)	Tmax ± SD (h)
0.25-2	42.079 ± 7.95	11.352 ± 2.85	1.35 ± 0.33
2-6	46.821 ± 13.142	9.28 ± 2.65	1.48 ± 0.52
6-8	50.111 ± 16.512	8.77 ± 1.96	1.99 ± 0.75

Valsartan

A pediatric pharmacokinetic study conducted by Thee et al was selected for comparison of simulated pediatric PK results, with those obtained from literature [107]. Subjects in the study received an oral dose of 2 mg/kg of valsartan, with a maximum single dose of 80 mg was obtained from literature [107]. Subjects were stratified into four age groups; 1-4 years, 4-6 years, 6-12 years, and 12-16 year olds. Up to a maximum of 1000 kids per age group were isolated to reflect the demographics of the study.

AUC and Cmax predictions for 6-12 year old children were not significant at a level of 5% (Table 66). Model derived AUC predictions from both workflows were not significant for the study groups corresponding to 6-12 and 12-16 year olds (Table 67). Workflow 1 derived Cmax estimates were not significant from observed data and Workflow 2 estimates within the latter two study groups. Workflow 1 managed to generate AUC predictions that were not significantly different from Workflow 2 for three of four age groups. The final age group, 12-16, AUC estimates were not statistically significant in comparison to observed data, within each respective workflow. All Tmax predictions were statistically significant from observed data.

To assess the question of which workflow is better, Workflow 1 and Workflow 2 were compared for prediction accuracy, bias, and precision (Table 68a). Aside from AAFE values corresponding to the 1-4 year old age group, all AAFE values were ≤ 2 fold accuracy (Table 68a). Observed data is shown in Table 68b.

Table 66. ANOVA F-test summary between model derived vs. observed means for valsartan

Parameter	Age (yr.)	F value	N: Observed, Workflows	p-value
$AUC_{0\text{-end}}$	1-4	2451.58	7, 908	0.0004
	4-6	1991.52	7, 603	0.0014
	6-12	4071.30	8, 1000	**0.3164**
	12-16	4868.50	8, 1000	<.0001
Cmax	1-4	4876.08	7, 908	<.0001
	4-6	3916.81	7, 603	<.0001
	6-12	7459.51	8, 1000	0.0084
	12-16	5026.94	8, 1000	**0.3989**
Tmax	1-4	465.96	7, 908	<.0001
	4-6	513.61	7, 603	<.0001
	6-12	822.45	8, 1000	<.0001
	12-16	833.61	8, 1000	<.0001

Differences not significant at a 5% level, shown in bold.

Table 67. P-values from post-hoc multiple comparison tests, of model derived PK predictions of observed data for valsartan			
Workflow 1 vs. Observed			
Study group age	$AUC_{0\text{-end}}$	Cmax	Tmax
1-4	0.0003	0.0052	<.0001
4-6	0.007	0.0025	<.0001
6-12	**0.3722**	**0.1177**	<.0001
12-16	**0.7529**	**0.8574**	<.0001
Workflow 2 vs. Observed			
1-4	0.0004	0.0006	<.0001
4-6	0.0036	<.0001	<.0001
6-12	**0.5126**	0.0296	<.0001
12-16	**0.3699**	**0.9243**	<.0001
Workflow 1 vs. Workflow 2			
1-4	**0.7002**	<.0001	<.0001
4-6	**0.1557**	<.0001	<.0001
6-12	**0.5675**	**0.1602**	<.0001
12-16	<.0001	**0.4079**	<.0001
Differences not significant at a 5% level, shown in bold.			

Table 68a. Precision and bias measurements for workflow 1 and workflow 2 derived PK estimates based on observed studies of valsartan						
	valsartan Workflow 1 – 1-4yr			valsartan Workflow 2 – 1-4yr		
	$AUC_{0\text{-end}}$	Cmax	Tmax	$AUC_{0\text{-end}}$	Cmax	Tmax
Mean	13878	2774	2.4	14137	2484	2.80
SD	7413	1161	0.3	6928	1254	0.33
AFE	0.47	0.59	1.2	0.5	0.52	1.40
AAFE	2.17	1.76	1.21	2.08	1.9	1.40
RMSE	0.40	0.3	0.1	0.37	0.36	0.16
	valsartan Workflow 1 – 4-6yr			valsartan Workflow 2 – 4-6yr		
Mean	16653	3095	2.41	15984	2639	2.86
SD	8829	1297	0.313	7267	1270	0.34
AFE	0.54	0.59	1.11	0.54	0.49	1.24
AAFE	1.93	1.76	1.21	1.9	2.0	1.42
RMSE	0.34	0.3	0.1	0.33	0.38	0.16
	valsartan Workflow 1 – 6-12yr			valsartan Workflow 2 – 6-12yr		
Mean	17546	3259	2.39	18413	2994	2.82
SD	5704	1045	0.73	8256	1403	0.34
AFE	0.8	0.72	1.19	0.83	0.63	1.4
AAFE	1.43	1.49	1.19	1.46	1.71	1.4
RMSE	0.2	0.22	0.09	0.21	0.29	0.16
	valsartan Workflow 1 – 12-16yr			valsartan Workflow 2 – 12-16yr		
Mean	18231	3163	2.45	20267	3088	2.84
SD	7721	1194	0.28	9318	1411	0.32
AFE	1.05	0.95	1.21	1.15	0.91	1.41
AAFE	1.41	1.38	1.22	1.46	1.45	1.41
RMSE	0.18	0.18	0.1	0.2	0.21	0.16

Table 68b. Observed pediatric pharmacokinetic data for valsartan			
Study (yr.)	$AUC_{0\text{-end}}$ ± SD (ng*h/mL)	Cmax ± SD (ng/mL)	Tmax ± SD (h)
1-4	25823 ± 11103	4307 ± 1852	2 ± 0.52
4-6	26800 ± 6968	4818 ± 1879	2 ± 0.19
6-12	20214 ± 7277	4254 ± 1148	2 ± 0.37
12-6	15944 ± 5580	3069 ± 1258	2 ± 0.34

4.3 Results for BCS class III compounds

Acyclovir

A pediatric study investigating the pharmacokinetics of acyclovir suspension in infants and children, conducted by Sullender et al was selected for comparison of model derived PK data [120]. In the study, a 600 mg/m^2 dose of acyclovir was administered to 13 children, divided into two groups based on age. The first group consisted of 0.5-4 year olds with a mean body surface area (BSA) of 0.6 m^2, whereas the second group consisted of 4-7 year olds with a mean BSA of 0.8 m^2. As a result, the two groups of participants received an approximate mean dose of 1000 mg, and 750 mg respectively.

All F-tests resulted in statistically significant differences at a 5% level (Table 69). Workflow 1 and Workflow 2 derived AUC and Tmax estimates for statistically different for both study groups, whereas Cmax was different than observed data obtained from the younger study group (Table 70). Workflow 1 and Workflow 2 derived AUC, Cmax and Tmax estimates were significant from observed means, with the exception of Workflow 1 derived Cmax and Workflow 2 derived Tmax corresponding to the 4-7 year old study group. For the assessment of each model's comparative ability to effectively predict observed PK data, only Workflow 1 derived AUC and Workflow 2 derived Tmax predictions were contained within the designated 2 fold bias benchmark (Table 71a). There was a strong bias for over-prediction of AUC and Cmax within both workflows. Overall Workflow 2 produced comparatively less bias predictions of observed AUC, Cmax and Tmax estimates. Observed data is shown in Table 68.

Table 69. ANOVA F-test summary between model derived vs. observed means of acyclovir

Parameter	Age (yr.)	F value	N: Observed, Workflows	p-value
$AUC_{0\text{-inf}}$	0.5-4	11.05	8, 1000	<.0001
	4-7	122.39	7,904	<.0001
Cmax	0.5-4	226.10	8, 1000	<.0001
	4-7	9.73	7,904	<.0001
Tmax	0.5-4	4599.08	8, 1000	<.0001
	4-7	3575.76	7,904	<.0001

Differences not significant at a 5% level, shown in bold.

Table 70. P-values from post-hoc multiple comparison tests, of model derived PK predictions of observed data for acyclovir			
Workflow 1 vs. Observed			
Obs. Study	$AUC_{0\text{-}inf}$	Cmax	Tmax
0.5-4 yr.	0.0317	<.0001	<.0001
4-7 yr.	**0.5626**	<.0001	<.0001
Workflow 2 vs. Observed			
0.5-4 yr.	0.0085	0.0015	<.0001
4-7 yr.	0.014	<.0001	**0.2070**
Workflow 1 vs. Workflow 2			
0.5-4 yr.	0.0004	<.0001	<.0001
4-7 yr.	<.0001	**0.9208**	<.0001
Differences significant at a 5% level, shown in bold			

Table 71a. Precision and bias measurements for Workflow 1 and Workflow 2 derived PK estimates based on observed studies of acyclovir						
	acyclovir Workflow 1: 0.5-4yr			acyclovir Workflow 2 – 0.5-4yr		
	$AUC_{0\text{-}inf}$	Cmax	Tmax	$AUC_{0\text{-}inf}$	Cmax	Tmax
Mean	11.7	3.87	0.66	12.5	2.65	2.44
SD	4.71	1.13	0.15	7.13	1.28	0.57
AFE	1.88	3.38	0.20	1.86	2.16	0.74
AAFE	1.89	3.38	5.00	2.08	2.33	1.38
RMSE	0.31	0.54	0.24	0.37	0.41	0.16
	acyclovir Workflow 1 – 4-7yr			acyclovir Workflow 2 – 4-7yr		
Mean	8.15	2.80	0.68	12.8	2.80	2.35
SD	4.21	0.55	0.17	8.15	1.40	0.57
AFE	1.40	3.07	0.25	1.99	2.72	0.87
AAFE	1.46	3.07	3.98	2.21	2.82	1.25
RMSE	0.21	0.49	0.61	0.40	0.50	0.11

Table 71b. Observed pediatric pharmacokinetic data for acyclovir			
Study (yr.)	$AUC_{0\text{-}inf}$ ± SD (ug*h/mL)	Cmax ± SD (ug/mL)	Tmax ± SD (h)
0.5-4	5.68 ± 2.4	1.07 ± 0.44	3.21 ± 0.99
4-7	5.38 ± 2.12	0.89 ± 0.30	2.64 ± 0.47

Cimetidine

A pediatric pharmacokinetic study conducted by Ziemniak et al was selected for comparison of simulated pediatric PK results, with those obtained from literature [126]. All participants received an oral dose of 20 mg/kg of cimetidine. Once pediatric populations following similar dosing regimen as in the study had been simulated, up to a maximum of 1000 kids per age group were isolated to reflect the demographics of the study.

All F-tests resulted in statistically significant differences at a 5% level (Table 72). To address the question of which workflow was a better predictor of pediatric PK data, both workflows were compared (Table 73). In the event that they predicted significantly different results, identifying which workflow was better could be addressed by data presented in Table 74a. AUC estimates generated from Workflow 1 and Workflow 2 were not significant from observed data. Workflow 1 and Workflow 2 derived Tmax, and Workflow 2 derived Cmax were significantly different from observed data. Model comparisons suggest Workflow 1 PK estimates were statistically significant from Workflow 2.

AUC and Cmax derived from Workflow 1 and AUC from Workflow 2 were within the designated 2 fold criteria for bias (Table 74a). Workflow 1 generated less bias and more precise AUC, Cmax and Tmax predictions of observed data. Observed data is shown in Table 74b.

Table 72. ANOVA F-test summary between model derived vs. observed means

Parameter	Age (yr.)	F value	N: Observed, Workflows	p-value
$AUC_{0\text{-inf}}$	9-16	19.61	8, 1000	<.0001
Cmax	9-16	2759.19	8, 1000	<.0001
Tmax	9-16	263.76	8, 1000	<.0001
Differences not significant at a 5% level, shown in bold.				

Table 73. P-values from post-hoc multiple comparison tests, of model derived PK predictions of observed data for cimetidine

Workflow 1 vs. Observed			
Study age group (yr.)	$AUC_{0\text{-inf}}$	Cmax	Tmax
9-16	**0.1949**	**0.4864**	<.0001
Workflow 2 vs. Observed			
9-16	**0.0534**	<.0001	<.0001
Workflow 1 vs. Workflow 2			
9-16	<.0001	<.0001	<.0001
Differences significant at a 5% level, shown in bold			

Table 74a. Precision and bias measurements for Workflow 1 and Workflow 2 derived PK estimates based on observed studies						
	cimetidine Workflow 1 - 9-16yr			cimetidine Workflow 2 - 9-16yr		
	$AUC_{0\text{-}inf}$	Cmax	Tmax	$AUC_{0\text{-}inf}$	Cmax	Tmax
Mean	30.05	7.62	0.93	32.93	15.20	0.68
SD	8.23	0.87	0.28	12.97	3.11	0.22
AFE	1.22	1.13	0.44	1.31	2.22	0.33
AAFE	1.31	1.15	2.28	1.40	2.22	3.06
RMSE	0.14	0.07	0.39	0.19	0.36	0.50

Table 74b. Observed pediatric pharmacokinetic data for cimetidine			
Study (yr.)	$AUC_{0\text{-}inf}$ ± SD (ug*h/mL)	Cmax ± SD (ug/mL)	Tmax ± SD (h)
9-16 [126]	21.64 ± 5.11	6.44 ± 3.6	1.75 ± 0.6

Azithromycin

Two studies conducted by Nahata et al were selected for comparison of simulated pediatric PK results, with those obtained from literature [137, 138]. Once pediatric populations following similar dosing regimen as in the study had been simulated, up to a maximum of 1000 kids were isolated from each population to reflect the distribution from each of three observed studies. Therefore, 1000 kids' ages 0.5-6 years, and 6-12 years were isolated for PK analysis.

All F-tests resulted in statistically significant differences at a 5% level (Table 75). With regards to determining which workflow was a better predictor of observed PK data in children, workflows 1 and 2 were compared (Table 76). Both workflows predicted statistically different AUC and Cmax estimates. In this instance, determining which workflow is better could be addressed by data presented in Table 77a. Both Workflow 2 derived Tmax estimates and Workflow 1 derived Tmax for 6-15 year olds was not significant from observed Tmax data. With regards to the PK metrics, there was a bias towards under-prediction of AUC and Cmax within both workflows; however there was not a clear trend for Tmax predictions. All AUC, Cmax, and Tmax predictions were within 2 fold bias for the study group consisting of 0.5-5 year old participants. Workflow 2 derived predictions corresponding to 6-15 year olds were less bias and more precise than those predicted by Workflow 1. Observed data is shown in Table 77b.

Table 75. ANOVA F-test summary between model derived vs. observed means of azithromycin

Parameter	Age (yr.)	F value	N: Observed, Workflows	p-value
$AUC_{t\text{-end}}$	0.5-5	73.88	13, 1000	<.0001
	6-15	703.54	15, 1000	<.0001
Cmax	0.5-5	198.65	13, 1000	<.0001
	6-15	419.91	15, 1000	<.0001
Tmax	0.5-5	294.87	13, 1000	<.0001
	6-15	189.50	15, 1000	<.0001
Differences not significant at a 5% level, shown in bold.				

Table 76. P-values from post-hoc multiple comparison tests, of model derived PK predictions of observed data

Workflow 1 vs. Observed			
Study group age (yr.)	$AUC_{t\text{-end}}$	Cmax	Tmax
0.5-5	<.0001	<.0001	<.0001
6-15	<.0001	<.0001	**0.1267**
Workflow 2 vs. Observed			
0.5-5	<.0001	0.0392	**0.2273**
6-15	<.0001	<.0001	**0.4008**
Workflow 1 vs. Workflow 2			
0.5-5	0.0003	<.0001	<.0001
6-15	<.0001	<.0001	<.0001
Differences significant at a 5% level, shown in bold			

Table 77a. Precision and bias measurements for Workflow 1 and Workflow 2 derived PK estimates based on observed studies of azithromycin						
azithromycin Workflow 1 - 0.5-5yr				azithromycin Workflow 2 - 0.5-5yr		
	$AUC_{t\text{-}end}$	Cmax	Tmax	$AUC_{t\text{-}end}$	Cmax	Tmax
Mean	1116.0	130.81	2.86	1077.5	182.9	2.09
SD	124.5	32.9	0.83	282.5	76.9	0.57
AFE	0.60	0.56	1.53	0.57	0.73	1.13
AAFE	1.66	1.78	1.53	1.76	1.53	1.20
RMSE	0.23	0.28	0.21	0.26	0.27	0.11
azithromycin Workflow 1 - 6-15yr				azithromycin Workflow 2 - 6-15yr		
Mean	1128.75	136.81	2.76	1444.06	238.14	2.21
SD	115.7	34.6	0.72	331.59	110.11	0.53
AFE	0.36	0.34	1.12	0.45	0.54	0.90
AAFE	2.77	2.90	1.19	2.21	1.89	1.23
RMSE	0.44	0.48	0.11	0.36	0.36	0.11

Table 77b. Observed pediatric pharmacokinetic data for azithromycin			
Study	$AUC_{t\text{-}end}$ ± SD (ug*h/mL)	Cmax ± SD (ug/mL)	Tmax ± SD (h)
0.5-5	1840.92 ± 651.25	236.83 ± 115.58	1.83 ± 0.39
6-15	3109.43 ± 1033.17	383.14 ± 142.02	2.43 ± 1.09

4.4 Summary of aim 1 and aim 2

To assess aim 1 and aim 2, an ANOVA test with Tukey-Kramer pairwise comparisons was conducted in order to determine the requirement of IV data based on statistical significance. Acceptance and rejection of the null hypotheses respective to aim 1 and aim 2 were based on the criteria established above. Looking at aim 1, which postulates the possibility that IV data may not be required for the derivation of pediatric PK estimates (Table 78), 9/25 (36%) of Workflow 1 derived AUC estimates were not different from observed data. Looking at aim 2, which postulates that that IV data would not be required (Table 78), 6/25 (24%) comparisons of Workflow 1 derived AUC estimates were not different from Workflow 2. Only 3/25 (12%) of AUC comparisons were comparable exclusively between Workflow 2 and observed data, and 7/25 (28%) did not fulfil any of the criteria, and were therefore subject to assessment by aim 3. Overall, 15/25 (60%) of AUC comparisons within Workflow 1 were comparable to either observed data or Workflow 2. There were 13/25 (52%) of Cmax and Tmax estimates from Workflow 1 that were comparable to either observed data or Workflow 2 (Table 78).

Table 78. Summary of aim 1 and aim 3 ANOVA and pairwise comparison

PK parameter	May not require IV data (Workflow 1 = Observed)	Do not require IV data (Workflow 1 = Workflow 2)	Inconclusive	May require IV data (only Workflow 2 = observed)
AUC	9 (36%)	6 (24%)	7 (28%)	3 (12%)
Cmax	3 (12%)	10 (40%)	11 (44%)	1 (4%)
Tmax	5 (20%)	8 (32%)	10 (40%)	2 (8%)

4.5 Summary of Chi squared statistic of BCS class comparison (Aim 3 & 4)

To assess aim 3, a Chi square test was conducted to assess the overall comparative predictive performance of each workflow to predict pediatric parameters within 2 fold AAFE. The objective of the Chi-square test for aim 3 was to evaluate if Workflow 1 performed differently than Workflow 2, and whether one workflow performed with an overall greater predictive performance than the other. Table 79 compares the total number of pediatric PK parameters, out of a possible 25 studies, that were predicted within, or greater than, 2 fold AAFE between workflows. Overall, 23/25 (92%) AUC estimates within Workflow 1 were within <2 fold AAFE compared to 20/25 (80%) within Workflow 2. A total of 22/25 (88%) Cmax estimates within both workflows were <2 fold AAFE. Lastly, 18/25 (72%) and 19/25 (76%) Tmax estimates were <2 fold AAFE respectively. Given that each p-value produced by the Chi squared test was >0.05, we may infer that there is no statistical significance in the predictive performance of Workflow 1, in comparison to Workflow 2 (Table 79).

Table 79. Chi squared statistic comparing overall predictive performance of each workflow to predict pediatric parameters within 2 fold AAFE

Parameter	2 < AAFE < 2	Workflow 1 (# of studies /25)	Workflow 2 (# of studies / 25)	p-value
AUC	AAFE<2 AAFE>2	23 2	20 5	1.00
Cmax	AAFE<2 AAFE>2	22 3	22 3	1.00
Tmax	AAFE<2 AAFE>2	18 7	19 6	1.00

To assess aim 4, a Chi square test was conducted to evaluate if there was a difference in the predictive performance of Workflow 1, based on BCS class stratification, in comparison to corresponding PK value predictions derived from Workflow 2 (Table 80). Within the BCS Class 1 stratification, 11/11 (100%) AUC and Cmax estimates were <2 fold AAFE within both workflows; 9/11 (82%) and 8/22 (73%) Tmax values within Workflow 1 and Workflow 2, respectively, were predicted within 2 fold AAFE. The Chi square test for evaluating a difference between Workflow 1 and Workflow 2 produced a p-value >0.05 for all respective PK parameters; from this we may infer that BCS Classification did not limit the ability of Workflow 1 to predict observed PK parameters as compared to Workflow 2 (Table 80). Within the BCS Class 2 stratification, 8/9 (89%) and 7/9 (78%) of AUC estimates were predicted within 2 fold AAFE within Workflow 1 and Workflow 2 respectively, 9/9 (100%) Cmax estimates and 7/9 (78%) Tmax estimates were predicted within 2 fold AAFE within both workflows. The Chi Square test for evaluating a difference between workflows based on BCS Class II stratification produced a p-value >0.05 for all respective PK parameters; from this, we may infer that limitations of solubility within BCS class II did not limit the predictive performance of Workflow 1 (Table 80). Lastly, Within the BCS Class 3

stratification, 4/5 (80%) and 2/5 (40%) of AUC estimates within Workflow 1 and Workflow 2 respectively, were predicted within 2 fold AAFE. Similarly, 2/5 (40%) Cmax estimates within both workflows, and 2/5 (40%) and 4/5 (80%) of Tmax estimates within Workflow 1 and Workflow 2 respectively, were predicted within 2 fold AAFE. The Chi square test for evaluating a difference between workflows based on BCS Class III stratification produced a p-value>0.05 for all respective PK parameters; from this we may infer that limitations of permeability and solubility within BCS Class 3 stratification did not limit the predictive performance of Workflow 1 (Table 80).

Table 80. Chi squared statistic comparing overall influence of BCS class on model prediction.

BCS Class	Parameter	2 < AAFE < 2	Workflow 1 (# of studies /25)	Workflow 2 (# of studies / 25)	p-value
BCS 1	AUC	AAFE<2 AAFE>2	11 0	11 0	1.00
	Cmax	AAFE<2 AAFE>2	11 0	11 0	1.00
	Tmax	AAFE<2 AAFE>2	9 2	8 3	1.00
BCS 2	AUC	AAFE<2 AAFE>2	8 1	7 2	0.2941
	Cmax	AAFE<2 AAFE>2	9 0	9 0	1.00
	Tmax	AAFE<2 AAFE>2	7 2	7 2	1.00
BCS 3	AUC	AAFE<2 AAFE>2	4 1	2 3	0.5238
	Cmax	AAFE<2 AAFE>2	2 3	2 3	1.00
	Tmax	AAFE<2 AAFE>2	2 3	4 1	0.5238

5. Discussion

This study proposed an alternate workflow method for pediatric PBPK modeling which yielded comparable pediatric pharmacokinetic predictions as the standard workflow of practice. Nine compounds were selected for this study based on current approval for administration in infants and children, availability of compound specific physicochemical data, organism specific plasma concentration profiles, as well as all relevant clearance processes data. Compounds were selected based on their respective BCS classification; three compounds from each of BCS I, II and III. The purpose of stratifying drug selection by BCS class was to assess whether uncertainties presented by the compound relative to solubility, and permeability would impede model performance. It was imperative that all *in vivo* and *in vitro* data were available for each drug included in the study.

The main objective of this study was to assess an alternate PBPK workflow which would serve as an acceptable replacement for the standard workflow as described by Maharaj and Edginton [22]. The proposed alternate workflow would ideally predict pediatric PK parameters (i.e. AUC, Cmax, and Tmax) that would statistically compare to observed data, when adult IV data is not available for a given compound. The null hypothesis for aim 1 of this study (H1) postulated that Workflow 1 and Workflow 2 derived predictions of pediatric PK data will not be significantly different from observed data at a significance level of 5%. Additionally the null hypothesis for aim 2 (H2), postulated that PK predictions derived from Workflow 1 would not be statistically significant from Workflow 2. The null hypothesis for aim 3 of this study (H3) postulated that the prediction accuracy of pediatric PK observed data using Workflow 1 will be comparable to Workflow 2 and within a 2 fold AAFE from observed data.

There were 11 age group stratifications within BCS I compounds where 6/11 predicted mean AUCs were not significantly different from observed within Workflow 1, whereas Workflow 2 had 9/11 mean AUCs that were not significantly different from observed. This would indicate that Workflow 2 was a more accurate model, as bolstered by comparison of AAFE outcomes discussed below. This was expected, given the availability of human IV data. All AUC predictions were statistically similar between Workflow 1 and Workflow 2 indicating that the starting point for model development does not alter the final product, which, in this case, were pediatric PK predictions. Based on model performance of AUC predictions, we fail to reject H1 for Workflow 1 derived estimates of BCS class 1 compounds, with moderate confidence and conclude that adult IV data is not required for BCS class I compounds when making pediatric PK predictions. Similarly, we fail to reject H1 for Workflow 2 derived AUC predictions with greater confidence than that of Workflow 1. The third aim of this study was to compare pediatric PK prediction accuracy within each workflow. Of the 11 age stratifications within BCS class 1, 11/11 AUC predictions were within a 2 fold of observed data for both workflows. As a result, H3 is accepted. In summary, for AUC, Workflow 2 was more accurate than Workflow 1 although for all predictions,

regardless of workflow, the predictions were within 2 fold of the observed data. While AUC was the most important metric to consider as it drives dosing, Cmax and Tmax may also be of importance and are considered here. Only 4/11 Cmax and 5/11 Tmax predictions within Workflow 1 were not significant from observed; however, >60% Cmax and >50% Tmax values were not different between Workflow 1 and Workflow 2. The majority of Cmax and Tmax predictions within Workflow 1 were comparable to observed or Workflow 2 derived means. We therefore fail to reject H1 for Workflow 1 and H2, and must conclude that IV data is not required for Cmax and Tmax estimates. Within Workflow 2, the majority of Cmax and Tmax predicted values were not different from observed or Workflow 1; as a result, we fail to reject H1 for Workflow 2 with respect to Cmax, and Tmax. All Cmax estimates, and most Tmax predictions were within a 2 fold AAFE of observed data within both workflows, we therefore fail to reject H3, and may conclude that both models were equally precise.

There were 9 age group stratifications within BCS class II compounds, where 4/9 mean AUC predictions within Workflow 1 were not significant from observed, compared to 3 of 9 within Workflow 2. This would indicate that both workflows were equally poor in model performance. There were 5/9 AUC predictions that were not statistically different between Workflow 1 and Workflow 2, thereby allowing us to accept H2 with moderate confidence. In total, 7/9 AUC predictions within Workflow 1 were either not significant from observed and/or not significant from Workflow 2, compared to 6 of 9 for Workflow 2. Although we fail to accept H1 for the majority of AUC predictions within both workflows, we fail to reject H2, from which we must conclude that that IV data is not a necessary component of pediatric model development for BCS class II compounds. Of the three compounds within BCS class II, ofloxacin, and valsartan undergo considerable biliary elimination which may very likely be the cause of such poor model performance. Biliary secretion creates great uncertainty towards model CL and mean residence time of the compound within an organism; it may also lead to enterohepatic recirculation which increases the possibility for first pass metabolism of the parent compound. With regards to the third aim of this study, 8/9 AUC predictions generated from Workflow 1 and 7/9 from Workflow 2 were within 2 fold AAFE of observed data. We fail to reject H3 with sufficient confidence, and must conclude that the accuracy of Workflow 1 was comparable to that of Workflow 2. In summary, neither workflow was able to generate accurate AUC estimates similar to observed data; however both workflows were equally precise in generating AUCs within a 2 fold AAFE of observed data. Only 3/9 predicted Cmax values within Workflow 1 and Workflow 1 independently, were not significant from observed; similarly only 3/9 Cmax values derived from Workflow 1 were not significant from Workflow 2. From this, we fail to accept H2 and H1 for both workflows, with respect to the prediction of Cmax. Similarly, only 2/9, and 1/9 Tmax predictions within Workflow 1 and Workflow 2, respectively, were not different from observed; there weren't any similar predictions between workflows. We therefore fail to accept H2 and H1 for both workflows. In summary, we are unable to conclude if IV data is a necessary component in pediatric model development in deriving Cmax and Tmax estimates. Looking at model prediction

accuracy, all 9 Cmax predictions, and 7/9 Tmax predictions, were within 2 fold AAFE. We therefore fail to reject H3 and must conclude that Workflow 1 was comparable to Workflow 2 in model precision, despite a lack of IV data.

Lastly, there were 5 age group stratifications within BCS class 3 compounds, of which only 2/5 predicted mean AUCs within Workflow 1 were not different from observed, compared to only 1/5 within Workflow 2. There were not any AUC predictions that were similar between Workflow 1 and Workflow 2. Based on model performance of AUC predictions, we fail to accept H2 and H1 for both workflows; therefore, we must conclude that it is unknown as to whether or not IV data is needed for sufficient model development. In assessing the third aim of this study for model precision, 4/5 Workflow 1 derived AUC estimates, and 2/5 within Workflow 2, were <2 fold AAFE. Although it would seem the majority of Workflow 2 derived AUC estimates fall outside of the acceptance range for the precision metric, a Chi-squared test suggests this result is of similar statistical power to the Workflow 1. Therefore, we fail to reject H3, and must conclude that Workflow 1 and Workflow 2 were not significant in model performance, despite a lack of adult IV data. For the comparison of PK prediction accuracy of Cmax and Tmax within each workflow, only 1/5 Cmax within Workflow 1 was not significant from observed, compared to 2/5 for Workflow 2; only 1/5 Cmax estimates were not different between both workflows. We therefore fail to reject H2, and H1 for both Workflow 1 and Workflow 2.Tmax was also poorly predicted by Workflow 1, as there were not any predictions within BCS class III that were similar to observed data. There were 3/5 predictions within Workflow 2 that were not different from observed, and only 1/5 which was similar between workflows. In summary, we fail to accept H2 and H1 for both workflows and must conclude that there is insufficient evidence to determine whether or not IV data is a necessary component of model development for the prediction of Cmax and Tmax. Although only 2/3 Cmax and Tmax predictions fell within a 2 fold AAFE for both workflows, according to the Chi-square test, we are able accept H3, and conclude, that although the models were not accurate, Workflow 1 model performance was not different from Workflow 2.

The final aim was to assess if the biopharmaceutical classification system holds significance over model predictive performance. The number of pediatric PK parameters, within each BCS class, that were accurately predicted within 2 fold AAFE using Workflow 1, were compared to the number of PK parameters that were accurately predicted within 2 fold AAFE using Workflow 2. A difference between workflow performances, stratified by BCS class, would indicate that compound permeability and solubility impede model prediction; this would therefore contribute to limitations in overall model performance. Workflow 1 did not perform differently than Workflow 2 overall, or within individual BCS classifications. As a result, BCS class does not significantly impact model predictive performance. This suggests that the absorption model that was used along with the optimization of CL and P_{int} led to accurate predictions of bioavailability regardless of BCS class and this filtered down to the pediatric

models. One limitation of this study was that there were few compounds chosen from each BCS class for modeling. This limits our confidence in factoring the effect of BCS classification on model performance. Although the results of this study, with respect to testing by BCS class, unanimously concluded that BCS class does not matter, an n = 3 within each class provides minimal confidence in the final conclusion. There were no BCS class 4 compounds selected for this study due to a scarcity of experimental data. For future research, it would be of value to examine the effects of BCS class stratification on compounds regulated by a diverse array of reaction mechanisms, as well as an overall larger sample size of compounds within each class.

In the final assessment of whether human IV data provides a significant advantage over pre-clinical rat IV data in the prediction of pediatric PK data, it would appear predictive performance of both workflows was comparable. Aim 1 and aim 2 of this study were established to examine model performance based explicitly on the statistical significance between model derived PK prediction and observed data. Based on conclusions drawn by a systematic assessment of the null hypotheses H1 and H2 (see Objectives section), for 15 of the 25 pediatric studies (60%), there was no advantage to having human IV data to predict observed data; of the remaining 10 studies, 3 required human IV data for accurate prediction (12%), while for 7 studies (28%) it was inconclusive whether the presence of human IV data was advantageous. In contrast to the initial two aims of this study, Aim 3 was established for an assessment of model performance within clinical relevance, rather than a strict assessment of statistical significance which suffered slightly from unbalanced comparisons. If the predicted mean of the PK parameter was within 2 fold (AAFE) of the observed mean, the model derived PK parameter was considered clinically similar. For example, this suggests that a predicted AUC value that is double or half of the observed value will derive a reasonable dose in children. Although there is currently no standard metric for deriving clinical relevance in this scenario, a 2 fold comparison is the most frequently applied metric within literature[148-150]. While this may be acceptable for drugs with wide therapeutic indices, this would not be ideal for compounds that exhibit a narrow therapeutic index in pediatrics, as an inadvertent doubling of dose may lead to concentrations that exceed toxicity threshold values and could potentially lead to various adverse events. On the other hand, under-dosing may lead to sub therapeutic concentrations that do not ameliorate the indication for which the drug is given.

Successful dose calculation relies on the accurate quantification of CL and F, as both these values will have a direct effect on the derivation of exposure (e.g. AUC). Given the purpose of this study, it would be beneficial to assess the ability of Workflow 1 to accurately predict total plasma CL. Total plasma CL is usually derived following IV administration where the systemic dose is known and CL can be precisely calculated. In the case of Workflow 1, CL was optimized based solely on the terminal slope of human oral data. The terminal slope is a function of the volume of distribution and CL. Volume of distribution is

dependent upon both the organism (e.g. K_p) and the drug's physico-chemistry where, in Workflow 1, drug physico-chemistry was optimized within the rat model. A comparison of Workflow 1 derived total CL values in adults to those obtained from adult IV data in Workflow 2 will help to assess the validity of the Workflow 1 derived CL. The total plasma CL values for 6 compounds (acetaminophen, levofloxacin, lorazepam, ofloxacin, acyclovir, and cimetidine) within Workflow 1 were within 25% of Workflow 2 total plasma CL values. Of the remaining 3 compounds (ciprofloxacin, valsartan, and azithromycin), total plasma CL was over predicted by 1.4, 3.6, and 1.8 fold error respectively. Much like CL, the precise derivation of F relies on complete systemic dose absorption which can only occur following IV dose administration. F is calculated as the ratio of AUC values from oral and IV dose administrations. Workflow 1 derived F values were within 20% of Workflow 2 value for the same 6 compounds for which CL was within 25% of Workflow 2. Of the remaining 3 compounds (ciprofloxacin, valsartan, and azithromycin), F values were over predicted by 1.6, 3.4, and 1.7 fold error, respectively. The over prediction of F values was proportional to the over prediction of CL values within the same compounds. This means that CL and F compensate for each other in the optimization procedure. It should be noted that this was the case for only some BCS II and III compounds and not for any BCS I compounds where bioavailability is predicted to be high. This CL and F over prediction did not appear to hinder prediction accuracy in children as it was determined that BCS class was irrelevant. This may become more problematic if human oral data is used to derive CL values as in Workflow 1 but is used to predict exposure following IV administration in children where F can no longer compensate for the over or under prediction of CL. In this case, it is expected that pediatric prediction would be less accurate than prediction of exposure following oral administration. Overall a large majority of total plasma CL and F values predicted from rat IV + human oral data were within 25% of those derived using human IV data. As discussed, care should be taken if exposure prediction following IV administration is completed for children without human IV data for drugs that are not BCS I.

6. Conclusion

In summary, this study has found that the proposed alternate workflow method for pediatric PBPK modeling (Workflow 1) may serve as a viable alternative to the standard workflow of practice (Workflow 2). Based on AUC predictions, approximately 60% of Workflow 1 derived pediatric AUC predictions were not statistically significant from either Workflow 2, and/or observed data; thereby suggesting that human IV data does not necessarily provide an advantage towards the prediction of pediatric AUC. The viability of Workflow 1 was further bolstered by the fact that approximately 92% of Workflow 1 derived pediatric AUC means were predicted within 2 fold of observed data. This lends itself to substantial clinical relevance, suggesting that predicted pediatric exposures can be reasonably scaled from adults using Workflow 1. The alternative workflow did not hinder prediction accuracy in children as a consequence of inaccurate CL and F prediction, given that the added limitations of the biopharmaceutical classification system were not relevant. In conclusion Workflow 1 has demonstrated that the substitution of rat IV data in the absence of human IV data, within the constructs of PBPK modeling, does not impede the model's ability to predict observed pediatric PK parameters.

References

1. Yamashiro W, Kazuya M, Masakazu H, Yasuhisa A, Zhuohan H, and Yuichi S. Involvement of transporters in the hepatic uptake and biliary excretion of valsartan, a selective antagonist of the angiotensin II AT1-receptor, in humans. Drug Metab and Dispos 2006; 34: 1247-54

2. Zhao P, Zhang L, Grillo JA, Li Q, Bullock JM, Moon YJ, Song P, Brar SS, Madabushi R, Wu TC, Booth BP, Rahman NA, Reynolds KS, Berglund GE, Lesko LJ, and Huang SM. Applications of physiologicall based pharmacokinetic (PBPK) modeling and simulation during regulatory review. Clin Pharmacol ther 2010; 89: 259-67

3. Sachs AN, Avant D, Lee C, Rodriquez W, and Murphy D. Pediatric information in drug product labeling. JAMA 2012; 307: 1914-1915

4. Rieder MJ. Better drug therapy for children: Time for action. Paediatr Child Health 2003; 8: 210-212

5. Leong R, Vieira ML, Zhao P, Mulugeta Y, Lee CA, Huang SM, and Burckart GJ. Regulatory experience with physiologically based pharmacokinetic modeling for pediatric drug trials. Nature 2012; 91: 926-931

6. Hsien L, Breddemann A., Frobel AK., Heusch A, Schmidt KG, and Läer S. Off-label drug use among hospitalized children: identifying areas with the highest need for research. Pharm World Sci 2008; 30: 497-502

7. Food and Drug Administration Modernization act of 1997. 2009; Available from: http://www.fda.gov/RegulatoryInformation/Legislation/FederalFoodDrugandCosmeticActFDCAct/SignificantAmendmentstotheFDCAct/FDAMA/

8. Hudachek SF, and Gustafson D L. Physiologically based pharmacokinetic model of laptinib developed in mice and scaled to humans. J Pharmacokinet Pharmacodyn 2013; 40: 157-176

9. Willman S, Hohn K, Edginton A, Sevestre M, Solodenko J, Weiss W, Jorg L, and Schmitt W. Development of a physiology based whole body population model for assessing the infludence of individual variability on the pharmacokinetics of drugs. J Pharmacokinet Pharmacodyn 2007;34: 401-431

10. Peters SA. Evaluation of a generic physiologically based parmacokinetic model for lineshape analysis. Clin Pharmacokinet 2008; 47: 261-275

11. Jones HM, Gardner IB, and Watson, KJ. Modelling and PBPK simulation in drug discovery. AAPS 2009; 11: 155-166

12. McNamara PJ, and Alcorn J. Protein binding predictions in infants. AAPS PharmSci 2002;4: 1-8

13. Peters SA. Physiologically based pharmacokinetic (PBPK) modeling and simulatons: Principles, methods and applications in the pharmaceutical industry. 2012, John Wiley & Sons

14. Bjorkman S. Prediction of the volume of distribution of a drug: which tissue plasma partition coefficients are needed? J Pharm Pharmacol 2002; 54: 1237-1245

15. Schmitt W. General approach for the calculation of tissue to plasma partition coefficients. Toxicol in vitro 2008; 22: 457-467

16. Berezhkovskiy B. The corrected traditional equations for calculation of hepatic clearance that account for the difference in drug ionization in extracellular and intracellular tissue water and the corresponding corrected PBPK equation. J Pharm Sci 2010; 100: 1167-1182

17. Edginton AN, Theil FP, Schmitt W, and Willmann S. Whole body physiologically based pharmacokinetic models: their use in clinical drug development. Expert Opin Drug Metab Toxicol 2003; 4: 1143-52

18. Edginton A, Schmitt W, and Willmann S. Development and evaluation of a generic physiologically based pharmacokinetic model for children. Clin Pharmacokinet 2006; 45:1013-1034

19. Bhattaram VA, Booth BP, Ramchandani RP, Beasley BN, Wang Y, Tandon V, Duan JZ, Baweja RK, Marroum PJ, Uppoor RS, Rahman NA, Sahajwalla CG, Powell R, Mehta MU, and Bhattaram J. Impact of pharmacometrics on drug approval and labeling decisions: a survey of 42 new drug applications. AAPS J 2005; 7: 503-512

20. Edginton AN. Knowledge-driven approaches for the guidance of first-in-children dosing. Paediatr Anesth 2010; 21: 1-9

21. Willmann S, Höhn K, Edginton A, Sevestre M, Solodenko J, Weiss W, Lippert J, and Schmitt W. Development of a physiology-based whole-body population model for assessing the influence of individual variability on the pharmacokinetics of drugs. J Pharmacokinet Pharmacodyn 2007; 34: 401-431

22. Maharaj AR, Barret JS, and Edginton AN. A Workflow example of PBPK modeling to support pediatric research and development: Case study with Lorazepam. AAPS J 2013; 15: 455-464

23. Gueorguieva I, Nestorov IA, Murby S, Gisbert S, Collins B, Dickens K, Duffy J, Hussain Z, and Rowland M. Development of a whole body physiologically based model to characterise the pharmacokinetics of benodiazepines. J Pharmacokinet Pharmacodyn 2004; 31: 269-298

24. Poulin P, and Theil FP. Development of a novel method for predicting human volume of distribution at steady-state of basic drugs and comparative asssessment with existing methods. J Pharm Sci 2009; 98: 4941-4961

25. Jones HM, Parrott N, Jorga K, and Lavé T. A novel strategy for physiologically basd predictions of human pharmacokinetics. Clin Pharmacokinet 2006; 45: 511-542

26. Rodgers, T., H.M. Jones, and M. Rowland, Tissue lipids and drug distribution: dog versus rat. J Pharm Sci 2012; 101: 4615-4626

27. Chaturvedy PR, Decker CJ, and Odinecs A. Prediction of pharmacokinetic properties using experimental approaches during early drug discovery. Curr Opin Chem Biol 2001; 452-463

28. Bjorkman, S. Prediction of drug disposition in infants and children by means of PBPK modelling: theophylline and midazolam as model drugs. BR J Clin Pharmacol 2005; 59: 691-704

29. McNamara PJ, and Alcorn J. Protein binding predictions in infants. AAPS PharmSci 2002; 4: 1-8

30. McNamara PJ, and Alcorn J. Using ontogeny information to build predictive models for drug elimination. Drug Discov Today 2008; 13: 507-512

31. Rhodin M, Anderson BJ, Peters AM, Coulthard MG, Wilkins B, Cole M, Chatelut E, Grubb A, Veal GJ, Keir MJ, Holford NHG. Human renal function maturation: a quantitative description using weight and post menstrual age. Pediatr Nephrol 2009; 24: 67-76

32. Edginton AN, Schmitt W, Voith B, and Willmann S. A mechanistic approach for the scaling of clearance in children. Clin Pharmacokinet 2006; 7: 683-704

33. Hayton WL. Maturation and growth of renal function: dosing renally cleared drugs in children. AAPS PharmSci, 2000; 2: 1-7

34. Di L, Keefer C, Scott DO, Strelevitz TJ, Chang G, Bi Y, Lai Y, Duckworth J, Fenner K, Troutman MD, and Obach RS. Mechanistic insights from comparing intrinsic clearance values between human liver microsomes and hepatocytes to guide drug design. Eur J Med Chem 2012; 57: 441-448

35. Parrott MN, Davies B, Hoffmann G, Koerner A, Lave T, Prinssen E, Theogaraj E, and Singer T. Development of a physiologically based model for oseltamivir and simulation of pharmacokinetics in neonates and infants. Clin Pharmacokinet 2011; 50: 613-623

36. Wu CY, and Benet LZ. Predicting drug disposition via application of BCS: transport/absorption/elimination interplay and development of a biopharmaceutics drug disposition classification system. Pharmaceut Res 2005; 22: 11-23

37. Medical, Statistical, and Clinical Pharmacology Reviews of Pediatric Studies Conducted under Section 505A and 505B of the Federal Food, Drug, and Cosmetic Act (the Act), as amended by the FDA Amendments Act of 2007 (FDAAA). 2013; Available from: http://www.fda.gov/Drugs/DevelopmentApprovalProcess/DevelopmentResources/ucm049872.htm

38. FDA, U. Summaries of Medical and Clinical Pharmacology Reviews - Summaries of Medical and Clinical Pharmacology Reviews as of January 15, 2008. 2013; Available from: http://www.fda.gov/Drugs/DevelopmentApprovalProcess/DevelopmentResources/ucm161894.htm

39. Agoram B, Woltosz WS, and Bolger MB. Predicting the impact of physiological and biochemical processes on oral drug bioavailability. Adv Drug Deliver Rev 2001; 50: S41-S67

40. Rodgers T, and Rowland M. Physiologically based pharmacokinetic modelling 2: predicting the tissue distribution of acids, very weak bases, neutrals and zwitterions. J Pharm Sci 2006; 95: 1238-1257

41. Watari N, Iwai M, and Kaneniwa N. Pharmacokinetic study of the fate of acetaminophen and its conjugates in rats. J Pharmacokinet Biop 1983; 11: 245-272

42. Kalantzi L, Reppas C, Dressman JB, Amidon GL, Junginger HE, Midha KK, Shah VP, Stavchansky SA, and Barends DM. Biowaiver monographs for immediate release solid oral dosage forms: acetaminophen (paracetamol). J.Pharm Sci 2006; 95: 4-14

43. Rawlins MD, Henderson DB, and Hijab AR. Pharmacokinetics of paracetamol (acetaminophen) after intravenous and oral administration. Eur J Clin Pharmacol 1977; 11: 283-286

44. Volak LP, Hanley MJ, Masse G, Hazarika S, Harmatz JS, Badmaev V, Majeed M, Greenblatt DJ, and Court MH. Effect of a herbal extract containing curcumin and piperine on midazolam, flurbiprofen and paracetamol (acetaminophen) pharmacokinetics in healthy volunteers. BR J Clin Pharmacol 2013; 75: 450-462

45. Wilson CG, Clarke CP, Starkey YYL, and Clarke GD. Comparison of a novel fast-dissolving acetaminophen tablet formulation (FD-APAP) and standard acetaminophen tablets using gamma scintigraphy and pharmacokinetic studies. Drug Dev Ind Pharm 2011; 37: 747-753

46. Prescott LF. Kinetics and metabolism of paracetamol and phenacetin. Br J Clin Pharmacol 1980; 10: 291S-298S

47. Court, M.H., Duan SX, von Moltke LL, Greenblatt DJ, Patten CJ, Miners JO, and Mackenzie PI. Interindividual variability in acetaminophen glucuronidation by human liver microsomes: identification of relevant acetaminophen UDP-glucuronosyltransferase isoforms. J Pharmacol Exp Ther 2001; 299: 998-1006

48. Adjei AA, Gaedigk A, Simon SD, Weinshilboum RM, and Leeder JS. Interindividual variability in acetaminophen sulfation by human fetal liver: Implications for pharmacogenetic investigations of drug-induced birth defects. Birth Defects-Orig 2008; 82: 155-165

49. Lee SS, Buters JT, Pineau T, Fernandez-Salguero P, and Gonzalez FJ. Role of CYP2E1 in the hepatotoxicity of acetaminophen. J Biol Chem 1996; 271: 12063-12067

50. Willmann S, Edginton AN, Kleine-Besten M, Jantratid E, Thelen K, and Dressman JB. Whole-body physiologically based pharmacokinetic population modelling of oral drug administration: inter-individual variability of cimetidine absorption. J Pharm Pharmacol 2009; 61:891-899

51. Van Biesen W, De Bacquer D, Verbeke F, Delanghe J, Lameire N, and Vanholder R. The glomerular filtration rate in an apparently healthy population and its relation with cardiovascular mortality during 10 years. Eur Heart J 2007; 28: 478-483

52. Bourrié M, Meunier V, Berger Y, and Fabre G. Cytochrome P450 isoform inhibitors as a tool for the investigation of metabolic reactions catalyzed by human liver microsomes. J Pharmacol Exp Ther 1996; 277: 321-332

53. Alhusainy W, Paini A, Punt A, Louisse J, Spenkelink A, Vervoort J, Delatour T, Scholz G, Schilter B, Adams T, van Bladeren PJ, Rietjens IM, and Alhusainy W. Identification of nevadensin as an important herb-based constituent inhibiting estragole bioactivation and physiology-based biokinetic modeling of its possible in vivo effect. Toxicol Appl Pharm 2010;

245: 179-190

54. Borlak J, Gasparic A, Locher M, Schupke H, and Hermann R. N-Glucuronidation of the antiepileptic drug retigabine: results from studies with human volunteers, heterologously expressed human UGTs, human liver, kidney, and liver microsomal membranes of Crigler-Najjar type II. Metabolism 2006; 55: 711-721

55. Clements JA, Critchley JA, and Prescott LF. The role of sulphate conjugation in the metabolism and disposition of oral and intravenous paracetamol in man. Br J Clin Pharmacol 1984; 18: 481-485

56. Khalil F, and Läer S. Physiologically based pharmacokinetic modeling: methodology, applications, and limitations with a focus on its role in pediatric drug development. BioMed Res 2011; 1-13

57. Alcorn J. and McNamara PJ. Ontogeny of hepatic and renal systemic clearance pathways in infants part II. Clin Pharmacokinet 2002; 41: 1077-1094

58. Willmann S, Becker C, Burghaus R, Coboeken K, Edginton AN, Lippert J, Siegmund H, Thelen K, and Mück W. Development of a paediatric population-based model of the pharmacokinetics of rivaroxaban. Clin Pharmacokinet 2014; 53: 89-102

59. Fujieda Y, Yamaoka K, Ito T, and Nakagawa T. Local absorption kinetics of levofloxacin from intestinal tract into portal vein in conscious rat using portal-venous concentration difference. Pharmaceut Res 1996; 13: 1201-1204

60. North DS, Fish DN, and Redington JJ. Levofloxacin, a second-generation fluoroquinolone. Pharmacotherapy 1998; 18: 915-935

61. Koeppe MO, Cristofoletti R, Fernandes EF, Storpirtis S, Junginger HE, Kopp S, Midha KK, Shah VP, Stavchansky S, Dressman JB, and Barends DM. Biowaiver monographs for immediate release solid oral dosage forms: Levofloxacin. J Pharm Sci 2011; 100: 1628-1636

62. Coceani N, Colombo I, and Grassi M. Acyclovir permeation through rat skin: mathematical modelling and in vitro experiments. Int J Pharm 2003; 254: 197-210

63. Chien SC, Chow AT, Natarajan J, Williams RR, Wong FA, Rogge MC, and Nayak RK. Absence of age and gender effects on the pharmacokinetics of a single 500-milligram oral dose of levofloxacin in healthy subjects. Antimicrob Agents Ch 1997; 41: 1562-1565

64. Chien SC, Wong FA, Fowler CL, Callery-D'Amico SV, Williams RR, Nayak R, and Chow AT. Double-blind evaluation of the safety and pharmacokinetics of multiple oral once-daily 750-milligram and 1-gram doses of levofloxacin in healthy volunteers. Antimicrob Agents Ch 1998; 42: 885-888

65. Fish DN, and Chow AT. The clinical pharmacokinetics of levofloxacin. Clin Pharmacokinet 1997; 32: 101-119

66. Tachibana M, Tanaka M, Masubuchi Y, and Horie T. Acyl glucuronidation of fluoroquinolone antibiotics by the UDP-glucuronosyltransferase 1A subfamily in human liver microsomes. Drug

Metab Dispos 2005; 33: 803-811

67. Fish DN, and Chow AT. The clinical pharmacokinetics of levofloxacin. Clin Pharmacokinet 1997; 32: 101-119

68. Chien S, Wells TG, Blumer JL, Kearns GL, Bradley JS, Bocchini JA, Natarajan J, Maldonado S, and Noel GJ. Levofloxacin pharmacokinetics in children. J Clin Pharmacol 2005; 45: 153-160

69. Atack JR, Scott-Stevens P, Beech JS, Fryer TD, Hughes JL, Cleij MC, Baron J, Clark JC, Hargreaves RJ, and Aigbirhio FI. Comparison of lorazepam [7-chloro-5-(2-chlorophenyl)-1, 3-dihydro-3-hydroxy-2H-1, 4-benzodiazepin-2-one] occupancy of rat brain γ-aminobutyric acidA receptors measured using in vivo [3H] flumazenil (8-fluoro 5, 6-dihydro-5-methyl-6-oxo-4H-imidazo [1, 5-a][1, 4] benzodiazepine-3-carboxylic acid ethyl ester) binding and [11C] flumazenil micro-positron emission tomography. J Pharmacol Exp Ther 2007; 320: 1030-1037

70. Divoll M, and Greenblatt DJ. Effect of age and sex on lorazepam protein binding. J Pharm Pharmacol 1982; 34: 122-123

71. Pyka A, Babuska M, and Zachariasz M. A comparison of theoretical methods of calculation of partition coefficients for selected drugs. Acta Pol Pharm 2006; 63: 159-167

72. Popović GV, Sladić DM, Stefanović VM, and Pfendt LB. Study on protolytic equilibria of lorazepam and oxazepam by UV and NMR spectroscopy. J Pharmaceut Biomed 2003; 31: 693-699

73. Yager JY, and Seshia SS. Sublingual lorazepam in childhood serial seizures. Am J Dis Child 1988; 142: 931-932

74. Greenblatt DJ, Divoll M, Harmatz JS, and Shader RI. Pharmacokinetic comparison of sublingual lorazepam with intravenous, intramuscular, and oral lorazepam. J Pharm Sci 1982; 71: 248-252

75. de Wildt SN, Kearns GL, Leeder JS, and van den Anker JN. Glucuronidation in humans. Clin Pharmacokinet 1999; 36: 439-452

76. Uchaipichat V, Suthisisang C, and Miners JO. The glucuronidation of R-and S-lorazepam: human liver microsomal kinetics, UDP-glucuronosyltransferase enzyme selectivity, and inhibition by drugs. Drug Metab Dispos 2013; 41: 1273-1284

77. Wang H, Liao ZX, Chen M, and Hu XL. Effects of hepatic fibrosis on ofloxacin pharmacokinetics in rats. Pharmacol Res 2006; 53: 28-34

78. Sakore S, Choudhari S, and Chakraborty BH. Biowaiver monograph for immediate release solid oral dosage forms: ofloxacin. Int J Pharm Pharm Sci 2010; Suppl 4: 156-161

79. Takács-Novák K, Józan M, Hermecz I, and Szász G. Lipophilicity of antibacterial fluoroquinolones. Int J Pharm 1992; 79: 89-96

80. Lode H, Höffken G, Olschewski P, Sievers B, Kirch A, Borner K, and Koeppe P. Pharmacokinetics of ofloxacin after parenteral and oral administration. Antimicrob Agents Ch 1987; 31: 1338-1342

81. Araki H, Ogake N, Minami S, Watanabe Y, Narita H, Tamai I, and Tsuji A. Application of muscle microdialysis to evaluate the concentrations of the fluoroquinolones pazufloxacin and ofloxacin in the tissue interstitial fluids of rats. J Pharm Pharmacol 1997; 49: 1141-1144

82. Peyret T, Poulin P, and Krishnan K. A unified algorithm for predicting partition coefficients for PBPK modeling of drugs and environmental chemicals. Toxicol Appl Pharm 2010; 249: 197-207

83. Lehto P, Kivisto KT, and Neuvonen PJ. The effect of ferrous sulphate on the absorption of norfloxacin, ciprofloxacin and ofloxacin. Br J Clin Pharmaco 1994; 37: 82-85

84. Yuk JH, Nightingale CH, Quintiliani R, and Sweeney KR. Bioavailability and pharmacokinetics of ofloxacin in healthy volunteers. Antimicrob Agents Ch 1991; 35: 384-386

85. Wingender W, Graefe KH, Gau W, Förster D, Beermann D, and Schacht P. Pharmacokinetics of ciprofloxacin after oral and intravenous administration in healthy volunteers. Eur J Clin Microbiol 1984; 3: 355-359

86. Höffken G, Lode H, Prinzing C, Borner K, and Koeppe P. Pharmacokinetics of ciprofloxacin after oral and parenteral administration. Antimicrob Agents Chemother 1985; 27: 375-379

87. Yamashiro W, Maeda K, Hirouchi M, Adachi Y, Hu Z, and Sugiyama Y. Involvement of transporters in the hepatic uptake and biliary excretion of valsartan, a selective antagonist of the angiotensin II AT1-receptor, in humans. Drug Metab Dispos 2006; 34: 1247-1254

88. Naora K, Ichikawa N, Hirano H, and Iwamoto K. Distribution of ciprofloxacin into the central nervous system in rats with acute renal or hepatic failure. J Pharm Pharmacol 1999; 51: 609-616

89. Olivera ME, Manzo RH, Junginger HE, Midha KK, Shah VP, Stavchansky S, Dressman JB, and Barends DM. Biowaiver monographs for immediate release solid oral dosage forms: ciprofloxacin hydrochloride. J Pharm Sci 2011; 100: 22-33

90. Ross DL, and Riley CM. Dissociation and complexation of the fluoroquinolone antimicrobials--an update. J Pharm Biomed Anal 1994; 12: 1325-1331

91. Ross DL, and Riley CM. Physicochemical properties of the fluoroquinolone antimicrobials II. Acid ionization constants and their relationship to structure. Int J Pharm 1992; 83: 267-272

92. Renau TE, Sanchez JP, Shapiro MA, Dever JA, Gracheck SJ, and Domagala JM. Effect of lipophilicity at N-1 on activity of fluoroquinolones against mycobacteria. J Med Chem 1995; 38: 2974-2977

93. Montero MT, Freixas J, and Hernandez-Borrell J. Expression of the partition coefficients of a homologous series of 6-fluoroquinolones. Int J Pharm 1997; 149: 161-170

94. Tang Y, and Gan K. Statistical evaluation of in vitro dissolution of different brands of ciprofloxacin hydrochloride tablets and capsules. Drug Dev Ind Pharm 1998; 24: 549-552

95. Lubasch A, Keller I, Borner K, Koeppe P, and Lode H. Comparative pharmacokinetics of ciprofloxacin, gatifloxacin, grepafloxacin, levofloxacin, trovafloxacin, and moxifloxacin after single oral administration in healthy volunteers. Antimicrob Agents Chemother 2000; 44: 2600-

2603

96. Brumfitt W, Franklin I, Grady D, Hamilton-Miller JM, and Iliffe A. Changes in the pharmacokinetics of ciprofloxacin and fecal flora during administration of a 7-day course to human volunteers. Antimicrob Agents Chemother 1984; 26: 757-761

97. Bergan T, Dalhoff A, and Rohwedder R. Pharmacokinetics of ciprofloxacin. Infection 1988; 16: S3-13

98. Wise R, Lockley RM, Webberly M, and Dent J. Pharmacokinetics of intravenously administered ciprofloxacin. Antimicrob Agents Chemother 1984; 26: 208-210

99. Peltola H, Ukkonen P, Saxén H, and Stab H. Single-dose and steady-state pharmacokinetics of a new oral suspension of ciprofloxacin in children. Pediatrics, 1998; 101: 658-662

100. Criscione L, Bradley WA, Bühlmayer P, Whitebread S, Glazer R, Lloyd P, Mueller P, and Gasparo M. Valsartan: preclinical and clinical profile of an antihypertensive angiotensin II antagonist. Cardiovasc Drug Rev 1995; 13: 230-250

101. Colussi DM, Parisot C, Rossolino ML, Brunner LA, and Lefèvre GY. Protein binding in plasma of valsartan, a new angiotensin II receptor antagonist. J Clin Pharmacol 1997; 37: 214-221

102. Chella N, Shastri N, and Tadikonda RR. Use of the liquisolid compact technique for improvement of the dissolution rate of valsartan. Acta Pharmaceutica Sinica B 2012; 2: 502-508

103. Flesch G, Miller P, and Lloyd P. Absolute bioavailability and pharmacokinetics of valsartan, an angiotensin II receptor antagonist, in man. Eur J Clin Pharmacol 1997; 52: 115-120

104. Macek J, Klima J, and Ptáček P. Rapid determination of valsartan in human plasma by protein precipitation and high-performance liquid chromatography. J Chromatogr B 2006; 832: 169-172

105. Waldmeier F, Glaenzel U, Wirz B, Oberer L, Schmid D, Seiberling M, Valencia J, Gilles-Jacques R, End P, and Vaidyanthan S. Absorption, distribution, metabolism, and elimination of the direct renin inhibitor aliskiren in healthy volunteers. Drug Metab Dispos 2007; 35: 1418-1428

106. Dorne JL, Walton K, and Renwick AG. Human variability in xenobiotic metabolism and pathway-related uncertainty factors for chemical risk assessment: a review. Food Chem Toxicol 2005; 43: 203-216

107. Blumer J, Batisky DL, Wells T, Shi V, Solar-Yohay S, and Sunkara G. Pharmacokinetics of valsartan in pediatric and adolescent subjects with hypertension. J Clin Pharmacol 2009; 49: 235-241

108. Ogiso T, Iwaki M, Tanino T, Fujii J, and Paku T. Rectal absorption of acyclovir in rats and improvement of absorption by triglyceride base. Biol Pharm Bull 1993; 3: 315-318

109. Ye J, Liu Q, Wang C, Meng Q, Sun H, Peng J, Ma X, and Liu K. Benzylpenicillin inhibits the renal excretion of acyclovir by OAT1 and OAT3. Pharmacol Rep 2013; 65: 505-512

110. Alcorn J, and McNamara PJ. Acyclovir, ganciclovir, and zidovudine transfer into rat milk. Antimicrob Agents Chemother 2002; 46: 1831-1836

111. Miranda, P, Good SS, Laskin OL, Krasny HC, Connor JD, and Lietman PS. Disposition of intravenous radioactive acyclovir. Clin Pharmacol Ther 1981; 30: 662-672

112. Laskin OL. Clinical pharmacokinetics of acyclovir. Clin Pharmacokinet 1983; 8: 187-201

113. Bank, D. Drugbank - Aciclovir. 2014 2014; Available from: http://www.drugbank.ca/drugs/DB00787

114. Balon K, Riebesehl BU, and Muller BW. Drug liposome partitioning as a tool for the prediction of human passive intestinal absorption. Pharm Res 1999; 16: 882-888

115. Koeppe MO, Cristofoletti R, Fernandes EF, Storpirtis S, Junginger HE, Kopp S, Midha KK, Shah VP, Stavchansky S, Dressman JB, and Barends DM. Biowaiver monographs for immediate release solid oral dosage forms: Levofloxacin. J Pharm Sci 2011; 100: 1628-1636

116. Bangaru RA, Bansal YK, Rao AR, and Gandhi TP. Rapid, simple and sensitive high-performance liquid chromatographic method for detection and determination of acyclovir in human plasma and its use in bioavailability studies. J Chromatogr B Biomed Sci Appl 2000; 739: 231-237

117. Yuen KH, Peh KK, Billa N, Chan KL, and Toh WT. Bioavailability and pharmacokinetics of acyclovir tablet preparation. Drug Dev Ind Pharm 1998; 24:193-196

118. Vergin H, Kikuta C, Mascher H, and Metz R. Pharmacokinetics and bioavailability of different formulations of aciclovir. Arzneimittelforschung 1995; 45: 508-515

119. Soul-Lawton J, Seaber E, On N, Wootton R, Rolan P, and Posner J. Absolute bioavailability and metabolic disposition of valaciclovir, the L-valyl ester of acyclovir, following oral administration to humans. Antimicrob Agents Chemother 1995; 39: 2759-2764

120. Sullender WM, Arvin AM, Diaz PS, Connor JD, Straube R, Dankner W, Levin MJ, Weller S, Blum MR, and Chapman S. Pharmacokinetics of acyclovir suspension in infants and children. Antimicrob Agents Chemother 1987; 31: 1722-1726

121. Adedoyin A, Aarons L, and Houston JB. Plasma concentration-response relationship for cimetidine inhibition of drug metabolism in the rat. Drug Metab Dispos 1987; 15: 127-132

122. Jantratid E, Prakongpan S, Dressman JB, Amidon GL, Junginger HE, Midha KK, and Barends DM. Biowaiver monographs for immediate release solid oral dosage forms: cimetidine. J Pharm Sci 2006; 95: 974-984

123. Jantratid E, PrakongpanS, Amidon GL, and Dressman JB. Feasibility of biowaiver extension to biopharmaceutics classification system class III drug products: cimetidine. Clin Pharmacokinet 2006; 45: 385-399

124. Yamasaki H, Arima T, and Nagashima H. Pharmacokinetic studies of cimetidine in patients with liver disease. Gastroenterol Jpn 1987; 22: 440-447

125. Somogyi A, and Gugler R. Clinical pharmacokinetics of cimetidine. Clin Pharmacokinet 1983; 8 463-495

126. Ziemniak JA, Assael BM, Padoan R, and Schentag JJ. The bioavailability and pharmacokinetics of cimetidine and its metabolites in juvenile cystic fibrosis patients: age related differences as compared to adults. Eur J Clin Pharmacol 1984; 26: 183-189

127. Taninaka C, Ohtani H, Hanada E, Kotaki H, Sato H, and Iga T. Determination of erythromycin, clarithromycin, roxithromycin, and azithromycin in plasma by high-performance liquid chromatography with amperometric detection. J Chromatogr B 2000; 738: 405-411

128. Shepard RM, and Falkner FC. Pharmacokinetics of azithromycin in rats and dogs. J Antimicrob Chemother 1990; 25(supple A): 49-60

129. McFarland JW, Berger CM, Froshauer SA, Hayashi SF, Hecker SJ, Jaynes BH, Jefson MR, Kamicker BJ, Lipinski CA, Lundy KM, Reese CP, and Vu CB. Quantitative structure-activity relationships among macrolide antibacterial agents: In vitro and in vivo potency against Pasteurella multocida. J Med Chem 1997; 40: 1340-1346

130. Foulds G, Shepard RM, and Johnson RB. The pharmacokinetics of azithromycin in human serum and tissues. J Antimicrob Chemother 1990; 25(suppl A): 73-82

131. Lipinski CA, Lombardo F, Dominy BW, and Feeney PJ. Experimental and computational approaches to estimate solubility and permeability in drug discovery and development settings. Adv Drug Deliver Rev 2012; 64: 4-17

132. Curatolo W, and Foulds G. Method of increasing the bioavailability and tissue penetration of azithromycin. US Patent Application 2001.

133. Matzneller P, Krasniqi S, Kinzig M, Sörgel F, Hüttner S, Lackner E, Muller M, and Zeitlinger M. Blood, tissue, and intracellular concentrations of azithromycin during and after end of therapy. Antimicrob Agents Chemother 2013; 57: 1736-1742

134. Iqbal Z, Khan MI, Khan A, Khan A, Shah Y, and Ahmad L. Bioequivalence of 2 azithromycin capsule formulations: a randomized, single-dose, open-label, 2-period crossover study in healthy male pakistani volunteers. Curr Ther Res 2011; 72: 95-108

135. Najib NM, Idkaidek N, Ghanem IE, Admour I, Mahmood Alam S, Zaman Q, and Dham R. Bioequivalence assessment of Azomycin®(Julphar, UAE) as compared to Zithromax®(Pfizer, USA)—two brands of azithromycin—in healthy human volunteers. Biopharm Drug Dispos 2001; 22: 15-21

136. Lode H. The pharmacokinetics of azithromycin and their clinical significance. Eur J Clin Microbiol 1991; 10: 807-812

137. Nahata MC, Koranyi KI, Gadgil SD, Hilligoss DM, Fouda HG, and Gardner MJ.Pharmacokinetics of azithromycin in pediatric patients after oral administration of multiple doses of suspension. Antimicrob Agents Chemother 1993; 37: 314-316

138. Nahata MC, Koranyi KI, Luke DR, and Foulds G. Pharmacokinetics of azithromycin in pediatric patients with acute otitis media. Antimicrob Agents Chemother 1995; 39: 1875-1877

139. Romsing J, Ostergaard D, Senderovitz T, Drozdziewicz D, Sonne J, and Ravn G. Pharmacokinetics of oral diclofenac and acetaminophen in children after surgery. Paediatr

Anaesth 2001; 11: 205-213

140. Walson PD, Galletta G, Braden NJ, and Alexander L. Ibuprofen, acetaminophen, and placebo treatment of febrile children. Clin Pharmacol Ther 1989; 46: 9-17

141. Hopkins CS, Underhill S, and Booker PD. Pharmacokinetics of paracetamol after cardiac surgery. Arch Dis Child 1990; 65: 971-976

142. Chien S, Wells TG, Blumer JL, Kearns GL, Bradley JS, Bocchini JA. Levofloxacin pharmacokinetics in children. J Clin Pharmacol 2005; 45: 153-160

143. McDermott CA, Kowalczyk AL, Schnitzler ER, Mangurten HH, Rodvold KA, and Metrick S. Pharmacokinetics of lorazepam in critically ill neonates with seizures. J Pediatr 1992; 120: 479-483

144. Muchohi SN, Obiero K, Newton CR, Ogutu BR, Edwards G, and Kokwaro GO. Pharmacokinetics and clinical efficacy of lorazepam in children with severe malaria and convulsions. Br J Clin Pharmacol 2008; 65: 12-21

145. Chamberlain JM, Capparelli EV, Brown KM, Vance CW, Lillis K, Mahajan P, and Lichenstein R. Pharmacokinetics of intravenous lorazepam in pediatric patients with and without status epilepticus. J Pediatr 2012; 160: 667-672

146. Peltola H, Väärälä M, Renkonen OV, and Neuvonen PJ. Pharmacokinetics of single-dose oral ciprofloxacin in infants and small children. Antimicrob Agent Chemother 1992; 36: 1086-1090

147. Thee S, Garcia-Prats AJ, McIlleron HM, Wiesner L, Castel S, Norman J, Draper HR, van der Merwe PL, Hesseling AC, and Schaaf HS. Pharmacokinetics of Ofloxacin and Levofloxacin for Prevention and Treatment of Multidrug-Resistant Tuberculosis in Children. Antimicrob Agent Chemother 2014; 58: 2948-2951

148. Gérard C, Bleyzac N, Girard P, Freyer G, Bertrand Y, and Tod M. Influence of dosing schedule on organ exposure to cyclosporin in pediatric hematopoietic stem cell transplantation: analysis with a PBPK model. Pharmaceut Res 2010; 27: 2602-2613

149. Johnson TN. The problems in scaling adult drug doses to children. Arch Dis Child 2008; 93: 207-211

150. Jones HM, Dickins M, Youdim K, Gosset JR, Attkins NJ, Hay TL, Gurrell IK, Logan YR, Bungay PJ, Jones BC, and Gardner IB. Application of PBPK modelling in drug discovery and development at Pfizer. Xenobiotica 2012; 42: 94-106